M. Phil Thesis

Tamjida Rahman Luna

04 June, 2011

Characterization of CoS and $Co_{1-x}Cd_xS$ Thin Films Deposited by Spray Pyrolysis Technique

by

Tamjida Rahman Luna

MASTER OF PHILOSOPHY IN PHYSICS

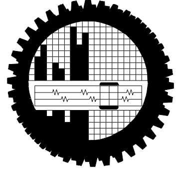

Department of Physics

BANGLADESH UNIVERSITY OF ENGINEERING & TECHNOLOGY
DHAKA-1000, BANGLADESH
04 JUNE, 2011.

Content

	Declaration	
	Dedication	
	Acknowledgement	I
	Abstract	IV

CHAPTER-I GENERAL INTRODUCTION

1.1	Introduction	1
1.2	Review of the earlier work	3
1.3.1	Physical properties of CoS	6
1.3.2	Physical properties of CdS	8
1.4	Characteristics of thin films	9
1.5	Application of thin films	11
1.6	Aim of the present work	12

CHAPTR-II THIN FILM DEPOSITION TECHNIQUES AND PROCESSES

2.1	Deposition techniques	15
2.1.1	Chemical Vapor Deposition (CVD)	17
2.1.2	Electrodeposition	19
2.1.3	Thermal oxidation	20
2.1.4	Epitaxy	21
2.1.5	Evaporation	22
2.1.6	Sputtering	23
2.1.7	Physical Vapor Deposition (PVD)	24
2.1.8	Casting	25
2.1.9	Sol-Gel	26
2.1.10	Molecular beam Epitaxy (MBE)	27
2.1.11	Spray pyrolysis method	29
2.2	Formation Stages of Thin Films	29
2.2.1	Condensation	29
2.2.2	Nucleation	31
2.2.3	Growth	31

CHAPTER-III THEORETICAL PRINCIPLES OF FILM CHARACTERIZATION

3.1	Surface Morphology and Structural Characterization	36
3.1.1	Scanning Electron Microscope	36
3.1.2	Scanning process of SEM	38
3.1.3	Energy Dispersive Analysis of X-ray	39
3.1.3.1	Energy dispersive X-ray spectroscopy	40

3.1.4	X-ray Diffraction	41
3.2	Optical Characterization	42
3.2.1	Beer-Lambert Law	42
3.2.2	Derivation of the Beer-Lambert law	43
3.2.2.1	Absorption coefficient	44
3.2.3	Electronic transitions	45
3.2.4	Direct and Indirect optical transitions	48
3.2.5	Working principle of UV-Visible spectrometer	50
3.3	Measurement of optical absorption of thin film	51
3.3.1	Measurement of thickness of thin film	52
3.3.2	Electrical Properties Measurement	54
3.3.3	Resistivity and Conductivity of thin film	55
3.3.4	Resistivity Measurement Techniques	55
3.3.5	Direct method	55
3.3.6	van-der Pauw's technique	56
3.3.7	Factors Affecting Resistivity Measurement	58
3.3.8	Sheet Resistance	58
3.3.9	Activation Energy	58
3.3.10	Temperature Coefficient of Resistance (T. C. R)	59
3.3.11	Annealing	60

CHAPTER-IV EXPERIMENTAL DETAILS

4.1	Experimental Equipment	61
4.1.1	Preparation of Masks	61
4.1.2	Heater	62
4.1.3	The Design of the Reactor	63
4.1.4	The Fume chamber	63
4.1.5	Air Compressor	64
4.1.6	Spray Head/ Spray Nozzle	64
4.2	Type of Substrate and substrate cleaning	64
4.3	Working Solution	65
4.4	Film Deposition Parameters	65
4.5	Sample Deposition	66
4.6	Rate of Deposition	68
4.7	Thickness Control	68
4.8	Optimization of the Deposition Process	68

CHAPTER-V RESULTS AND DISCUSSION

5.1	Introduction	70
5.2	Deposition of $Co_{1-x}Cd_xS$ thin films	70
5.3	Thickness Measurement	70
5.4	Surface morphology of as-deposited $Co_{1-x}Cd_xS$ and annealed $Co_{0.8}Cd_{0.2}S$ thin films	71
5.5	Compositional studies	74
5.6	X-ray diffraction (XRD)	77

5.7	Optical Properties	79
5.7.1	Absorbance and Transmittance	79
5.7.1.1	Absorption coefficient and optical band gap	81
5.7.2	Extinction coefficient	84
5.7.3	Refractive index	85
5.7.4	Dielectric constants	86
5.7.5	Dielectric loss	88
5.7.6	Optical conductivity	89
5.8	Optical Properties of annealed $Co_{0.8}Cd_{0.2}S$ thin film	89
5.8.1	Absorbance, Transmittance and Optical band gap of annealed $Co_{0.8}Cd_{0.2}S$ thin film	90
5.8.2	Extinction coefficient	93
5.8.3	Refractive index	93
5.8.4	Dielectric constants	94
5.8.5	Dielectric loss	95
5.8.6	Optical conductivity	96
5.9	Electrical Properties of as-deposited $Co_{1-x}Cd_xS$ thin films	96
5.9.1	Variation of Resistivity with Temperature	97
5.9.2	Variation of Conductivity with Temperature	98
5.9.3	Variation of Sheet Resistance with Temperature	99
5.9.4	Variation of Activation Energy	100
5.9.5	Variation of Temperature Coefficient of Resistance (T. C. R)	101

CHAPTER-VI CONCLUSIONS AND SUGGESTIONS FOR FUTURE WORK

6.1	Conclusions	102
6.2	Suggestions for Future Work	104

CHAPTER-VII

	References	105
	Appendix	110

LIST OF FIGURES

1.1	Crystal structure of CoS.	7
1.2	Crystal structure of CdS	8
2.1	Classification of most common deposition process.	17
2.2	Chemical Vapor Deposition (CVD) Process.	18
2.3	Typical setup for electrodeposition process.	19
2.4	Typical wafer oxidation furnace.	20
2.5	Typical cold-wall vapor phase epitaxial reactor.	21
2.6	Typical system for e-beam evaporation process.	22
2.7	Schematic drawing of the magnetron sputtering system.	24
2.8	Physical vapor deposition process.	25

2.9	The spin casting process as used for photoresist in photolithography	26
2.10	Generalized scheme of sol-gel synthesis.	27
2.11	Schematic of the Molecular beam epitaxy system	28
2.12	Different stages of film growth.	32
2.13	Schematic of shape changes during coalescence (Pashley et al., 1964).	33
2.14	Electron micrograph of islands during and after coalescence (a) at zero (b) after 1 to 2 sec. (c) after 60 sec. (Pashley, 1954).	33
3.1	Photograph of Scanning Electron Microscopy (SEM).	37
3.2	Schematic diagram of a scanning electron microscope.	39
3.3	Photograph of Energy dispersive X-ray spectroscopy (Inspect IS50 FEI Company) in AECD, Dhaka.	40
3.4	Absorption of light by a sample.	43
3.5	Vibrational and rotational energy levels.	46
3.6	Possible electronic transitions.	46
3.7	Diagram of the components of a spectrometer.	50
3.8	Photograph of a recording Spectrophotometer (UV-1601PC, SHIMADZU, JAPAN) in BCSIR, Dhaka.	51
3.9	Interferometer arrangement for producing reflection Fizeau fringes of equal thickness.	53
3.10	Circuit arrangement for resistivity measurement by direct method.	56
3.11	Experimental arrangements for measuring resistivity by using van-der Pauw's method.	56
4.1	Mask for the sample.	62
4.2	Design of a reactor.	63
4. 3	Experimental set up of spray pyrolysis method.	67
5.1(a-f.)	SEM photographs of as-deposited $Co_{1-x}Cd_xS$ films at x=0.0, 0.2, 0.4, 0.6, 0.8 and 1.0 respectively under 1000 magnification.	72
5.1(g-i)	SEM photographs of $Co_{0.8}Cd_{0.2}S$ annealed films at 673, 773 and 873 K respectively under 5000 magnification.	73
5.2 (a-d)	EDX spectra of $Co_{1-x}Cd_xS$ thin films (x=0.0, 0.2, 0.6, 0.8 and 1 respectively).	75-76
5.3.(a)	X-ray diffraction patterns of as-deposited $Co_{1-x}Cd_xS$ thin films.	78
5.3.(b)	X-ray diffraction patterns of annealed $Co_{0.8}Cd_{0.2}S$ thin films.	79
5.4.(a)	Variation of absorbance as a function of wavelength for $Co_{1-x}Cd_xS$ films for different concentrations.	80
5.4(b)	Variation of transmittance as a function of wavelength for $Co_{1-x}Cd_xS$ films for different concentrations.	80
5.4 (c)	Variation of Absorption coefficient as a function of photon energy for as-deposited $Co_{1-x}Cd_xS$ films	82
5.4(d-i)	Plots of (αhν) 2 vs. photon energy (hν) for as-deposited $Co_{1-x}Cd_xS$ thin films.	83
5.5	Variation of extinction coefficient as a function of wavelength for as-deposited $Co_{1-x}Cd_xS$ films of different concentrations.	85
5.6	Variation of refractive index as a function of wavelength for $Co_{1-x}Cd_xS$ films of different concentrations.	86

5.7(a)	Variation of real part of dielectric constant as a function of wavelength of $Co_{1-x}Cd_xS$ films of different concentrations.	87
5.7(b)	Variation of imaginary part of dielectric constant as a function of wavelength for $Co_{1-x}Cd_xS$ films of different concentration.	87
5.8	Variation of dielectric loss as a function of photon energy for as-deposited $Co_{1-x}Cd_xS$ films of different concentrations.	88
5.9	Variation of optical conductivity as a function of photon energy for $Co_{1-x}Cd_xS$ films of different concentrations.	89
5.10 (a)	Variation of absorbance as a function of wavelength for annealed $Co_{0.8}Cd_{0.2}S$ films.	90
5.10(b)	Variation of Transmittance as a function of wavelength for annealed $Co_{0.8}Cd_{0.2}S$ films.	90
5.10(c-e)	Plots of $(\alpha h\nu)^2$ vs. photon energy ($h\nu$) for annealed $Co_{0.8}Cd_{0.2}S$ films.	91-92
5.11	Variation of extinction coefficient as a function of wavelength for annealed $Co_{0.8}Cd_{0.2}S$ films.	93
5.12	Variation of refractive index as a function of wavelength for annealed $Co_{0.8}Cd_{0.2}S$ films.	94
5.13(a)	Variation of real part of dielectric constants as a function of wavelength for $Co_{0.8}Cd_{0.2}S$ films.	94
5.13(b)	Variation of imaginary part of dielectric constants as a function of wavelength for annealed $Co_{0.8}Cd_{0.2}S$ films.	95
5.14	Variation of dielectric loss as a function of photon energy for annealed $Co_{0.8}Cd_{0.2}S$ films.	95
5.15	Variation of optical conductivity as a function of photon energy for annealed $Co_{0.8}Cd_{0.2}S$ films	96
5.16	Variation of electrical resistivity with temperature for as-deposited $Co_{1-x}Cd_xS$ thin films.	97
5.17	Variation of electrical conductivity with temperature for as-deposited $Co_{1-x}Cd_xS$ thin films.	98
5.18	Variation of sheet resistance with temperature for $Co_{1-x}Cd_xS$ thin films.	99
5.19	Plot of $\ln\sigma$ versus 1000 / T for as-deposited $Co_{1-x}Cd_xS$ thin films.	100
5.20	Variation of Temperature coefficient resistance (T. C. R) with temperature for as-deposited $Co_{1-x}Cd_xS$ thin films.	101

LIST OF TABLES

Table 1.1	Atomic % of different compositions of $Co_{1-x}Cd_xS$ thin films.	74
Table 1.2	Variation of thickness and direct band gap with the doping concentration value, (x=0-100 % Cd) of $Co_{1-x}Cd_xS$ thin films.	84
Table 1.3	Variation of direct E_g with different annealing temperatures for annealed $Co_{0.8}Cd_{0.2}S$ thin films.	92
Table 1.4	Variation of activation energy with different compositions of $Co_{1-x}Cd_xS$ thin films.	101

ACKNOWLEDGEMENT

First of all I am very much grateful to the **Almighty Allah** for giving me strength, patience and ability to complete this research work.

I would like to express my sincere gratitude and acknowledgement to my respected supervisor **Dr. Jiban Podder,** Professor, Department of Physics, BUET, Dhaka. I am very much grateful to him for his able supervision, good guidance, constant encouragement, profound cordiality, constructive discussion, valuable suggestions, untold patience and continuous support during the course of this work. I am especially thankful to him for allowing me to work under his supervision.

I would like to express my gratefulness to **Prof. Dr. A. K. M. Akther Hossain,** Head, Department of Physics, BUET, Dhaka, for his instructive discussions, helpful suggestions, cordial supports to carry out this work and also allowing me to use the instrument facilities of his laboratory for this work as well.

I would like to express my gratefulness to **Prof. Dr. Md. Abu Hashan Bhuiyan** for his constructive criticism, stimulating encouragement, various advice and suggestions to shape this work in many ways. I also like to thank all the respected teachers of Physics department, BUET, Dhaka including **Prof. Dr. Md. Feroz Alam Khan**, **Prof. Nazma Zaman, Mrs. Fahima Khanam, Prof. Dr. Md. Mostak Hossain, Dr. Afia Begum, Dr. Md. Farhad Mina, Dr. Md. Rafi Uddin, Mr. Muhammad Rakibul Islam, Mr. Mohammad Abu Sayem Karal, Mr. Mohammad Jellur Rahman** and **Mr. Muhammed Samir Ullah**.

I want to give my special thanks to **Mr. Md. Maidul Islam**, Scientific Officer, AECD for his contributions to the design of SPD unit at BUET.

The help provided by **Dr. Dilip Kumar Saha,** C. S. O.**,** Materials Science Division, AECD for XRD analysis, **Dr. M. A. Gafur**, S. S. O. BCSIR, for UV-VIS

measurements and **Mr. Harinarayan Das,** Scientific officer, AECD for EDX and SEM analysis is greatly appreciated.

I would like to express my cordial thanks to **Mr. Md. Julkarnain** and **Mr. Jaker Hossain**, Lecturers, Department of Applied Physics & Electronic Engineering, University of Rajshahi for their kind help during the study of electrical properties in their laboratory.

I am also thankful to all of fellow graduate students. Working with them during these past years has truly been a delight experience. There are too many names to list them all, but I will try to highlight a few. Thanks are also due to **Ms. Ferdousi, Ms. Lubna, Mr. Kazi Md. Amjad Hussain, Mr. Sonjit Sen Roy, Akas, Puspen, Rasel, Ranjit, Gobindo, Nupur, Sanjoy, Khorshed, Rimi, and Mr. Sunirmal Majumder** for their suggestions and sincere help during my research time. I am also thankful to **Mr. Idris Munsi, Mr. Liaquat Ali** and **Sawpan vai** for their help throughout the working time.

I would like to express my heartfelt thanks to **Mr. Kamal Uddin Azad,** Assistant Professor, Department of Physics, Sherpur Govt. Mohila College and **Mr. Md. Kamruzzaman,** Lecturer, Department of Physics, Begum Rokeya University, Rangpur for their cordial cooperation, valuable suggestions and instructive discussion from the beginning of my thesis work.

I need to mention some of my colleagues name for their appreciation and cordial support to me in many ways. Thanks to **Mr. Ataur Rahman**, **Mrs. Shamima Ferdous, Mr. Shahin Sakawat Chowdhury, Mr. Shahidul Azad, Dr. Mizanur Rahman**, **Mr. Safayet Alom, Mr. Tarikul Islam, Mr. Md. Kabir Hossain, Mrs. Lima** and **Mrs. Rafia**. I am specially thankful to **Mr. Mohammed Enamul Hye, FCS,** Associate Professor, Department of Accounting, Bandarban Govt. College and

Mr. K. M. Rafiqul Islam, Project Director, 306 Model School Project for their supportive guidance during my deputation process.

I need to thank some individuals on the personal side of my life. I am blessed with some cordial friends and wish to say my warm thanks to **Shimu apa, Jhuma apa, Ruma, Sompa, Supti, Kajol, Bappi, Aunnesh** and **Zakaria** for their love, support and encouragement. I would like to express my heartfelt thanks to **Mr. Manzoor Murshed Siddiqui**, Associate Professor, Department of Physics, Govt. Carmichael College, Rangpur, for his friendly encouragement and constant inspiration to complete this dissertation.

Last but not least, I would like to convey my deep gratitude and love to my **family** who has been the pillar of support during each and every phase of my educational and professional career. I am grateful to **my parents** and two younger brothers **Tanim, Tarik** and other relatives **Rana vaia, Moni**, **Moshiur, Sahadot vai-vabi, Nazma apa-Kafi dulavai and Lima aunty-Jillur uncle** for their blessings and encouragement throughout my entire life.

I acknowledge with thanks to the **University Grant Commission** (**UGC)** for giving me the 2 years M. Phil scholarship.

I acknowledge with thanks to the **Bangladesh University of Engineering & Technology** for giving me the opportunity to do this thesis work and for the financial assistance.

Abstract

Pure cobalt sulfide (CoS) and cadmium (Cd) doped CoS ($Co_{1-x}Cd_xS$) thin films with different values of x (viz, 0.0, 0.2, 0.4, 0.6, 0.8, 1.0) were deposited on glass substrate from aqueous solutions of $Co(CH_3COO)_2.4H_2O$, $Cd(CH_3COO)_2.3H_2O$ and NH_2CSNH_2 at 523 K using a low cost spray pyrolysis technique. The surface morphology, elemental, structural, optical and electrical properties of the as-deposited films were studied by scanning electron microscopy (SEM), energy dispersive X-ray (EDX) analysis, X-ray diffraction (XRD), UV-Visible spectroscopy and van-der Pauw method respectively.

The $Co_{0.8}Cd_{0.2}S$ film was annealed at 673, 773, and 873 K for one hour. The surface morphology of the as-deposited $Co_{1-x}Cd_xS$ films was found to be inhomogeneous and the film became homogenous after annealing. With the increase of annealing temperature the defects and surface roughness of the film was reduced. The elemental compositions revealed the presence of Co, S and Cd in the film. The XRD analysis showed that as-deposited films were amorphous and the formation of crystalline nature of the film was started after annealing. The absorption coefficient, optical band gap, refractive index, extinction coefficient, optical conductivity and dielectric constant of the films were calculated from UV-VIS spectroscopy analysis. The optical band gap of the as-deposited $Co_{1-x}Cd_xS$ films was increased from 2.2 to 3.10 eV with increasing Cd content from x = 0.0 to 1.0. This indicated that the presence of Cd in the system greatly affected the optical band gap. The optical band gap of annealed $Co_{0.8}Cd_{0.2}S$ films also increased from 3.25 to 3.45 eV with the increase of annealing temperature. The increase of electrical conductivity with the increase of temperature indicated semiconducting behavior of the as-deposited films. Activation energy of $Co_{1-x}Cd_xS$ films increased between 0.25 to 0.50 eV with the increase of Cd in the solution.

Characterization of CoS and $Co_{1-x}Cd_xS$ Thin Films Deposited by Spray Pyrolysis Technique

by

Tamjida Rahman Luna

MASTER OF PHILOSOPHY IN PHYSICS

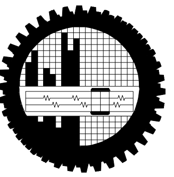

Department of Physics

BANGLADESH UNIVERSITY OF ENGINEERING & TECHNOLOGY
DHAKA-1000, BANGLADESH.
04 JUNE, 2011.

Characterization of CoS and $Co_{1-x}Cd_xS$ Thin Films Deposited by Spray Pyrolysis Technique

by

Tamjida Rahman Luna

Roll No. 100614027 F

Session: October, 2006

A Dissertation submitted to the Department of Physics, Bangladesh University of Engineering & Technology (BUET), Dhaka, Bangladesh, in partial fulfillment of the requirements for the degree of Master of Philosophy (M. Phil).

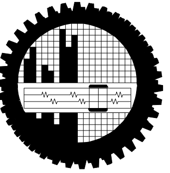

Department of Physics

BANGLADESH UNIVERSITY OF ENGINEERING & TECHNOLOGY

DHAKA-1000, BANGLADESH.

04 JUNE, 2011.

BANGLADESH UNIVERSITY OF ENGINEERING AND TECHNOLOGY
DEPARTMENT OF PHYSICS, DHAKA-1000.

Certification of Thesis

The thesis titled "**CHARACTERIZATION OF CoS AND $Co_{1-x}Cd_xS$ THIN FILMS DEPOSITED BY SPRAY PYROLYSIS TECHNIQUE"** submitted by **TAMJIDA RAHMAN LUNA**, Roll No: 100614027F, Registration No: 100614027, Session: October/2006, has been accepted satisfactory in partial fulfillment of the requirement for the degree of **Master of Philosophy (M. Phil.) in Physics** on **04 June, 2011.**

BOARD OF EXAMINERS

1. ______________________________
DR. JIBAN PODDER (Supervisor) — Chairman
Professor
Department of Physics, BUET, Dhaka

2. ______________________________
DR. A. K. M. AKTHER HOSSAIN — Member
Professor& Head (Ex-Officio)
Department of Physics, BUET, Dhaka

3. ______________________________
DR. MD. ABU HASHAN BHUIYAN — Member
Professor
Department of Physics, BUET, Dhaka

4. ______________________________
DR. DEBA PRASAD PAUL — Member (External)
Professor
Department of Physics
University of Chittagong, Chittagong.

CANDIDATE'S DECLARATION

It is hereby declared that this thesis or any part of it has not been submitted elsewhere for the award of any degree or diploma.

Signature of the candidate

____

Tamjida Rahman Luna
Roll No. 100614027 F
Session: October, 2006

Dedication

This thesis is dedicated to my family for their everlasting love and support.

CHAPTER-I

GENERAL INTRODUCTION

1.1 INTRODUCTION

Current trend of research in the physical properties of matter has progressed so much during the last ten decades that today physics is divided into a large number of groups of special branches, which are often very different from each other. In recent years thin film technology is an important special branch of research area of Physics in which the characteristics of different materials such as metals, semiconductors, and insulators are investigated in the form of thin film. This new special branch of physics has become known as “thin solid films” which has been developed very rapidly since 1940.

The word “Thin” gives a relative measurement of any dimension but not to any absolute value and “Film” means a coating of layer. Thin films are thin material layers ranging from fractions of a nanometer (monolayer) to several micrometers in thickness. Thin film is defined as a coating of layer that is so thin (<wave length) that only its surface properties are of potential importance. When a thin layer of solid material is formed on another solid substrate and if the thickness of the layer becomes comparable in magnitude with mean free path of the conduction electrons of solid material then this layer is termed as ‘Thin Film’. Thin films exhibit different structural, electrical, mechanical and magnetic properties than their corresponding bulk bodies. Successful application of thin films in various scientific, industrial and engineering purposes and the increasing demand of microelectronic components in different branches of technology have greatly expanded the sphere of thin films research [1, 2].

Systematic study of semiconducting thin films has been continued for more than half a century. Initially thin films of single semiconductor (Si, Ge, etc.) were studied. Now attention has been concentrated to study the compound semiconducting thin

films and metal doped compound semiconducting thin films because of their wide applications as optical and microelectronic coatings, selective surface coatings, antiglare and antistatic coatings for television and computer monitors. Among these, selective surface coatings are used for utilization of solar energy and thermal energy [3]. According to design and structure of the devices, these coatings may be either a single or multilayer on a suitable neutral substrate or may be a layer forming composite structure [4, 5].

In recent years, metal sulfide semiconductor thin films have received intensive attention due to their very important role on the photovoltaic technology, optoelectronic devices and solar cell fabrication [6]. Of paramount technological importance is that micro-crystallite of pure Cobalt sulfide (CoS) and Cadmium (Cd) doped Cobalt sulfide ($Co_{1-x}Cd_xS$) have high optical and mechanical properties that can be harnessed for possible application as filter materials, temperature sensors, optical waveguide, absorber coating, photodiodes etc [7]. Various technological applications mentioned above need new and alternative materials with developed properties. Our aim was to study and improve some physical characteristics of CoS films by Cd incorporation.

Recent trend of research is dedicated towards the fabrication of small-sized particle. This includes the growth of semiconductor nanocrystalline materials. Among the materials of interest are II-IV and IV-VI compound semiconductors such as pure CoS and $Co_{1-x}Cd_xS$ alloys. These groups of semiconductors show a large optical band gap when the crystallite size becomes less than the Bohr exciton radius [8, 9]. CoS is an intrinsic semiconductor and a suitable candidate for photovoltaic or photothermal applications which has an optical band gap of 1.15 eV with cubic structure [10] and CdS is hexagonal closed packed structure with band gap of 2.53eV [11]. The alloying of CoS with Cd may tune the optical band gap by reducing the grain size in nanometer range which may provide the suitability of this material for photovoltaic applications.

In thin film preparation a variety of deposition techniques have been used to grow CoS and $Co_{1-x}Cd_xS$ thin films such as, chemical bath deposition [10, 12], surfactant-

assisted method [13], implantation-assisted method [14], modified Bridgeman method [15], spray pyrolysis technique (SPD) [16]. Spray pyrolysis deposition technique can also be considered as a viable technique for production of Co doped CdS thin films due to its many advantages over the conventional methods, viz., low cost experimental set up., high spatial selectivity, precise control over maneuvering the impurity concentration and possibility to overcome the solubility limit. In addition, this technique could be used for the production of large scale area for thin film deposition without employing any high vacuum system [17]. There are very few reports available on the CoS thin films but there is no such report available on the ternary $Co_{1-x}Cd_xS$ thin films prepared by spray pyrolysis technique. From this point of view, binary CoS and ternary $Co_{1-x}Cd_xS$ alloys will be deposited on glass substrate using SPD method at a relatively low temperature 523K to reduce the preparation cost and their structural, optical and electrical properties will be studied in details.

1.2 REVIEW OF THE EARLIER WORK

Yu Zenrui et al [10] deposited cobalt sulfide (CoS) thin films on glass substrates using a modified chemical bath deposition method with cobalt dichloride ($CoCl_2$) and sodium sulfide (Na_2S) aqueous solutions. Microcrystalline features appear in the as-deposited states which grow after thermal annealing. The CoS film has an indirect optical band gap of 1.10 eV in the as-deposited state. One hour thermal annealing at 300^0 C decreases the band gap to 1.02 eV. At 300^0 C, the conductivity (initial value of 5.08 X 10^{-8} ohm-cm^{-1}) is increased by a factor of 2700, which is probably originated from the growth of the grain size and crystal volume fraction and the conductivity activation energy is decreased from 0.66 to 0.48 eV. Further annealing at 450^0 C decreases the conductivity. Surface oxidization is one of the reasons for the reduction of conductivity.

Mishack et al 2010 [11] investigated ternary CdCoS thin film has been deposited on microscopic glass substrate using the chemical bath deposition method. The optical

property of the film was characterized using the UNICO UV-2102 PC spectrophotometer in the UV-VIS-NIR region. The optical and dielectric properties of the film show that it has high transmittance in the VIS-NIR range (>50%) which moderate at the UV range (<50%) with low reflectance (3.52 – 20.57%) that declined albeit exponentially within the entire wavelength range. The observed band gap energy of the deposited films for 14h and 17h are 2.1eV and 2.53eV respectively.

F. I. Ezema and R. U. Osuji [12] investigated the optical characterization of cobalt doped cadmium sulfide ($CdCoS_2$) thin film deposited on glass slide from aqueous solutions of $CoCl_2.6H_2O$, $CdCl_2.2^{1/2}H_2O$ and thiourea in which ammonium solution and TEA were employed as complexing agents using chemical bath deposition technique. The optical properties of $CdCoS_2$ thin film were obtained in UV-VIS-NIR regions by means of PYE UNICAM SP8-100 double beam spectrophotometer. They investigated the absorbance, transmittance, reflectance spectra, band gap, refractive index, extinction coefficient, real and imaginary dielectric constant and optical conductivity of the $CdCoS_2$ thin film. The FTIR spectroscopy of the films showed the percentage transmittance that ranged between 7 and 46% in the far infrared regions. The films were found to have average transmittance of greater than 50% in the VIS-NIR regions and exhibits high reflectance of greater than 12% in the same regions. The film exhibits poor transmittance in the UV regions. $CdCoS_2$ thin films with thickness of 0.461μm and the found energy band gap ranged between 2.50 and 2.70eV which indicated that the deposited films were rich in cadmium.

R. Sathyamoorthy et al [13] deposited the $Cd_{1-x}Co_xS$ nanocluster alloys for different doping concentrations (x = 0.10, 0.20, 0.30) using surfactant-assisted synthesis technique. The lattice parameters of CdS nanoclusters were altered with respect to Co doping concentrations and it exhibits hexagonal-greenockite structure. Grain size of the CdS increased with increase in Co doping concentration. The value of the optical band gap energy for different Co concentrations in $Cd_{1-x}Co_xS$ nanoclusters obtained from the diffused reflectance spectra at RT varied from 2.56 to 2.70 eV was observed. In the present work Co-doped CdS samples with x=0.3 could

result in better ferromagnetic behavior than the lower doping concentrations (x=0.1 and 0.2).

S. Chandramohan et al [14] studied structural, optical, vibrational and morphological properties of Co doped CdS thin films from 0.34 to 10.8 at % by ion implantation technique at room temperature (RT). With increasing Co concentration a decrease in the optical band gap, from 2.39 to 2.26 eV, observed in this work. This reduction addressed on the basis of band tailing due to the creation of localized energy states in association with Urbach energy calculations. It is founded that implantation caused stain in the CdS lattice which was inhomogeneous at higher fluences due to size and shape fluctuations of individual CdS grains. Implantation increased surface roughness also.

E. Bacaksiz et al [16] investigated structural, optical and magnetic properties of CdS thin films with the addition of Co prepared by (i) Spray Pyrolysis deposition (SPD) technique of $Cd_{1-x}Co_xS$ ($x \leq 0.10$) thin films (type1) and (ii) Co diffusion doped CdS films (type2). The undoped film has a hexagonal structure with a strong (112) preferred orientation. As the Co concentration in CdS increased, the preferred orientation changed from (112) to (002) direction. X-ray photoelectron spectroscopy (XPS) analysis showed that Co atoms on the surface of films were found to be bounded either to S atoms or O atoms. The transmittance spectra indicated the four characteristic absorption maxima at the wavelengths of 680, 685, 729 and 744 nm, which were not observed for the undoped CdS film. Observed band gap energy E_g of the film decreased from 2.43 to 2.37 eV with increasing Co content from x=0 to 0.10. The Co doped $Cd_{1-x}Co_xS$ films grown by SPD (Type 1) did not show any sign of ferromagnetic behavior. However, the Co diffused CdS films (Type2) showed clear ferromagnetic loops.

P. Raji et al [18] studied the thermal and structural properties of cadmium sulfide (CdS) thin films grown by spray pyrolysis measured using photo acoustic technique. From XRD, the films are found to be in the single phase of CdS with hexagonal structure and the identification of the peaks indicates that the film is polycrystalline.

In this report the absorbance spectrum shows a sharp increase in absorption at wavelength near to the absorption edge of the threshold wavelength for onset of absorption. The absorption coefficient (α) of CdS film is $5x10^4$ cm^{-1} and the direct band gap of CdS film is found to be 2.41 eV. The dependence of thermal diffusivity on the thickness of the layer or the size of the particles on the glass substrate is analyzed in this work. As the spray time increases, thermal conductivity decreases i.e. when thickness of the film is increased, more layers are deposited but the thermal diffusion length can not be altered and so further thermal diffusion is not possible, after this thermal diffusion length. Thermal diffusivity and thermal conductivity of the CdS film decreases when the temperature is increased consequently the mean free path decreases. It is found that the thermal diffusivity of CdS thin films decrease at least by two orders compared to the bulk.

E. I. Ugwu and D. U. Onah [19] used the solution grown technique for growing CdS thin film. The effect of the solid state properties on spectral absorbance, transmission and reflectance were obtained using a PYEUNICAM® SP 8-100 spectrophotometer in the range of UV-VIS-NIR regions in this report. The film showed the visible transmitting behavior. The absorbance at the near infrared domain is low with high transmittance (70%) at the same region. In the same region the percentage reflectance were found to be 14%. They found an indirect band gap of CdS films ranged from 1.80-2.0 eV and the band gap for visible transmitting film ranged 1.5 - 3.0 eV. The other optical properties of the films such as refractive index (n), extinction coefficient (k), dielectric constant (ϵ) and optical conductivity (σ) were also measured in this study.

1.3.1 PHYSICAL PROPERTIES OF CoS

CoS is an intrinsic semiconductor of II-IV group and a suitable candidate of metal sulfide thin films. In recent years, metal sulfide semiconductor thin films have received intensive attention due to their very important role on the technology and

the different branches of applied science. Some of the standard values relating to the physical properties of CoS are mentioned below:

- Synonyms and molecular formula : Cobalt (II) sulfide, Cobalt sulfide, CoS
- Molar mass : 90.999 gm/mol
- Color : Black
- Appearance: Powder
- Specific gravity : 1.7
- Density : 5.45 gm/cm^3
- Melting point : 1182 ^{0}c
- Crystal structure : Cubic
- Lattice parameter : a
- Solubility in water : Negligible
- Direct Band gap : 1.15 eV
- Semiconductor type : n-type

The crystal structure of cobalt sulfide (CoS) is shown in Fig. 1.1.

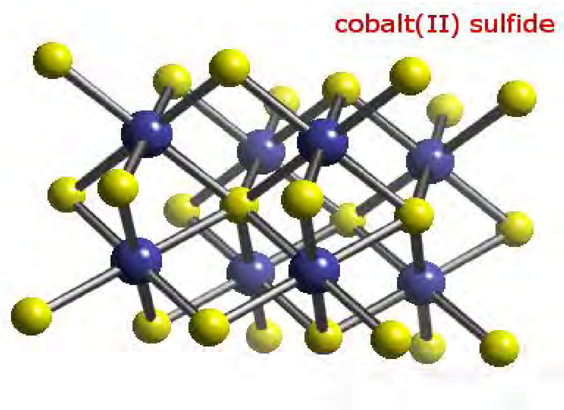

Fig. 1.1 Crystal structure of CoS.

Figure shows a ball model illustration of a nearly perfect (ideal) CoS surface based on the ionic radii of the ions. The blue color balls represent Co^{2+} cations, while the yellow color balls represent S^{2-} anions.

1.3.2 PHYSICAL PROPERTIES OF CdS

CdS is an important member of IV-VI semiconductor group which has various applications in modern science. Some of the standard values relating to the physical properties of CdS are mentioned below:

- Synonyms and formula: Cadmium (II) Sulfide: Cadmium Sulfide, CdS
- Molar mass: 144.477 gm/mol
- Color: Yellow
- Appearance : Crystalline solid
- Density: 4.83 gm/cm^3
- Melting point: 1750 ^{0}C
- Crystal Structure: Hexagonal wurtzite or cubic
- Lattice constant : a = 4.160 Å and c = 6.756 Å
- Solubility in water : Negligible
- Direct band gap energy: 2.42 eV
- Semiconductor type: n-type

The crystal structure of cadmium sulfide (CdS) is shown in Fig. 1.2.

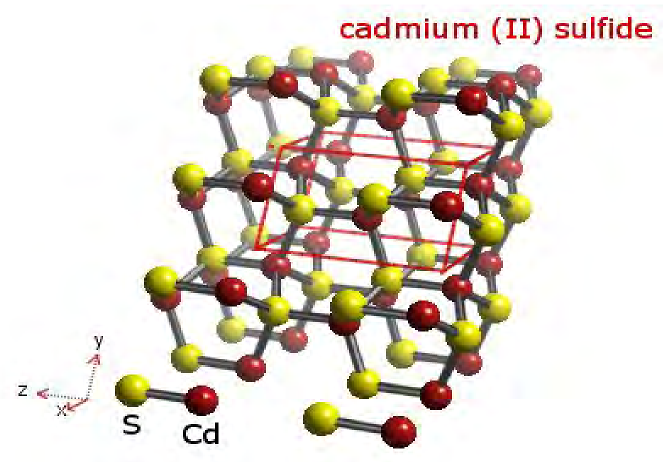

Fig. 1.2 Crystal structure of CdS

Figure shows a ball model illustration of a nearly perfect (ideal) CdS surface based on the ionic radii of the ions. The red color balls represent Cd^{2+} cations, while the yellow color balls represent S^{2-} anions.

1.4 CHARACTERISTICS OF THIN FILMS

Thin films can be characterized in many different ways such as: structural, electrical and optical properties, etc. The properties of thin film change appreciably when it is cooled to a very low temperature or heated to a higher temperature (above room temperature). The study of the changes in the properties of thin film with temperature provides a great deal of information about the properties of thin films.

On the other hand, a number of factors that affects the physical properties of thin films, such as:

The nature of substrate:

It may be non-crystalline solids e.g. glass of vitreous silica or crystalline material such as cleavage plates of rock-salt or mica. Films characteristics may be different for each type of substrate. It is also necessary to consider the melting point of the substrate material. It should be comparable with that of the film materials.

Deposition conditions:

The properties of thin films strongly depend on the deposition conditions, such as source to substrate height, source temperature, deposition angle, ambient chamber pressure, substrate temperature, etc.

Substrate temperature during deposition:

The temperature of substrate during deposition of film may affect the film properties. At low temperature poly- crystalline films with high densities of structural imperfections are formed on both vitreous and crystalline substrates, but

at high temperature oriented single-crystal films are formed on crystalline substrates.

The annealing temperature:

The as-deposited films seem to be associated with the formation of highly unstable phases along with innumerable defects and imperfections, i.e., vacancies, interstitials, impurities, grain boundaries, dislocations. On annealing (keeping the film for one hour at a constant high temperature), some of these defects will diffuse out with time and the crystallites or grains tend to assume a minimum potential energy configuration. This leads to the stabilization of the film. The relative value of the minimum annealing temperature i.e. heating the film to a higher temperature and cooling it back to the room temperature (RT) after deposition.

Annealing cycle:

Annealing cycle, however, also plays an important role for the surface mobility of the atoms at the temperature of the substrate after deposition.

Pressure and nature of residual gas in deposition chamber:

If the deposition chamber is not evacuated the evaporated atoms cannot reach the surface of the substrate. They interact with the gas molecules within the chamber and scattered inside the chamber. So, sufficient low pressure is necessary for deposition of the thin film on the substrate.

Temperature of evaporation source:

If the temperature of the evaporation source is increased uniformly, then the film is likely to be uniform; otherwise it may not be uniform due to sudden increase in temperature.

Deposition rate and film thickness:

The temperature at which epitaxy occurs is dependent on the deposition rate. Film thickness mainly depends on deposition rate and deposition time. If the deposition rate increases, the film thickness also increases having the same deposition time.

1.5 APPLICATIONS OF THIN FILM

Thin films are widely used in today's technology and their applications are expected to be even more widespread in future. It is not possible to give an exhaustive survey over thin film applications, but a listing may, nevertheless, be of some interest. The application areas for thin films are:

Optical Functional:

- Mirrors
- Architectural glazing
- Automotive windows
- Spacecraft temperature control
- Solar absorbing coatings
- Anti- reflection layers on optical components
- Coatings for laser optics
- Display devices (CD)

Electrically Functional:

- Conductors, Insulators (resistors, capacitors)
- Semiconductor, Super-conductors devices
- Contacts
- Micro electronic devices
- Solar cells

Magnetically functional:

- Computer memories, Computer logic elements
- Radio-frequency and microwave
- Miscellaneous applications

Mechanically functional:

- Adhesion, lubrication, micromechanics
- Hard coatings for cutting tolls

- Tribiological (wear and erosion resistant) coating

Chemically functional:

- Barriers to diffusion or alloying
- Catalytic coatings
- Batteries
- Protection against oxidation or corrosion
- Gas/liquid sensors

Decorative:

- Watch bezels and bands
- Eyeglass frames
- Costume jewelry

Thermal:

- Barrier layers
- Heat sink

1.6 AIM OF THE PRESENT WORK

Thin film technique and research are strongly related to the activities of the basic research in nanotechnology. In recent years there has been increasing interest in the size-dependent electrical and optical properties of semiconductors [20, 21]. In nanocrystallites, the electrons confined in a narrow potential that well exhibit extraordinary characteristics in the optical and electrical properties. When the width of such confining potential is very small i.e. of the order of few hundred angstroms, quantum size effect arises. During the last few years, the research on the growth of nanoparticle CoS and $Co_{1-x}Cd_xS$ thin films have increased, for its technological applications in optoelectronic devices, photodetectors, solar energy absorber, solar cell fabrication, temperature sensors, optical waveguides, filter materials, etc [7, 22-24].

The spray pyrolysis deposition (SPD) method is suitable for scientific studies and for many applications in technology and industry. Particularly SPD is attractive coating deposition technique because the process equipment is very simple, fast, inexpensive, vacuum less and suitable for mass production.

From the practical and technological point of interest, the main objective of this research is to synthesize binary CoS and ternary $Co_{1-x}Cd_xS$ thin films in different doping concentrations by spray pyrolysis deposition system to reduce the preparation cost. The alloying of CoS with Cd may tune the optical band gap by reducing the grain size in nanometer range which may provide the suitability of this material for the applications mentioned above. The optimum condition for growing a good quality and homogeneous deposition of CoS and $Co_{1-x}Cd_xS$ thin films can be achieved by detailed investigations of structural, optical and electrical properties in detailed. Based on these research challenges, the objectives of this work are as follows:

(a) Surface morphology of the deposited films is to be studied by scanning electron microscopy (SEM).

(b) The elemental compositions are to be estimated by energy dispersive X-ray (EDX) analysis.

(c) The structural properties of the deposited films are to be analyzed by X-ray diffraction (XRD).

(d) The thickness of the films is to be measured by Fizeau fringe interferometer method.

(e) The optical constants e. g. optical band gap (E_g), extinction coefficient (k), refractive index (n), dielectric constants (ϵ), dielectric loss, optical conductivity (σ) etc. are to be determined by Ultra-violet Visible (UV-VIS) spectrophotometer in the wavelength range 300 nm ~ 1100 nm.

(f) The annealing effect on optical constants e. g absorption coefficient, optical band gap, refractive index, dielectric constants, dielectric loss, optical

conductivity etc. are to be determined by UV-visible spectroscopy in the wavelength range 300 nm ~ 1100 nm.

(g) Electrical conductivity measurement is to be carried out by van-der Pauw method.

CHAPTR-II

THIN FILM DEPOSITION TECHNIQUES AND PROCESSES

2.1 DEPOSITION TECHNIQUES

Thin films are defined as coatings of a thickness from about 5 Angstroms (Å) to a few micrometers (µm) [25, 26]. Several materials may be deposited as thin films on passive substrates such as glass or ceramic or on active substrates such as silicon. The act of applying a thin film to a surface is known as thin-film deposition. Thin film deposition is a technique for depositing a thin film of material onto a substrate or onto previously deposited layers. "Thin" is a relative term, but most deposition techniques allow layer thickness to be controlled within a few tens of nanometers, and some (molecular beam Epitaxy) allow single layers of atoms to be deposited at a time.

It is useful in the manufacture of optics (for reflective or anti-reflective coatings, for instance), electronics (layers of insulators, semiconductors, and conductors form integrated circuits), packaging (i.e., aluminum-coated PET film) and in contemporary art. Similar processes are sometimes used where thickness is not important: for instance, the purification of copper by electroplating and the deposition of silicon and enriched uranium by a CVD-like process after gas-phase processing.

Deposition techniques fall into two broad categories:

i) Chemical Techniques
ii) Physical Techniques

(i) Chemical Techniques

These processes exploit the creation of solid materials directly from chemical reactions in gas and/or liquid compositions or with the substrate material. The solid material is usually not the only product formed by the reaction. Byproducts can include gases, liquids and even other solids. Thin films from chemical deposition techniques tend to be conformal, rather than directional.
Depositions that happen because of a chemical reaction:

- Chemical Vapor Deposition (CVD)
- Electrodeposition
- Epitaxy
- Thermal oxidation

(ii) Physical Techniques

Physical deposition uses mechanical or thermodynamic means to produce a thin film of solid. Common for all these processes are that the material deposited is physically moved on to the substrate. In other words, there is no chemical reaction which forms the material on the substrate. This is not completely correct for casting processes, though it is more convenient to think of them that way. This is by no means an exhaustive list since technologies evolve continuously.

Depositions that happen because of a physical reaction:

- Physical Vapor Deposition (PVD)
- Casting

The classification of the different deposition processes is illustrated in the Fig 2.1:

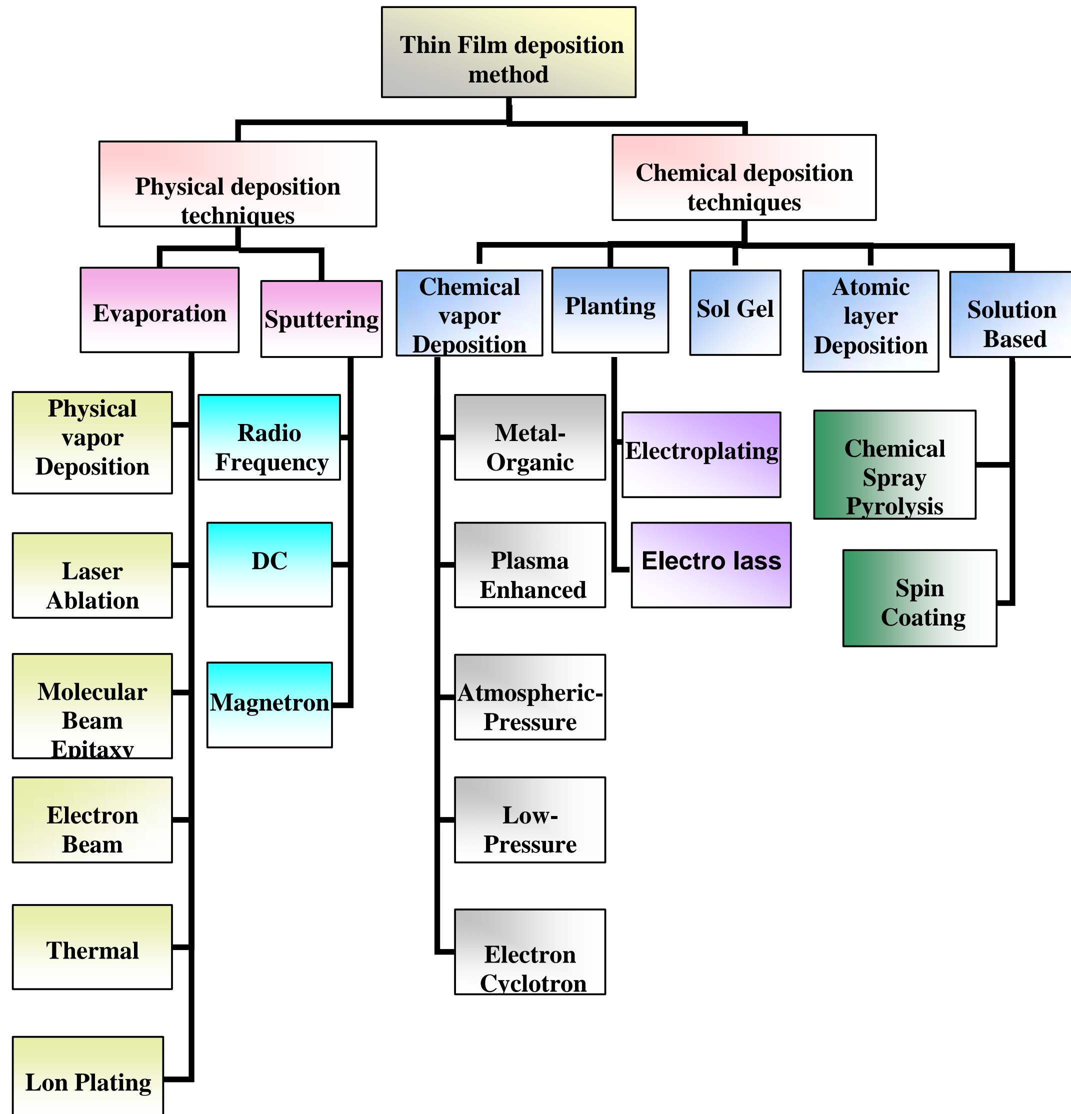

Fig. 2.1. Classification of most common deposition process.

Some of the commonly used methods for depositing large area thin film on a variety of commercially available substrates are described below:

2.1.1 CHEMICAL VAPOR DEPOSITION (CVD)

Chemical vapor deposition (CVD) is a generic name for a group of processes that involve depositing a solid material from a gaseous phase. Precursor gases (often

diluted in carrier gases) are delivered into the reaction chamber at approximately ambient temperatures. As they pass over or come into contact with a heated substrate, they react or decompose forming a solid phase and which are deposited onto the substrate. The substrate temperature is critical and can influence what reactions will take place.

Chemical Vapor Deposition (CVD)

Fig. 2.2. Chemical Vapor Deposition (CVD) Process.

Chemical Vapor Deposition is chemical reactions which transform gaseous molecules **,** called precursor, into a solid material **,** in the form of thin film or powder, on the surface of a substrate **.**

CVD covers processes such as:

1. Atmospheric Pressure Chemical Vapor Deposition (APCVD)

2. Metal-Organic Chemical Vapor Deposition (MOCVD)

3. Plasma Enhanced Chemical Vapor Deposition (PECVD)

4. Photochemical Vapor Deposition (PCVD)

CVD coatings are usually only a few microns thick and are generally deposited at fairly slow rates, usually of the order of a few hundred microns per hour. CVD is an extremely versatile process that can be used to process almost any metallic or ceramic compound. Some of these include: Elements, Metals and alloys, Nitrides Carbides, Borides, Oxides, Intermetallic compounds.

2.1.2. ELECTRODEPOSITION

This process is also known as "electroplating" and is typically restricted to electrically conductive materials. There are basically two technologies for plating: Electroplating and Electroless plating. In the electroplating process the substrate is placed in a liquid solution (electrolyte). When an electrical potential is applied between a conducting area on the substrate and a counter electrode (usually platinum) in the liquid, a chemical redox process takes place resulting in the formation of a layer of material on the substrate and usually some gas generation at the counter electrode.

In the electroless plating process a more complex chemical solution is used, in which deposition happens spontaneously on any surface which forms a sufficiently high electrochemical potential with the solution. This process is desirable since it does not require any external electrical potential and contact to the substrate during processing. Unfortunately, it is also more difficult to control with regards to film thickness and uniformity. A schematic diagram of a typical setup for electroplating is shown in the Fig. 2.3.

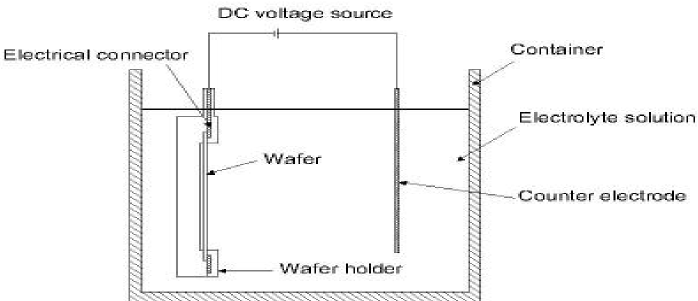

Fig. 2.3. Typical setup for electrodeposition process.

The electrodeposition process is well suited to make films of metals such as copper, gold and nickel. The films can be made in any thickness from ~1μm to 100 μm. The deposition is best controlled when used with an external electrical potential, however, it requires electrical contact to the substrate when immersed in the liquid bath. In any process, the surface of the substrate must have an electrically conducting coating before the deposition can be done.

2.1.3 THERMAL OXIDATION

This is one of the most basic deposition technologies. It is simply oxidation of the substrate surface in an oxygen rich atmosphere. The temperature is raised to 800 - 1100° C to speed up the process. This is also the only deposition technology which actually consumes some of the substrate as it proceeds. The growth of the film is spurned by diffusion of oxygen into the substrate, which means the film growth is actually downwards into the substrate. As the thickness of the oxidized layer increases, the diffusion of oxygen to the substrate becomes more difficult leading to a parabolic relationship between film thickness and oxidation time for films thicker than ~100nm. This process is naturally limited to materials that can be oxidized, and it can only form films that are oxides of that material. This is the classical process used to form silicon dioxide on a silicon substrate. A schematic diagram of a typical wafer oxidation furnace is shown in the Fig. 2.4.

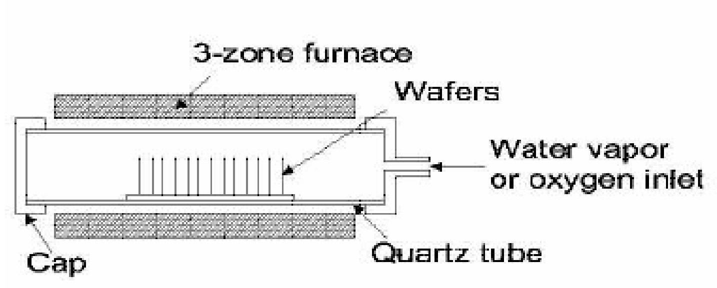

Fig. 2.4. Typical wafer oxidation furnace.

2.1.4 EPITAXY

This technology is quite similar to what happens in CVD processes, however, if the substrate is an ordered semiconductor crystal (i.e. silicon, gallium arsenide), it is possible with this process to continue building on the substrate with the same crystallographic orientation with the substrate acting as a seed for the deposition. If an amorphous/polycrystalline substrate surface is used, the film will also be amorphous or polycrystalline.

There are several technologies for creating the conditions inside a reactor needed to support epitaxial growth, of which the most important is Vapor Phase Epitaxy (VPE). In this process, a number of gases are introduced in an induction heated reactor where only the substrate is heated. The temperature of the substrate typically must be at least 50 % of the melting point of the material to be deposited.

An advantage of Epitaxy is the high growth rate of material, which allows the formation of films with considerable thickness (>100μm). Epitaxy is a widely used technology for producing silicon on insulator (SOI) substrates.

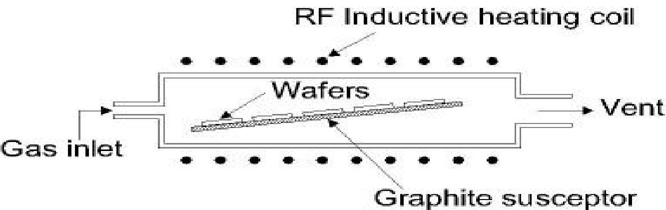

Fig. 2.5 Typical cold-wall vapor phase epitaxial reactor.

The process can be used to form films of silicon with thicknesses of ~1μm to >100μm. Some processes require high temperature exposure of the substrate, whereas others do not require significant heating of the substrate. Some processes can even be used to perform selective deposition, depending on the surface of the substrate.

2.1.5 EVAPORATION

In evaporation the substrate is placed inside a vacuum chamber, in which a block (source) of the material to be deposited is also located. The source material is then heated to the point where it starts to boil and evaporate. The vacuum is required to allow the molecules to evaporate freely in the chamber, and they subsequently condense on all surfaces. This principle is the same for all evaporation technologies, only the method used to the heat (evaporate) the source material differs. There are two popular evaporation technologies, which are e-beam evaporation and resistive evaporation each referring to the heating method. In e-beam evaporation, an electron beam is aimed at the source material causing local heating and evaporation. In resistive evaporation, a tungsten boat, containing the source material, is heated electrically with a high current to make the material evaporate. Many materials are restrictive in terms of what evaporation method can be used (i.e. aluminum is quite difficult to evaporate using resistive heating), which typically relates to the phase transition properties of that material. A schematic diagram of a typical system for e-beam evaporation is shown in the Fig. 2.6.

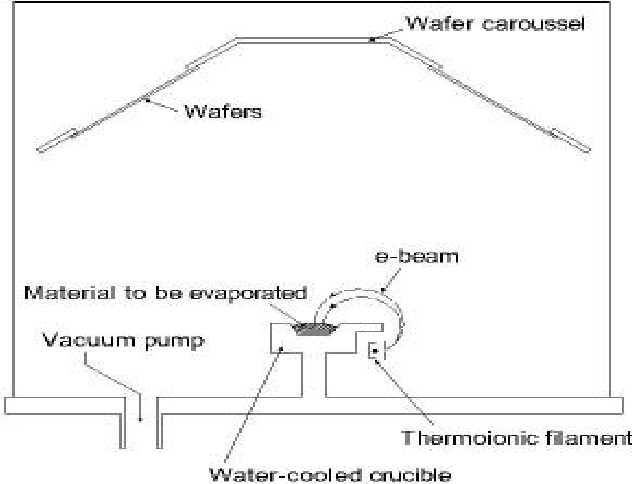

Fig. 2.6. Typical system for e-beam evaporation process.

2.1.6 SPUTTERING

Sputtering is a method used to deposit both thin metal films and insulators onto a substrate. Unlike evaporation, the material to be sputtered does not have to be heated. During sputtering an atom or molecule is knocked out of a target material by accelerated ions which are produced from excited plasma. The atom or molecule is then condensed on a substrate either in its original or in a modified form [27]. Prior to the sputtering procedure a vacuum of less than one ten millionth of an atmosphere must be achieved. From this point a closely controlled flow of an inert gas such as argon is introduced. Specifically, a sputtering system consists of an evacuated chamber, a target (cathode) and a substrate table (anode). It is a process in which the chemically inert atoms, e.g. argon (Ar) as mentioned above, are ionized in a glow discharge which is called plasma [28]. The ions are accelerated into a target by the electric field at the boundary of the plasma. Atoms from the target are knocked out and these atoms are allowed to reach the substrate.

If the plasma ions are accelerated by a DC field then the sputtering technique is called DC [29]. If an RF field is used then the technique is called RF sputtering and Magnetron if magnets with alternating polarity are arranged behind or sometimes at the sides of the target to enable lower pressures to be used and thus a cleaner film to be created [30-33]. In particular, during sputtering secondary electrons can be captured close to the target from a magnetic field. The electrons follow helical paths around the magnetic field lines and undergo more ionizing collisions with neutral gaseous near the target than they would without the magnetic field. Therefore, a higher sputter rate is achieved trough this enhancement of the ionization. Additionally, with this method the plasma can be sustained at a lower pressure. The magnetic trap does not affect the sputtered atoms since they are neutrally charged.

Sputtering is a procedure that takes place in a low pressure gas environment and is less directional than electron beam evaporation and can typically achieve much higher deposition rates. It can be used with metallic targets but also dielectric films such as silicon dioxide (SiO_2) can be sputtered even though usually chemical vapor

deposition methods. Yet, some specialty materials such as piezoelectric zinc oxide and aluminum nitride films are well suited to sputtering [28].

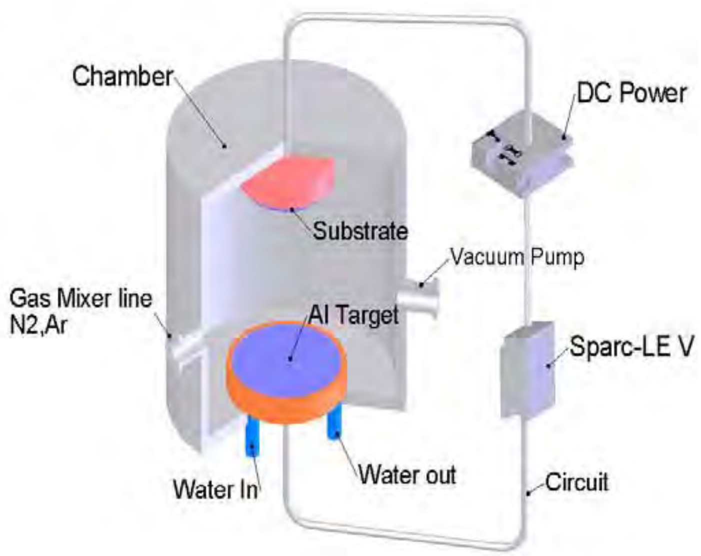

Fig. 2.7. Schematic drawing of the magnetron sputtering system**.**

2.1.7 PHYSICAL VAPOR DEPOSITION (PVD)

Physical vapor deposition (PVD) is a method to deposit thin films by the condensation of a vaporized material onto various surfaces (e.g., onto semiconductor wafers). The coating method involves purely physical processes such as high temperature vacuum evaporation rather than involving a chemical reaction at the surface to be coated as in chemical vapor deposition. One of the main industrial fields where PVD is extensively used is the fabrication of semiconductor devices. PVD covers a number of deposition technologies in which material is released from a source and transferred to the substrate.

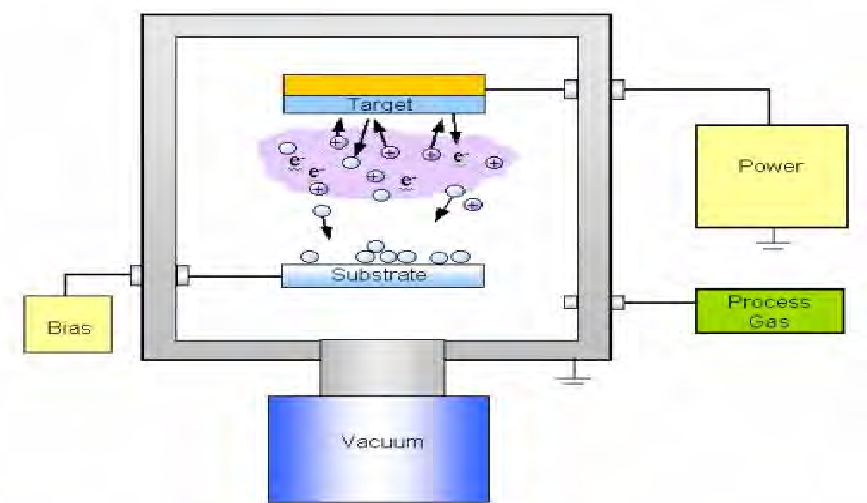

Fig. 2.8. Physical vapor deposition process.

PVD comprises the standard technologies for deposition of metals. It is far more common than CVD for metals since it can be performed at lower process risk and cheaper in regards to materials cost. The quality of the films is inferior to CVD, which for metals means higher resistivity and for insulators more defects and traps. The step coverage is also not as good as CVD. Evaporation/sputtering of a target material onto a substrate:

- Evaporation of a solid
- Transport of the gaseous species to the substrate
- Condensing gaseous species on the substrate, followed by nucleation and growth.

2.1.8 CASTING

In this process the material to be deposited is dissolved in liquid form in a solvent. The material can be applied to the substrate by spraying or spinning. Once the solvent is evaporated, a thin film of the material remains on the substrate. This is particularly useful for polymer materials, which may be easily dissolved in organic solvents, and it is the common method used to apply photoresist to substrates (in photolithography). The thicknesses that can be cast on a substrate range all the way

from a single monolayer of molecules (adhesion promotion) to tens of micrometers. In recent years, the casting technology has also been applied to form films of glass materials on substrates. The spin casting process is illustrated in the Fig. 2.9.

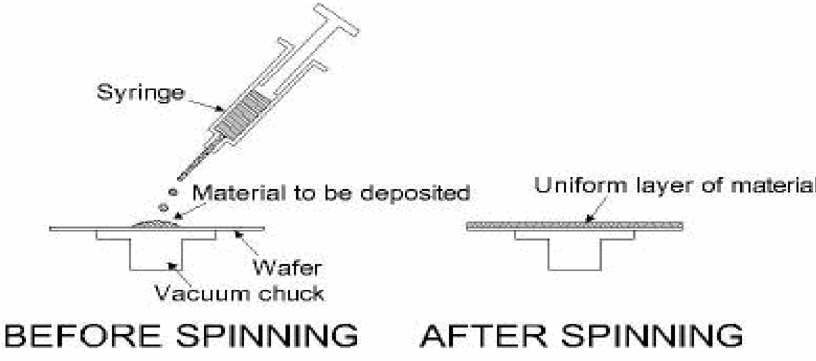

Fig. 2.9. The spin casting process as used for photoresist in photolithography.

2.1.9 SOL-GEL

Sol-gel method is a wet chemical route for the synthesis of colloidal dispersions of oxides which can be altered to powders, fibers, thin films and monoliths as shown in Figure 2.10. In general, sol-gel method consists of hydrolysis and condensation reactions. Sol-gel coating is a process of preparation of single or multicomponent oxide coating which may be glass, glass ceramic or crystalline ceramic depending on the process. Also, the nanomaterials used in modern ceramic and device technology require high purity and facilitate to control over composition and structure. The solgel coating is one of the interesting methods because it has many advantages. Examples are as the followings-

1. The chemical reactants for sol-gel process can be conveniently purified by distillation and crystallization.
2. All starting materials are mixed at the molecular level in the solution so that a high degree of homogeneity of films can be expected.

3. The trace elements in the form of organometallic compounds or soluble organic or inorganic salts can be added to adjust the microstructure or to improve the structural, optical and electrical properties of oxide films.
4. Large-area films of desired composition and thickness can be easily formed on a complex geometry substrate.
5. It facilitates to form films of complex oxides and eases to control of composition and microstructure of the deposited films. The solgel coating is almost exclusively applied for fabrication of transparent layers with a high degree of planarity and surface quality.[34]

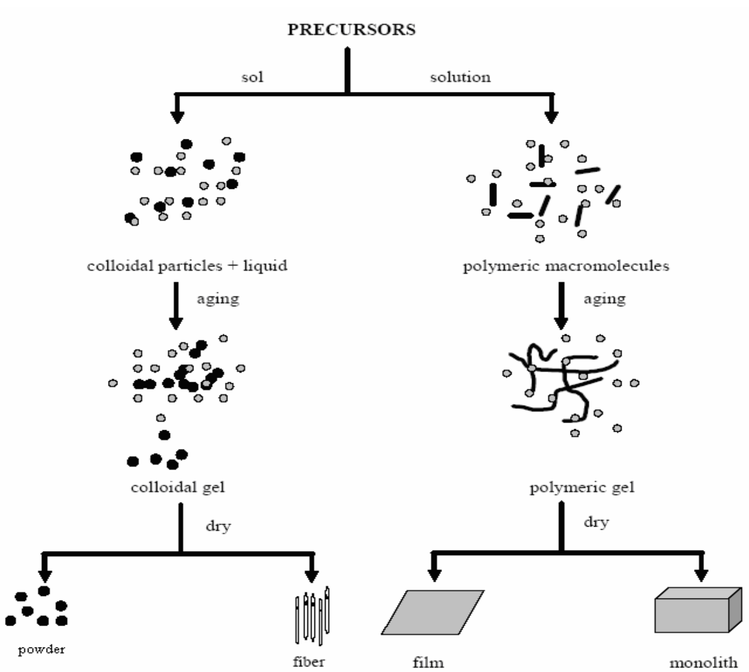

Fig. 2.10. Generalized scheme of sol-gel synthesis.

2.1.10 MOLECULAR BEAM EPITAXY (MBE)

Molecular beam epitaxy (MBE) is a technique for epitaxial growth via the interaction of one or several molecular or atomic beams that occurs on a surface of a heated crystalline substrate. Angular distribution of atoms or molecules in a beam is provided by placing the solid sources of materials in evaporation cells. The substrate is heated to the necessary of temperature and, when required, continuously rotated in

order to improve the growth homogeneity. During the MBE technique the atoms are arranged in a single-crystal manner upon a crystalline substrate which acts as a seed crystal. Thus the lattice of the grown film is the same as that of the substrate. In MBE the heated, e.g. between 400 - 800° C, single-crystal is placed in an ultrahigh vacuum, e.g. 133 x 10^{-11} Pa, together with atomic streams from heated cells that contain the materials of interest. The most important aspect of MBE is the slow deposition rate (typically less than 1000 nm per hour), which allows the films to grow epitaxial. The slow deposition rates require proportionally better vacuum to achieve the same impurity levels as other deposition techniques evaporation of elemental sources independently at a controlled rate. Molecular beams intercept at the substrate surface UHV conditions (10-10 bar), low growth rates, line-of-sight, high purity, complex layer structures, good control of doping. [35]

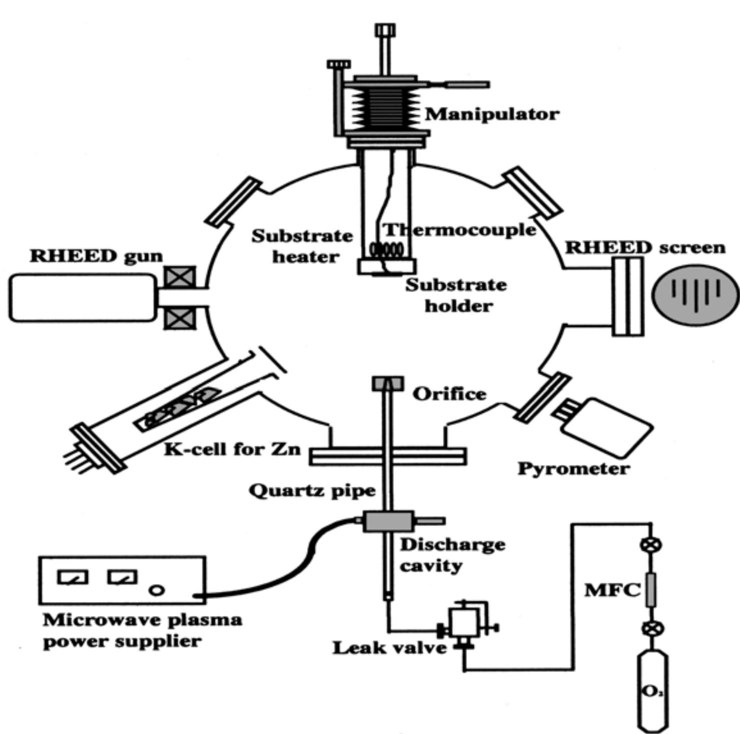

Fig. 2.11. Schematic of the Molecular beam epitaxy system.

2.1.11 SPRAY PYROLYSIS METHOD

Spray pyrolysis is a convenient, low-cost, very simple and rapid method for the deposition of thin films, and is suitable for industrial applications and has been used for about 30 years for the manufacture of conductive glass. It is also an excellent method for preparing films of semiconductor alloys and complex compounds. This technique involves spraying of an ionic solution, usually aqueous containing soluble salts of the constituent atoms of the desired compound onto heated substrates. Hydrolysis and pyrolysis are the main chemical reactions involved in the process. In this technique, the chemicals are sprayed onto the heated surface of the glass substrate and the film is grown by heat mechanism. In principle spray pyrolysis technique is very simple and is suitable for industrial applications. The apparatus needed to carry out the chemical spray process consists of an optimizer the spray solution and a substrate heater. In this experiment a modified spray pyrolysis technique has been used and this will be discussed in details in Chapter 4. [36]

2.2 FORMATION STAGES OF THIN FILM

There are three mechanisms of thin film condensation can be distinguished, depending on the strength of interaction between the atoms of the growing film and between the atoms of the film and substrate: These are (a) The layer by layer growth (Vander Mcrwe mechanism); (b) A three-dimensional nucleation, forming, growth and coalescence of islands (Volmer Weber mechanism); (c) Absorption of a monolayer and subsequent nucleation on the top of this layer (Stranski-Krastanov mechanism). In most cases mechanism (b) takes place and a brief description of it is given below.

2.2.1 CONDENSATION

Condensation simply means the transformation of a gas into a liquid or solid. The condensation of vapor atom is determined by its interaction with the impinged surface in the following manner. The impinging atom is attracted to the surface by

the instantaneous dipole and quadruple moments of the surface atoms. As a result, the atoms lose its velocity component normal to the surface in a short time, provided the incident kinetic energy is not too high [37]. The vapor atom is then physically absorbed (called “adatom”), but it may or may not be completely thermally equilibrated. It may move over the surface by jumping from one potential well to the other, because of thermal activation from the surface and /or its own kinetic energy parallel to the surface. The adatom has a finite stay or residence time on the surface during which it may interact with other adatoms to form a stable cluster and be chemically absorbed with the release of the heat of condensation. If not absorbed, the adatom reevaporates or desorbs into the vapor phase. Therefore, the condensation is the net result of equilibrium between the absorption and de absorption processes.

The probability that an impinging atom will be incorporated into the substrate is called the “condensation” or “sticking coefficient”. It is measured by the ratio of the amount of material condensed on a surface to the total amount impinged. In fact, often the sticking coefficient is so small that observation is not observable by ordinary techniques. On the other hand, the sticking coefficient is found to be strongly dependent on the total time during which the substrate was subject to impingement, and also on the substrate temperature. A non unity sticking coefficient is usually explained in terms of monomers re-evaporation from the areas on the substrate which are outside the capture zones around each stable nucleus.

Langmuir and **Frenkel** [38] formulated condensation model (This model considers vapor→ solid transformation. At high deposition temperatures, a vapor→ liquid (amorphous)→ solid condensation mode may occur. **Semenoff** [39] suggested that heterogeneous nucleation always proceeds by formation of an amorphous film followed by nucleation of crystallites within the amorphous film in which the absorbed atoms move over the surface during their lifetimes to form pairs which in turn acts as condensation centers for other atoms.

2.2.2 NUCLEATION

Nucleation is the birth stage of film. Consideration is initiated by the formation of small cluster through the combination of several adsorbed atoms. These clusters are called nuclei and the process of cluster formation is called nucleation.

There are two types of nucleation that occur during the formation of film: homogeneous and heterogeneous nucleation. A homogeneous nucleation theory which takes into account the total free energy of formation of a cluster of adatoms was postulated by **Volmer** and **Weber** [40], and **Becker** and **Doring** [41]. It was later extended to heterogeneous nucleation by **Volmer** [42] and to the particular shapes of clusters in a thin film case by **Pound et al** [43]. In this theory, clusters are formed by collisions of atoms on the substrate surface, and in the vapor phase if super saturation is sufficiently high. They develop initially with an increase in free energy until a critical size is reached, above which growth continues with a decrease in free energy. In atomistic theory, at low substrate temperature or very high super saturations, the critical nucleus may be single atom, which will form a pair with another atom by random occurrence to become a stable cluster and grow spontaneously.

2.2.3 GROWTH

Growth is the final and completion stage of thin film formation. The process of enlargement of the nuclei to finally form a coherent is termed as growth. The growth sequence of a film was originally deduced by **Andrade** [44] from the observed optical transmission behavior of Ag films. This deduction is in remarkable agreement with the electron-microscopic observations first made by **Uyeda** [45] and later in detailed by **Levinstein** [46]. The clusters become larger and ultimately continuous film is produced. **Pashley et al**. [47], distinguished four stages of the growth process based on the electron microscopic observations are:

- The island stage
- The coalescence stage

- The channel stage
- The continuous film stage

The stages of film formation are shown in Fig.2.12.

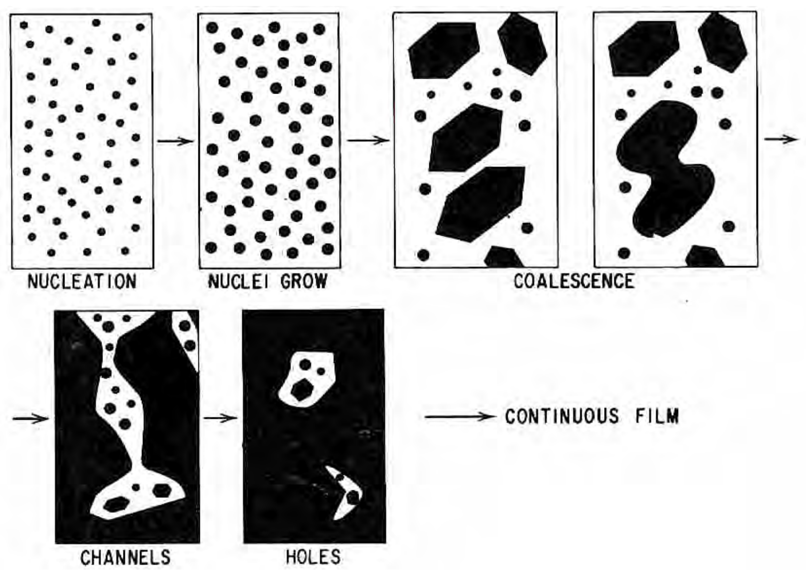

Fig. 2.12. Different stages of film growth.

(i)The island stage

When a substrate under impingement of condensate state monomers is observed in the electron microscope, the first evidence of condensation is a sudden burst of nuclei of fairly uniform size. The smallest nuclei detected have a size of 20 to 30 Å. Growth of nuclei is three-dimensional, but the growth parallel to the substrate is greater than that normal to it. This is probably because growth occurs largely by the surface diffusion of monomers on the substrate, rather than by direct impingement from the vapor phase. The tendency to form an island structure is increased by (1) at high substrate temperature, (2) at low boiling point film material, (3) at low deposition rate, (4) weak binding energy between film material and substrate, (5) a high surface energy of the film material and (6) a low surface energy of the substrate.

(ii) The coalescence stage

As islands increases their size by further deposition and come closer to each-other, the larger one appear to grow by coalescence of the smaller ones. Fig.2.13 illustrates the manner of coalescence of two rounded nuclei. The coalescence occurs in less than 0.1 s for the small nuclei and is characterized by a decrease in total projected area of the nuclei on the substrate (and an increase in their height). In addition, nuclei having well-defined crystallographic shapes before coalescence become rounded during the event [47]. The composite island takes on a crystallographic shape again if left for a sufficiently long time before interacting with its neighbors. The triangular profile of the crystallites is characteristic of the nucleation stage. After coalescence has taken place, the islands assume a more hexagonal profile and are often faulted. A sequence of micrographs illustrating the effects is shown in Fig.2.14, where islands A and B have formed a compound island which eventually becomes crystallographically shaped.

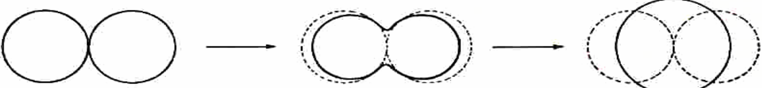

Fig. 2.13. Schematic of shape changes during coalescence (Pashley et al**.,** 1964 **).**

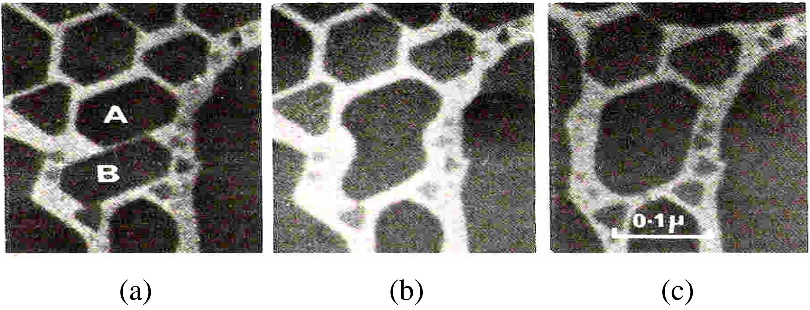

(a) (b) (c)

Fig.2.14. Electron micrographs of islands during and after coalescence (a) at zero (b) after 1 to 2 sec. (c) after 60 sec. (Pashley, 1954).

The liquid like character of the coalescence leads to enlargements of the uncovered areas of the substrate, with the result that secondary nuclei form between the islands. This effect becomes noticeable when the primary islands have grown to about 1000 Å and continues until the final hole-free film is formed. The small nuclei

surrounding island B are examples of those secondary nuclei. A secondary nucleus grows until it touches a neighbor, and if this happens to be a much larger island, the secondary nucleus coalesces very rapidly and becomes completely incorporated in the large island.

(iii) The channel stage

As the islands grow, there is a decreasing tendency for them to become completely rounded after coalescence. Large shape changes still occur, but these confined mainly to the regions in the immediate vicinity of the junction of the islands. Consequently, the islands become elongated and join to form a continuous network structure in which the deposit material is separated by long, irregular, and narrow channels of width 50 to 200 Å. As deposition continues, secondary nucleation occurs in these channels, and the nuclei are incorporated into the bulk of the film as they grow and touch the sides of the channel. At the same time, channels are bridged at some points and fill in rapidly in a liquid like manner.

Eventually, most of the channels are eliminated and the film is continuous but contains many small irregular holes. Secondary nucleation takes place on the substrate within these holes, and the growing nuclei are incorporated (in a liquid like manner) into the continuous regions of the deposit. The hole contains many secondary nuclei which coalescence with each other to form secondary islands, which then touch the edge of the hole and coalesce with the main film to leave a clean hole. Further, secondary nuclei then form and the process are repeated until the hole finally fills in.

(iv) The continuous film stage

The final stage of film growth is a slow process of filling the empty channels, which requires a considerable amount of deposits. In channel stage large areas are vacated by coalescence. These empty channels are filled by secondary nucleation, growth and coalescence and in this way a continuous film is formed.

Considerable changes in the orientation of islands occur during the growth of the film, particularly in the coalescence stage. This is of considerable importance in the growth of epitaxial films. The general mechanism of the growth of polycrystalline layers is similar to that of epitaxial layers, except that the coalescing pairs of islands have a relative orientation, which is randomly distributed.

CHAPTER-III

THEORETICAL PRINCIPLES OF FILM CHARACTERIZATION

In recent years thin film science has grown world-wide into a major research area. Thin films are usually characterized by their structural, stoichiometric, optical, electrical, magnetic and mechanical properties. In this section, the characterization methods used in this work are reviewed briefly. These techniques include Scanning Electron Microscopy (SEM) for surface morphology, Energy Dispersive X-ray (EDX) Diffraction for compositional study, X-ray diffraction (XRD) for structural characterization, absorption spectra for the optical characterization.

3.1 SURFACE MORPHOLOGY AND STRUCTURAL CHARACTERIZATION

The techniques employed for structural analysis of thin films may be classified under two groups, one dealing primarily with the “surface” structure and the other with “volume and surface” structure [48]. This arbitrary classification is obviously meaningless for ultra thin films. The two groups consist of the following techniques [48].

(a) Optical interference, light-figure reflectograms, low-energy electron diffraction (LEED), field-emission and field-ion microscopy, sputter-ion microscopy, electron-reflection diffraction and electron microscopy.

(b) X-ray microscopy, X-ray diffraction (XRD), scanning electron microscopy (SEM).

3.1.1 SCANNING ELECTRON MICROSCOPE

The scanning electron microscopy (SEM) is one of the most useful techniques for the investigation of surface morphology of thin film [49]. The SEM is a type of electron microscope that creates various images (surface morphology) by focusing a high energy beam of electrons onto the surface of a sample and detecting signals

from the interaction of the incident electron with the sample's surface. The type of signals gathered in a SEM varies and can include secondary electrons, characteristic X-rays, and back scattered electrons. In a SEM, these signals come not only from the primary beam impinging upon the sample, but from other interactions within the sample near the surface. The SEM is capable of producing high resolution images of a sample surface in its primary use mode, secondary electron imaging. The SEM is capable of producing high resolution images of a sample surface in its primary use mode, secondary electron imaging. Due to the manner in which this image is created, SEM images have great depth of field yielding a characteristic three-dimensional appearance useful for understanding the surface structure of a sample. This great depth of field and the wide range of magnifications are the most familiar imaging mode for specimens in the SEM. Characteristic X-rays are emitted when the primary beam causes the ejection of inner shell electrons from the sample and are used to tell the elemental composition of the sample. The back-scattered electrons emitted from the sample may be used alone to form an image or in conjunction with the characteristic X-rays as atomic number contrast clues to the elemental composition of the sample.

Fig.3.1. Photograph of a Scanning Electron Microscope (SEM).

3.1.2 SCANNING PROCESS OF SEM

In a typical SEM, electrons are thermionically emitted from a tungsten or lanthanum hexaboride (LaB_6) cathode and are accelerated towards an anode; alternatively, electron scan be emitted via field emission (FE). Tungsten is used because it has the highest melting point and lowest vapor pressure of all metals, thereby allowing it to be heated for electron emission. The electron beam, which typically has an energy ranging from a few hundred eV to 100 keV, is focused by one or two condenser lenses into a beam with a very fine focal spot sized 0.4 to 5 nm. The beam passes through pairs of scanning coils or pairs of deflector plates in the electron optical column, typically in the objective lenses, which deflect the beam horizontally and vertically so that it scans in a raster fashion over a rectangular area of the sample surface. When the primary electron beam interacts with the sample, the electrons lose energy by repeated scattering and absorption within a teardrop-shaped volume of the specimen known as the interaction volume, which extends from less than 100 nm to around 5 µm into the surface. The size of the interaction volume depends on the electrons' landing energy, the atomic number of the specimen and the specimen's density. The energy exchanges between the electron beam and the sample results in the emission of electrons and electromagnetic radiation, which can be detected to produce an image [50].

Electron Microscopes function exactly as their optical counterparts except that they use a focused beam of electrons instead of light to "image" the specimen and gain information as to its structure and composition. The basic steps involved in all electron microscopes are shown in Fig. 3.2.

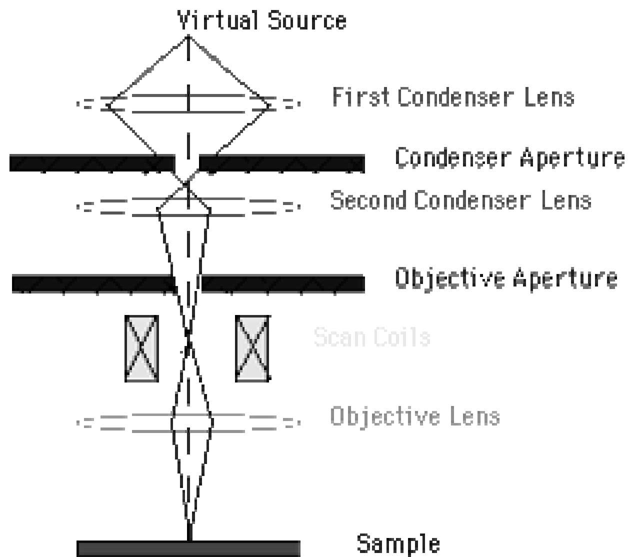

Fig. 3.2. Schematic diagram of a scanning electron microscope.

1. A stream of electrons is formed (by the Electron Source) and accelerated toward the specimen using a positive electrical potential.
2. This stream is confined and focused using metal apertures and magnetic lenses into a thin, focused, monochromatic beam.
3. This beam is focused onto the sample using a magnetic lens.
4. Interactions occur inside the irradiated sample, affecting the electron beam. These interactions and effects are detected and transformed into an image. The above steps are carried out in all EMs regardless of type.

3.1.3 ENERGY DISPERSIVE ANALYSIS OF X-RAY

Energy Dispersive Analysis of X-ray (EDAX) describes the compositional analysis of the thin films. This is done by the scanning electron microscopy (SEM) by focusing the X-ray beam on the full frame or a particular spot of the thin films. The analysis represents the individual weight (%) of the element that is present in the thin films. The optical and electrical properties of thin films are very sensitively influenced by the crystallographic and microstructural characteristics of the film. Similarly, the structural features of the interface at the film also affect the electronic

behavior of the photovoltaic materials. Several techniques have been developed which provide image of the morphological, crystallographic and defect structure of materials component.

3.1.3.1 ENERGY DISPERSIVE X-RAY SPECTROSCOPY

Energy dispersive X-ray spectroscopy (EDS, EDX or EDXRF) is an analytical technique used for the elemental analysis or chemical characterization of a sample. It is one of the variants of XRF. As a type of spectroscopy, it relies on the investigation of a sample through interactions between electromagnetic radiation and matter, analyzing X-rays emitted by the matter in response to being hit with charged particles. Its characterization capabilities are due in large part to the fundamental principle that each element has a unique atomic structure allowing X-rays that are characteristic of an element's atomic structure to be identified uniquely from each other.

Fig.3.3. Photograph of Energy dispersive X-ray spectroscopy (Inspect IS50 FEI Company) in AECD, Dhaka.

To stimulate the emission of characteristic X-rays from a specimen, a high energy beam of charged particles such as electrons or protons, or a beam of X-rays, is focused into the sample being studied. At rest, an atom within the sample contains

ground state (or unexcited) electrons in discrete energy levels or electron shells bound to the nucleus. The incident beam may excite an electron in an inner shell, ejecting it from the shell while creating an electron hole where the electron was. An electron from an outer, higher-energy shell then fills the hole, and the difference in energy between the higher-energy shell and the lower energy shell may be released in the form of an X-ray. The number and energy of the X-rays emitted from a specimen can be measured by an energy dispersive spectrometer. As the energy of the X-rays is characteristic of the difference in energy between the two shells, and of the atomic structure of the element from which they were emitted, this allows the elemental composition of the specimen to be measured.

3.1.4 X-RAY DIFFRACTION

X-ray diffraction is the most precise technique for studying the crystal structure of solids, generally requiring no elaborate sample preparation and is essentially nondestructive [51]. Thin surface film, up to about 1000 Å thick, can be investigated using X-ray diffraction [52]. Thicker films can be characterized by reflection high-energy electron diffraction (RHEED). Analysis of the diffraction patterns obtained by these techniques and comparison with standard ASTM data can reveal the existence of different crystallographic phases in the film, their relative abundance, the lattice parameters, and any preferred orientations.

One has to determine whether a given deposit is a single crystal or polycrystalline either with a random distribution of orientation with respect to the coating plane. For a single crystal coating, it is important to know its orientation relationship with respect to the substrate [53] X-ray diffraction is a suitable tool to determine the crystal structure of any unknown materials, whether the sample is a single crystal or polycrystals [51], either with a random distribution of orientations or with a preferred orientation with respect to the film plane.

XRD is one of the oldest and effective tools for the determination of the atomic arrangement in a crystal; X-rays are the electromagnetic waves and its wavelength ≈

0.1nm. The wavelength of an X-ray is thus of the same order of magnitude as the lattice constant of crystals. When X-rays are incident on a crystal surface, they are reflected from it. The reflection obeys the following Bragg's law,

$$2d \sin\theta = n\lambda$$

where, d is the distance between crystal plane, θ is the X-ray incident angle; λ is the wavelength of the X-ray and n is a positive integer. Bragg's law also suggests that the diffraction is only possible when $\lambda<2d$.

From the width of the diffraction line, it is possible to estimate the average grain size in the film [54]. The X-ay line broadening is commonly used to determine the crystallite size, which is given by:

$$D_g = 0.9\lambda / \Delta\cos\theta$$

where, D_g is the average grain size, λ is the wavelength of the radiation used as the primary beam of CuK_α (λ= 1.54178 Å), θ is the angle of incidence in degree and Δ is the full width at half maximum (FWHM) of the peak in radian. The dimensionless shape factor has a typical value of about 0.9, but varies with the actual shape of the crystallite [51].

3.2 OPTICAL CHARACTERIZATION

3.2.1 BEER-LAMBERT LAW

The Beer-Lambert law is the linear relationship between absorbance and concentration of an absorbing species. The general Beer-Lambert law is usually written as:

$$A = \varepsilon bc$$

where, A is the measured absorbance, ε is the is the molar absorbtivity with units of L mol^{-1} cm^{-1}, b is the path length of the sample - that is, the path length of the curette in which the sample is contained. The unit of b is centimeter and c is the concentration of the compound in solution, expressed in mol L^{-1}.

3.2.2 DERIVATION OF THE BEER-LAMBERT LAW

The Beer-Lambert law can be derived from an approximation for the absorption coefficient for a molecule by approximating the molecule by an opaque disk whose cross-sectional area (σ), represents the effective area seen by a photon of frequency (ν). If the frequency of the light is far from resonance, the area is approximately 0, and if ν is close to resonance the area is a maximum. Taking an infinitesimal slab, dz, of sample:

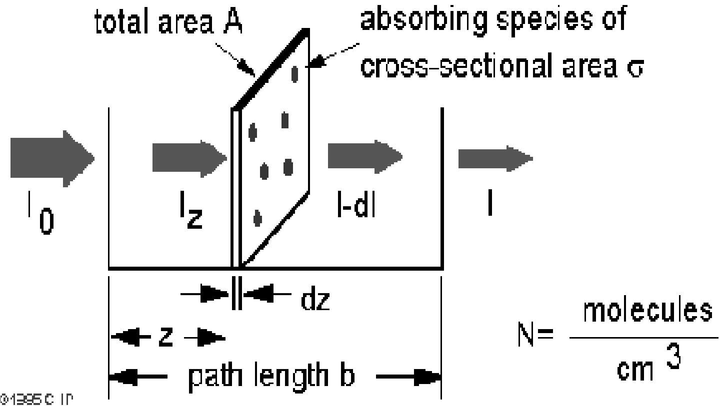

Fig. 3.4. Absorption of light by a sample.

I_o is the intensity entering the sample at z=0, I_z is the intensity entering the infinitesimal slab at z, dI is the intensity absorbed in the slab, and I is the intensity of light leaving the sample. Then, the total opaque area on the slab due to the absorbers is σNA dz. Then, the fraction of photons absorbed will be σNA dz / A so,

$$\frac{dI}{I_z} = -\sigma N dz$$

Integrating this equation from z = 0 to z = b gives:

$$\ln(I) - \ln(I_o) = -\sigma N b$$

or

$$-\ln(I / I_o) = -\sigma N b$$

Since N (molecules/cm^3) (1 mole / 6.023×10^{23} molecules) 1000 cm^3 / liter = c (moles/liter) and 2.303 * log(x) = ln(x)

$$\text{then, } -\log(I / I_o) = \sigma(6.023 \text{ X } 10^{20} / 2.303) cb$$

$$\text{or} \quad -\log(I / I_o) = A = \varepsilon bc$$

where, $\varepsilon = \sigma (6.023 \text{ X}10^{20} / 2.303) = \sigma (2.61 \text{ X } 10^{20})$, and ε is called the molar absorptivity.

Thus the intensity of the transmitted light can be expressed as $I = I_0 e^{-\alpha d}$ where, d is the path length through the sample and α is the absorption coefficient.

3.2.2.1 ABSORPTION COEEFECIENT

When a semiconductor is illuminated by light, photon strikes the surface, a fraction of photons are reflected, some of these are absorbed within the semiconductor and the remainder transmitted into the semiconductor. The absorption of radiation by any medium occurs through the excitation of electrons and photons.

For semiconductor, it is convenient to consider several types of absorption arising from

i) Electronic transitions between different energy bands.
ii) Electronic transitions within energy band.
iii) Electronic transitions to localized states of impurity atoms.
iv) Lattice vibrations.
v) Vibrations of impurity atoms.

When a narrow (collimated) beam of light passes through a substance, the beam will lose intensity due to two processes: The light can be absorbed by the substance or the light can be scattered (i.e., the photons can change direction) by the substance. Just looking at the narrow beam itself, the two processes cannot be distinguished. However, if a detector is set up to measure light leaving in different directions or conversely using a non-narrow beam, one can measure how much of the lost

intensity was scattered, and how much was absorbed. The "absorption coefficient" measures how quickly the beam would lose intensity due to the absorption.

The intensity of the transmitted light can be expressed as $I = I_0 e^{-\alpha t}$ where, t is the path length through the sample and α is the absorption coefficient. Using Beer-Lambert's formula the absorption coefficient can be written as,

$$\alpha = \frac{2.303A}{d}$$

where, A is the absorbance and d is the film thickness.

3.2.3 ELECTRONIC TRANSITIONS

The absorption of UV or visible radiation corresponds to the excitation of outer electrons. There are three types of electronic transition which can be considered;

1. Transitions involving π, σ, and *n* electrons
2. Transitions involving charge-transfer electrons
3. Transitions involving *d* and *f* electrons

When an atom or molecule absorbs energy, electrons are promoted from their ground state to an excited state. In a molecule, the atoms can rotate and vibrate with respect to each other. These vibrations and rotations also have discrete energy levels, which can be considered as being packed on top of each electronic level.

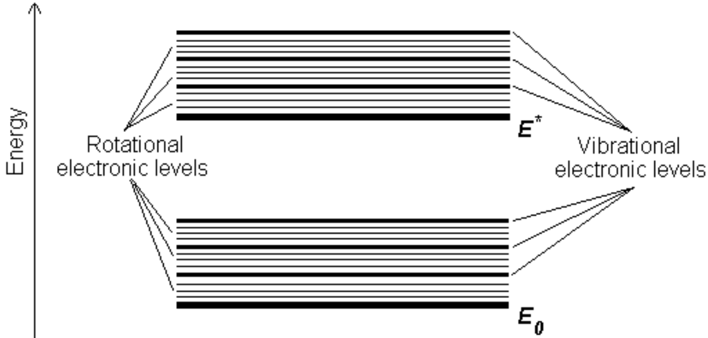

Fig. 3.5. Vibrational and rotational energy levels.

Absorbing species containing π, σ, and n electrons

Absorption of ultraviolet and visible radiation in organic molecules is restricted to certain functional groups (*chromophores*) that contain valence electrons of low excitation energy. The spectrum of a molecule containing these chromophores is complex. This is because the superposition of rotational and vibrational transitions on the electronic transitions gives a combination of overlapping lines. This appears as a continuous absorption band.

Possible electronic transitions of π, σ, and n electrons are;

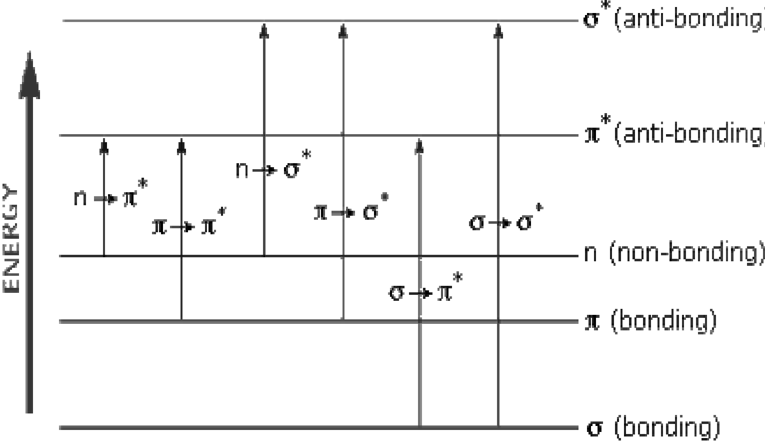

Fig. 3.6. Possible electronic transitions.

$\sigma \rightarrow \sigma^*$ Transitions

An electron in a bonding σ orbital is excited to the corresponding antibonding orbital. The energy required is large. For example, methane (which has only C-H bonds, and can only undergo $\sigma \rightarrow \sigma^*$ transitions) shows an absorbance maximum at 125 nm. Absorption maxima due to $\sigma \rightarrow \sigma^*$ transitions are not seen in typical UV-VIS. spectra (200 - 700 nm).

$n \rightarrow \sigma^*$ Transitions

Saturated compounds containing atoms with lone pairs (non-bonding electrons) are capable of $n \rightarrow \sigma^*$ transitions. These transitions usually need less energy than $\sigma \rightarrow \sigma^*$ transitions. They can be initiated by light whose wavelength is in the range 150 - 250 nm. The number of organic functional groups with $n \rightarrow \sigma^*$ peaks in the UV region is small.

$n \rightarrow \pi^*$ and $\pi \rightarrow \pi^*$ Transitions

Most absorption spectroscopy of organic compounds is based on transitions of *n* or π electrons to the π^* excited state. This is because the absorption peaks for these transitions fall in an experimentally convenient region of the spectrum (200 - 700 nm). These transitions need an unsaturated group in the molecule to provide the π electrons.

Molar absorbtivities from $n \rightarrow \pi^*$ transitions are relatively low, and range from 10 to100 L mol^{-1} cm^{-1}. $\pi \rightarrow \pi^*$ transitions normally give molar absorbtivities between 1000 and 10,000 L mol^{-1} cm^{-1}.

The solvent in which the absorbing species is dissolved also has an effect on the spectrum of the species. Peaks resulting from $n \rightarrow \pi^*$ transitions are shifted to shorter wavelengths (*blue shift*) with increasing solvent polarity. This arises from increased solvation of the lone pair, which lowers the energy of the *n* orbital. Often

(but *not* always), the reverse (i.e. *red shift*) is seen for $\pi \rightarrow \pi^*$ transitions. This is caused by attractive polarization forces between the solvent and the absorber, which lower the energy levels of both the excited and unexcited states. This effect is greater for the excited state, and so the energy difference between the excited and unexcited states is slightly reduced - resulting in a small red shift. This effect also influences $n \rightarrow \pi^*$ transitions but is overshadowed by the blue shift resulting from solvation of lone pairs.

3.2.4 DIRECT AND INDIRECT OPTICAL TRANSITIONS

The band gap generally refers to the energy difference between the top of the valence band and the bottom of the conduction band. Fundamental absorption refers to the annihilation or absorption of photons by the excitation of an electron from the valence band up into the conduction band, leaving a hole in the valence band. Both energy and momentum must be conserved in such a transition.

In the case of an indirect-band gap semiconductor, the minimum energy in the conduction band and the maximum energy in the valence band occur at different values of crystal momentum. Photon energies much larger than the forbidden gap are required to give direct transitions of electrons from the valence to the conduction band. However, transitions can occur at lower energies by a two-step process. Involving not only photon and electron but also a third particle, a phonon.

To estimate the nature of absorption a random phase model is used where the k momentum selection rate is completely relaxed. The integrated density of states N (E) has been used and defined by,

$$N(E) = \int_{-\infty}^{+\infty} g(E)dE$$

The density of states per unit energy interval may be represented by,

$$g(E) = \frac{1}{V}\sum \delta(E - E_n)$$

where, V is the volume, E is the energy at which $g(E)$ is to be evaluated and E_n is the energy of the nth state. If $g_v \propto E^p$ and $g_c \propto (E-E_{opt})$, where energies are measured from the valance band mobility edge in the conduction band (mobility gap) and substituting these values into an expression for the random phase approximation, the relationship obtained,

$$\nu^2 I_2(\nu) \propto (h\nu - E_0)^{p+q+1},$$

where, $I_2(\nu)$ is the imaginary part of the complex permittivity. If the density of states of both band edges is parabolic, then the photon energy dependence of the absorption becomes

$$\alpha h\nu \propto \nu^2 I_2(\nu) \propto (h\nu - E_{opt})^2.$$

So for higher photon energies the simplified general equation which is known as Tauc relation is,

$$\alpha h\nu = B(h\nu - E_{\mathrm{opt}})^n$$

where, $h\nu$ is the energy of absorbed light, n is the parameter connected with distribution of the density of states and B, a constant or Tauc parameter and here n = 1/2 for direct and n = 2 for indirect transitions [54].

The above equation can be written as

$$\frac{d[\ln(\alpha h\nu)]}{d[h\nu]} = \frac{n}{h\nu - E_{opt}}$$

When finding the n, type of transition can be obtained from the absorption spectrum. A discontinuity in the d[ln($\alpha h\nu$)] / d($h\nu$) versus $h\nu$ plot at the band gap energy (E_{opt} or E_g), i.e. at $h\nu = E_g$ can be observed. The discontinuity at a particular energy value gives the band gap E_g.

Thus from the straight-line plots of $(\alpha h\nu)^2$ versus $h\nu$ and $(\alpha h\nu)^{1/2}$ versus $h\nu$ the direct and indirect energy gaps of thin films can be determined.

3.2.5 WORKING PRINCIPLE OF UV-VISIBLE SPECTROMETER

A diagram of the components of a typical spectrometer is shown in the following Fig. 3.7. The functioning of this instrument is relatively straightforward. A beam of light from a visible and/or UV light source (colored red) is separated into its component wavelengths by a prism or diffraction grating. Each monochromatic (single wavelength) beam in turn is split into two equal intensity beams by a half-mirrored device. One beam, the sample beam (colored magenta), passes through a small transparent container (curette) containing a solution of the compound being studied in a transparent solvent. The other beam, the reference (colored blue), passes through an identical curette containing only the solvent. The intensities of these light beams are then measured by electronic detectors and compared. The intensity of the reference beam, which should have suffered little or no light absorption, is defined as I_0. The intensity of the sample beam is defined as I. Over a short period of time, the spectrometer automatically scans all the component wavelengths in the manner described. The ultraviolet region scanned is normally from 200 to 400 nm, and the visible portion is from 400 to 800 nm. If the sample compound does not absorb light of a given wavelength, $I = I_0$. However, if the sample compound absorbs light then I is less than I_0 and this difference may be plotted on a graph.

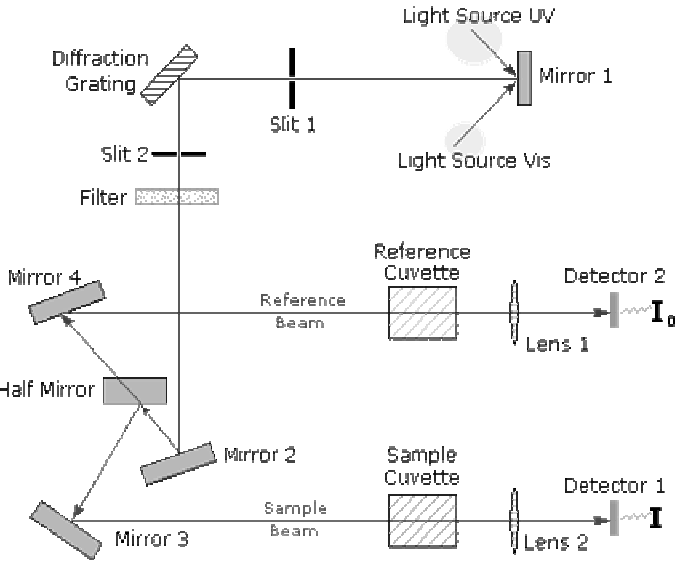

Fig. 3.7. Diagram of the components of a spectrometer.

Absorption may be presented as transmittance or absorbance. If no absorption has occurred, T = 1.0 and *A*= 0. Most of the sample compound does not absorb light of a given wavelength, $I = I_0$. Most spectrometers display absorbance on the vertical axis, and the commonly observed range is from 0 (100% transmittance) to 2 (1% transmittance). The wavelength of maximum absorbance is a characteristic value, designated as λ_{max}. Different compounds may have very different absorption maxima and absorbances. Intensely absorbing compounds must be examined in dilute solution, so that significant light energy is received by the detector, and this requires the use of completely transparent (non-absorbing) solvents. The most commonly used solvents are water, ethanol, hexane and cyclohexane.

3.3 MEASURMENT OF OPTICAL ABSORPTION OF THIN FILM

The optical properties of the thin films deposited onto glass substrates having a dimension of 18mm × 9mm × 2mm were studied by UV-visible spectroscopic measurements. UV-visible absorption spectra were recorded using a dual beam UV-visible spectrophotometer (SHIMADZU, JAPAN, UV-1601) in the wavelength range of 300-1100 nm at room temperature. The absorption spectra were recorded both for as-deposited and annealed films. Annealed were performed at 673, 773, and 873 K for 1 hour. Samples of Cd concentration 0.00, 0.20, 0.40, 0.60, 0.80 and 1.00 were used for UV-visible spectroscopic studies. A blank glass slide was used as the reference during the optical absorption measurement of thin films.

Fig. 3.8. Photograph of a Spectrophotometer (UV-1601PC, SHIMADZU, JAPAN) in BCSIR, Dhaka.

3.3.1 MEASUREMENT OF THICKNESS OF THIN FILM

Thickness is the single most significant film parameter. It may be measured either by in-situ monitoring of the rate of deposition, or after the film is taken out of deposition chamber. Techniques of the first type often called as monitor method generally allow both monitoring and controlling of the deposition rate and film thickness. Other techniques are also used for thickness measurement. Any physical quantity related to film thickness can in principle be used to measure the film thickness. It may be measured either by several methods with varying degrees of accuracy. The methods are chosen on the basis of their convenience, simplicity and reliability. Since the film thicknesses are generally of the order of a wavelength of light, various types of optical interference phenomena have been found to be most useful for measurement of film thicknesses.

Multiple-Beam Interferometry

During evaporation, i) Multiple-Beam Interferometry, (Tolansky Fezeau fringes method, Fringes of equal chromatic order.) ii) Michelson interferometer iii) Using a Hysteresis graph relative and other methods used in film-thickness determination with particular reference to their merits and accuracies. Multiple-Beam Interferometry technique was employed for the measurement of thickness of the thin films. A brief description of the method is given below. This method utilizes the resulting interference effects when two silvered surfaces are brought close together and are subjected to optical radiation. This interference technique, which is of great value in studying surface topology in general, may be applied simply and directly to film-thickness determination. When a wedge of small angle is formed between unsilvered glass plates, which are illuminated by monochromatic light, broad fringes are seen arising from interference between the light beams reflected from the glass on the two sides of the air wedge. At points along the wedge where the path difference between these two beams are an integral and odd number of wavelengths, bright and dark fringes occur respectively. If the glass surfaces of the plates are coated with highly reflecting layers, one of which is partially transparent, then the

reflected fringe system consists of very fine dark lines against a bright background. A schematic diagram of the multiple-beam interferometer along with a typical pattern of Fizeau fringes from a film step is shown in Fig. 3.9. As shown in this figure, the film whose thickness is to be measured is over coated with a silver layer to give a good reflecting surface and a half-silvered microscope slide is laid on top of the film whose thickness is to be determined. A wedge is formed by the two microscope slides and light multiply reflected between the two silvered surfaces forms an interference pattern with a discontinuity at the film edge.

The thickness of the film "*d*" can then be determined by the relation, $d = \frac{\lambda}{2}\frac{b}{a}$ where, λ is the wavelength and *b/a* is the fractional discontinuity identified in the figure 3.9.

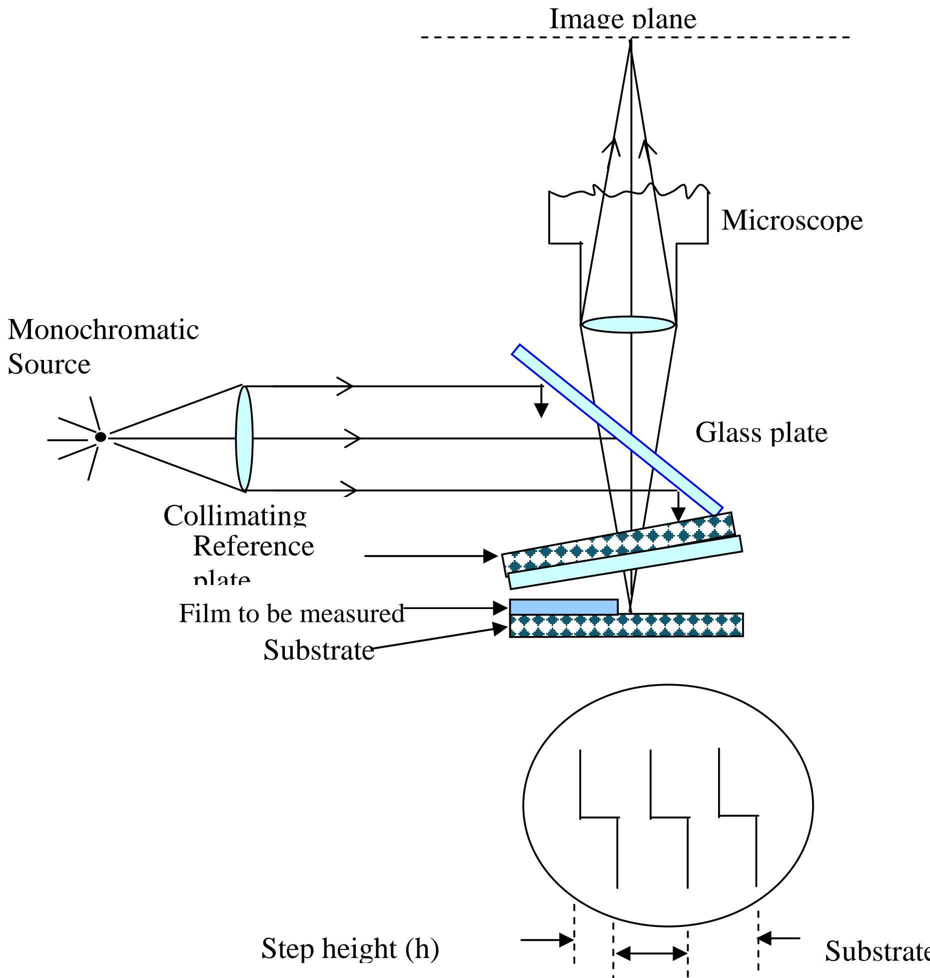

Fig. 3.9. Interferometer arrangement for producing reflection Fizeau fringes of equal thickness.

In general, the sodium light is used, for which $\lambda = 5893$ Å. In conclusion, it might be mentioned that the Tolansky method of film-thickness measurement is the most widely used and in many respects also the most accurate and satisfactory one [55].
The thickness of the films deposited on glass substrates was measured by using a multiple-beam interferometric method. For film thickness measurement separate glass slide has been used in addition to the sample substrates. The step generated on the surface of the glass slide was used to measure the film thickness.

3.3.2 ELECTRICAL PROPERTIES MEASURMENT

Electrical parameters like resistivity, conductivity, sheet resistance, activation energy etc. of the $Co_{1-x}Cd_xS$ ($0 \leq x \leq 1$) films were measured by the van-der Pauw method from the laboratory of Applied Physics Department, Rajshahi University. D.C electrical resistivity measurements were made in air for freshly deposited films from room temperature 303 to 403 K by van-der Pauw method and data were taken by increasing the temperature of the film slowly. On increasing up to a maximum temperature (403 K) and then film cooled down slowly to room temperature. Variation of current and voltage corresponding temperature recorded in data and then calculated electrical parameters. For dc conductivity measurement, a 15V dc fixed bias was maintained. A power supply (Heathkit, Model: IP-2717A) was used to pass a constant dc current through the test sample. An electrometer (Keithley, Model: 614) was used to monitor the current through the sample and a digital multimeter (Model: DM-206) was used to measure the potential differences across each sample. The glass substrate was heated by a specially designed heater and the temperature was measured by a chromel-alumel thermocouple placed on the middle of the substrate.

3.3.3 RESISTIVITY AND ELECTRICAL CONDUCTIVITY OF THIN FILM

The property of a material to resist the flow of electrical current is called the resistance and the resistance per unit length of unit cross-section is called resistivity. It is denoted by ρ and mathematically defined as

$$\rho = \frac{RA}{L} \tag{3.1}$$

where, A is the cross-sectional area, R is the resistance and L is the length of the material along the direction of current flow. Resistivity is an intrinsic property of a material and depends only on the crystal structure of the material. Electrical conductivity of a material is reciprocal of resistivity of the material. Electrical conductivity is denoted by σ_{elec} and defined as:

$$\sigma_{elec} = \frac{1}{\rho} \tag{3.2}$$

Conductivity depends only on the structural and physical property of the material.

3.3.4 RESISTIVITY MEASUREMENT TECHNIQUES

A number of methods are used to measure the resistivity of a material. Only two of them are discussed below.

3.3.5 DIRECT METHOD

The resistivity of a thin film can be measured easily by direct method using the relation

$$\rho = R\frac{bt}{L} \tag{3.3}$$

where, b and t are the breadth and thickness of the sample. For simplicity, if we consider, b = L, the above equation becomes

$$\rho = Rt \tag{3.4}$$

Measuring the resistance, R and thickness, t one can easily determine the resistivity. The experimental arrangement is shown in Fig. 3.10.

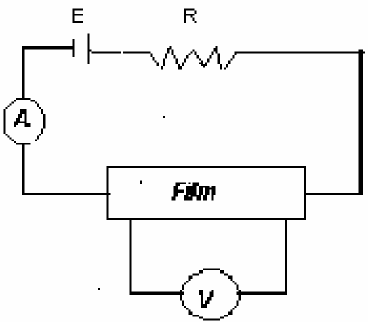

Fig. 3.10. Circuit arrangement for resistivity measurement by direct method.

3.3.6 van-der Pauw's Technique

Electrical resistivity of metal and semiconductor film of any shape may be measured by using van-der Pauw's method. The resistivity of film having any arbitrary shape can be uniquely determined by using this method.

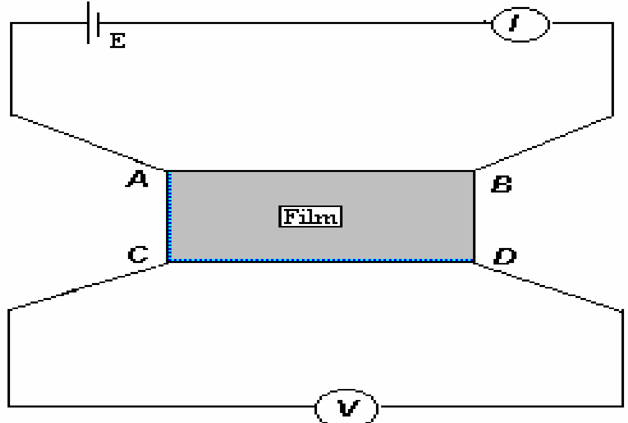

Fig. 3.11. Experimental arrangements for measuring resistivity by using van-der Pauw's method.

At first we select a region on the sample where four electrical contacts were made at four corners, say A, B, C, and D as shown in Fig. 3.11. Silver paste or indium was used to the contact. If a current I_{AB} entering the specimen through the contact A and

leaving through the contact, B produces a potential difference V_D-V_C between C and D then the resistance $R_{AB, CD}$ is defined as

$$R_{AB,CD} = \frac{V_D - V_C}{I_{AB}} = \frac{V_{CD}}{I_{AB}} \quad (3.5)$$

Similarly,

$$R_{BC,DA} = \frac{V_A - V_D}{I_{BC}} = \frac{V_{DA}}{I_{BC}} \quad (3.6)$$

$$R_{CD,AB} = \frac{V_B - V_A}{I_{CD}} = \frac{V_{AB}}{I_{CD}} \quad (3.7)$$

and

$$R_{DA,BC} = \frac{V_C - V_B}{I_{DA}} = \frac{V_{BC}}{I_{DA}} \quad (3.8)$$

The resistivity of a thin film can be expressed by the equation

$$\rho = \frac{\pi t}{\ln 2}\left[\frac{R_{AB.CD} + R_{BC,AD}}{2}\right] \times f\left[\frac{R_{AB.CD}}{R_{BC.DA}}\right] \quad (3.9)$$

$$\rho = 4.53t \times \left[\frac{R_{AB.CD} + R_{BC,DA}}{2}\right] \times f\left[\frac{R_{AB.CD}}{R_{BC.AD}}\right] \quad (3.10)$$

where, t is the thickness of the film and the function f can be evaluated from the equation

$$\left[\frac{R_{AB.CD} - R_{BC.DA}}{R_{AB.CD} + R_{BC.DA}}\right] = \frac{f}{\ln 2}\, arc\cosh\, \frac{\exp(\ln 2/f)}{2} \quad (3.11)$$

If $R_{AB, CD}$ and $R_{BC, DA}$ is almost equal, f may be approximately equal to unity and then the equation (3.10) takes the form,

$$\rho = 2.265\ t\ (R_{AB, CD} + R_{BC, DA})\ \Omega\text{-cm}\ . \quad (3.12)$$

It is very difficult to get f, so we have taken the value of f from the chart for different ratio greater than unity.

3.3.7 FACTORS AFFECTING RESISTIVITY MEASUREMENT

The effects of the following factors are remarkable in the measurement of resistivity:

a) Length to breadth ratio, L/b of the film
b) Current electrodes
c) Current density
d) Microscopic inhomogenity of the film
e) Sensitivity of the measuring devices
f) Electrical contact resistivity

3.3.8 SHEET RESISTANCE

The resistance of a thin film directly proportional to the resistivity ρ and inversely proportional to the thickness t and we can write for a rectangular film of length L and width W.

$$R = (\frac{\rho}{t}) \times (\frac{L}{W}) = R_s \ (\frac{L}{W}) \quad (3.13)$$

where, R_S is known as the sheet resistance and expressed in ohm.

$$R_s = \frac{\rho}{t} \text{ ohm} \quad (3.14)$$

The ratio (L/W) is called the number of squares.

The number of “squares” is a pure number have no dimensions. It is very useful quantity that is widely used for comparing films, particularly those of the same material deposited under similar conditions.

3.3.9 ACTIVATION ENERGY

The energy required to transfer charge from one initially neutral island to another is known as activation energy and denoted by ΔE. This is equivalent to the electrostatic

binding energy of the charge to the island. When these charge carriers are excited to at least this energy from the Fermi-level, there will be tunneling from one island to another. These islands or small particles are called crystallites. The activation energy is related with film conductivity and given by the relation,

$$\sigma = \sigma_0 \exp\left(-\frac{\Delta E}{2kT}\right) \qquad (3.15)$$

where, σ_0 is the conductivity at 273 K and k is the Boltzmann constant and T is the absolute temperature. Equation (3.15) can be written as

$$\ln\sigma = -\frac{\Delta E}{2kT} + \ln\sigma_0 \qquad 3.16)$$

Equation (3.16) is equivalent to a straight line equation, y = mx + c. So that ΔE can be determined from the slope of the straight line $\ln\sigma = -\frac{\Delta E}{2kT} + \ln\sigma_0$. From the graph of lnσ vs.1/T, ΔE can be calculated by using the relation

$$\Delta E = -\left(\frac{\ln\sigma}{\frac{1}{T}}\right) \times 2k \text{ (eV)} \qquad (3.17)$$

3.3.10 TEMPERATURE COEFFICIENT OF RESISTANCE (T. C. R)

The temperature coefficients of resistance (T.C.R) plays an important role for film characterization and it is very important circuit functions where ambient temperature changes could cause unexpected changes in circuit performance.

The resistivity of any metal and semiconductor are usually dependent on temperature. According to the law of Ghosh and Deb [56], the relation between resistivity and temperature is given by,

$$\rho_T = \rho_o (1+\alpha_{T.C.R}\, T+\beta T^2 + \cdots\cdots\cdots) \qquad (3.18)$$

where, ρ_o is the resistivity at 0^0C and ρ_T is the resistivity at T^0 C and $\alpha_{T.C.R}$ is the temperature coefficient of resistance (T.C.R) and β is a constant. Generally $\alpha_{T.C.R} >> \beta$ at low temperature and we can write from first approximation,

$$\rho_T = \rho_o (1+\alpha_{T.C.R}\, T) \qquad (3.19)$$

At temperatures T_2 and T_1 equation (3.19) can be written as,

$$\rho_{T2} = \rho_o (1+\alpha_{T.C.R}\, T_2) \qquad (3.20)$$

$$\rho_{T1} = \rho_o (1+\alpha_{T.C.R}\, T_1) \qquad (3.21)$$

After some mathematical manipulation Equation-3.20 and 3.21 may be written as,

$$\%\ \text{T. C. R.} = \frac{\rho_{T2} - \rho_{t1}}{\rho_{T1}(T_2 - T_1)} \times 100 \qquad (3.22)$$

Generally ρ_{T1} is the resistivity at room temperature and ρ_{T2} is the resistivity at temperature T_2.

3.3.11 ANNEALING

Annealing is a form of heat treatment by which crystals of varying composition may be homogenized, relieve internal stresses and instabilities. It consists of heating the specimen to a specified temperature (below the melting temperature) for sufficient length of time to allow diffusion to occur followed by a slow cooling process.

Annealing was conducted using a horizontal tube furnace. The prepared $Co_{0.8}Cd_{0.2}S$ film substrates to be annealed were inserted in a long Pyrex cylinder. The heat was raised to the desired temperature (673, 773 and 873 K) for the same samples, under air and was left for 1 hour before cooling. The system was left to cool, in the desired method slow cooling.

CHAPTER-IV

EXPERIMENTAL DETAILS

Film Preparation

The spray pyrolysis method is particularly attractive because of its simplicity. It is fast, inexpensive, vacuum less and is suitable for thin film production. The spray pyrolysis method is basically a chemical deposition method in which fine droplets of the desired material are sprayed onto a heated substrate. A continuous film is formed on the hot substrate by thermal decomposition of the material droplets.

Thin films can be prepared from a variety of materials such as metals, semiconductors, insulators or dielectrics etc., and for this purpose various preparation techniques has also been developed. Spray pyrolysis is the most commonly used technique adopted for the deposition of metals, alloys and many compounds.

This chapter deals mainly with the description of the apparatus and the preparation of the sample. In this chapter the preparation of $Co_{1-x}Cd_xS$ thin films on glass substrate by spray pyrolysis process is discussed. Various steps of the film deposition procedure of the spray pyrolysis method have been discussed below.

4.1 EXPERIMENTAL EQUIPMENT

4.1.1 PREPARATION OF MASKS

The direct deposition of thin film pattern requires a suitably shaped aperture, commonly referred to as a mask. For the purpose of various experimental studies, film of specific size and shape are required. Mask was made from stainless steel plate with the desired pattern cut into it. The aperture was made in a bath machine.

The most commonly used method of patterning thin film is the physical masking, which is accomplished by placing the mask of desired shape on the substrate. In the present work, thin mica sheet was used for the preparation of masks as shown in figure 4.1.

Regardless of mask material and fabrication process all masks should be thoroughly cleaned and inspected before use. Surface contaminants, particularly oil, grease or other organic materials may become volatile when the mask is heated and then be absorbed by the substrate and this may be a cause of weak film adhesion.

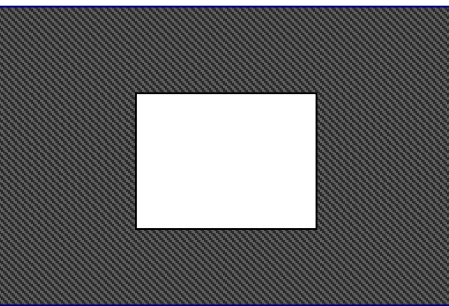

Fig. 4.1. Mask for the sample.

The mask is placed in proximity to the substrate, thereby allowing condensation of the evaporate only in the exposed substrate areas. The mask was prepared in such a way that the edge of the mask is smooth so that it is helpful for determining the film thickness accurately.

4.1.2 HEATER

The heater 'H' is an ordinary hot plate 2 k-watt nichrome wire heater. The top of the plate is covered with a piece of asbestos sheet having a small open area at the center where a mica sheet is attached. A thick stainless steel plate is placed on this mica sheet. Substrate is placed on this susceptor plate to have a uniform temperature

throughout the substrate surface. An electrical voltage variac controls the heater power.

4.1.3 THE DESIGN OF THE REACTOR

The design of the reactor is shown in Fig. 4.2. It is a vertical bath type reactor composed of a galvanized iron enclosure ‘E’, heater ‘H’ and heat susceptor ‘G’. For the rapid expulsion of the by-product gases there are opening at the side and at the top of the reactor. It helps focusing the incoming sprayed solution towards the substrate and also provides a chimney action to the exhaust gas upwards.

Fig. 4.2. Design of a reactor.

4.1.4 THE FUME CHAMBER

It is a large type chamber with a slanting top and is provided with a chimney. There is an exhaust fan fitted at the mouth of the chimney to remove the unused gases from the chamber. The slanting top and the sidewalls are made of glass and wood. There are airtight doors in the front side. The chamber has purging facilities. The whole spray system and the reactor are kept inside this fume chamber at the time of film deposition because of the safety grounds and to check air current disturbances at the deposition site. These two points just stated are very important for the spray process when deposition is carried out in open-air atmosphere.

4.1.5 AIR COMPRESSOR

It is reservoir type electrical air compressor. A rotary pump in this section mode draws atmospheric air and keeps it reserved in a large capacity air tank. At the outlet of the tank a pressure gauge is attached which records the pressure of the air at the time of supplying it from the tank. There is a by pass control valve which can keep the output pressure constant.

4.1.6 SPRAY HEAD / SPRAY NOZZLE

The single spray nozzle consists of capillary tubes (stainless steels) fitted perpendicular to the other tube as shown in Fig. 4.3. When compressed air is passed rapidly through the upper tube ‘P’ in direction tangential to the mouth of the lower tube ‘A’, a partial vacuum is created at the front part of the tube ‘A’ whose other end is kept immersed in the spray liquid. Due to this partial vacuum the liquid rises up through the tube ‘A’ and the compressed air drives it away in the form of fine spray particles. The thinner spray nozzle would give the finer spray particles. A very fine needle shaped capillary tube was used for the spray nozzle and it may vary from nozzle to nozzle.

4.2 TYPE OF SUBSTRATE AND SUBSTRATE CLEANING

For thin film deposition, several types of substrates are used. Generally, glass, quartz, plastic and ceramic substrates are used for polycrystalline films. However, in the present work, thin films were deposited on glass substrates. The most commonly microscope glass slides having 5 cm long, 2 cm wide and 0.1 cm thickness were used. These were fine smooth high quality microscope glass slides.

The cleaning of substrate has a major influence on the properties of the thin film deposited onto them. Surface contaminations manifest in it pinholes, which can cause open resistor or localized high resistance. The following procedures were used

for substrate cleaning. The gross contamination of each of the substrates were first removed by ethyl alcohol (C_2H_5OH) and then boiled with distilled water. After boiling in distilled water, the substrates were dipped at first into acetone for some time. Taking them out of acetone one by one and then these were washed and thoroughly rinsed with distilled water for several times. Finally, these were dried in hot air and preserved for use. During the whole process the substrates were always held by slide holding forceps.

4.3 WORKING SOLUTION

The working solution was prepared by taking cobalt acetate [Co ($CH_3COO)_2$. $4H_2O$], [Cd($CH_3COO)_2$.$3H_2O$] and thiourea [NH_2CSNH_2] as source material of Co, Cd and S respectively. The most commonly used solvents are water and ethanol. As [Co($CH_3COO)_2$.$4H_2O$] dissolves in water at room temperature (RT), water was taken as solvent. Since the spray system used in the present experiment operates via a partial vacuum path as the mouth of the spray nozzle, the concentration of the solution prepared by the solvent was made in such a way that it could be at least be drawn by the nozzle.

In order to prepare the $Co_{1-x}Cd_xS$ thin films for different concentrations ($x = 0.0$ - 1.0), the aqueous solution of cobalt acetate [Co($CH_3COO)_2$.$4H_2O$], cadmium acetate [Cd($CH_3COO)_2$.$3H_2O$] and thiourea [NH_2CSNH_2] as the precursor solution were taken. In this work the concentration of the solution was kept at 0.1 M.

4.4 FILM DEPOSITION PARAMETERS

In the chemical spray deposition technique the structure, composition and other characteristics of the deposited films depend on a number of process variables [deposition parameters]. The variable quantities such the substrate temperature, solution and gas flow rate, deposition time, quality of the substrate material, size of

atomized particles, solution concentration, and substrate to spray outlet distance, etc. are affected on the film properties. It is obvious that the substrate temperature is the most important deposition parameter and it is controlled with grate care.

For the deposition of $Co_{1-x}Cd_xS$ thin film, all the above mentioned parameters except

(i) Substrate temperature (T_s)
(ii) Deposition time (t_d)
(iii) Solution concentration (C)
(iv) Spray rate (S_r)
(v) Spray outlet to substrate distance (d_s) and
(vi) Carrier air pressure (P_a), were kept at their optimum values. To study the effect of any one of these six parameters on the film properties the remaining other were kept constant.

Air current disturbances become another parameter, which creates problem to get uniformity of thickness and homogeneity of the film.

4.5 SAMPLE DEPOSITION

It has been stated earlier that spray pyrolysis method for preparing Cobalt sulfide thin film is an economically attractive method, which consist basically of spraying solution on a heated glass substrate. The apparatus needed to carry out the chemical spray process consists of a device to atomize the spray solution and a substrate heater. Fig. 4.3 shows a typical experimental setup of spray pyrolysis technique.

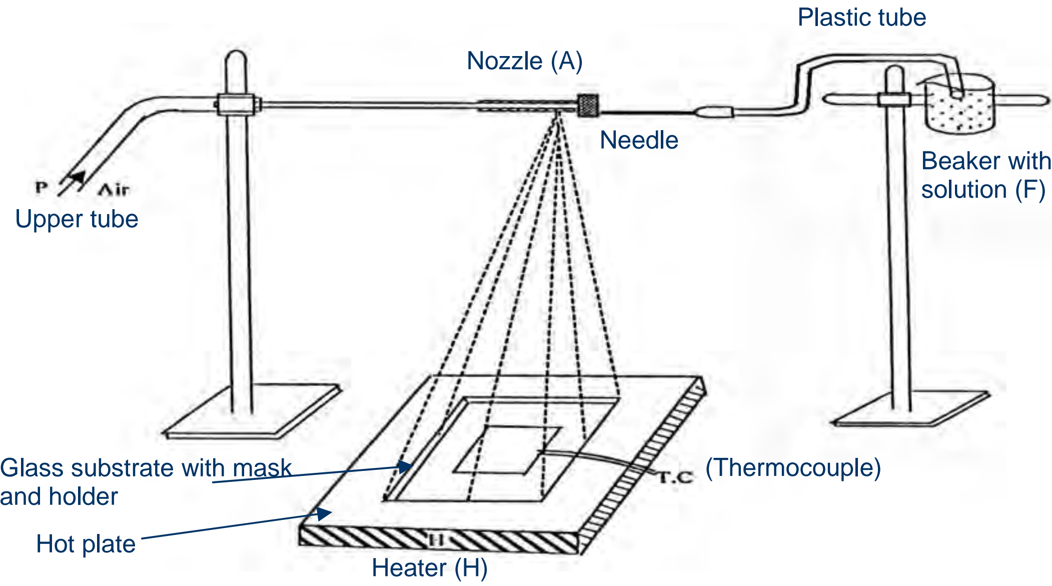

Fig.4. 3. Experimental set up of spray pyrolysis method.

A considerable amount of (100 ml) solution taken in the container 'F' fitted with the spray nozzle 'A'. The clean substrate with a suitable mask was put on the susceptor of the heater 'H'. The distance between the tip of the nozzle and the surface of the glass substrate was kept 25 cm. Before supplying the compressed air the substrate temperature 'T_s' was to be kept at a level slightly higher than the required substrate temperature because at the onset of spraying a slight fall of temperature is likely. The temperature of a substrate was controlled by controlling the heater power using a variac. The substrate temperature was measured by placing a copper constantan thermocouple on the substrate.

When compressed air is passed through 'P' at constant pressure (0.50 bar), a fine $Co_{1-x}Cd_xS$ was produced and was automatically carried to the reactor zone where film was deposited on the heated substrate. A situation has been adjusted such that 5 minutes of spray produces $Co_{1-x}Cd_xS$ thin film keeping substrate temperatures at 523 K. The possible chemical reaction that takes place on the heated substrate to produce $Co_{1-x}Cd_xS$ may be as follows:

$$\left.\begin{array}{l} Co(CH_3COO)_2.4H_2O+ \\ Cd(CH_3COO)_2.3H_2O+ \\ NH_2CSNH_2 \end{array}\right\} \xrightarrow[\text{Decomposes}]{523\ K} Co_{1-x}Cd_xS + CO_2\uparrow + NH_3\uparrow + CH_4\uparrow + \text{Steam}\uparrow$$

4.6 RATE OF DEPOSITION

The rate of flow of the working solution can be controlled by a suitable nozzle 'A' and adjusting the airflow rate.

4.7 THICKNESS CONTROL

In the present spray deposition process, the deposition time is the main factor for the thickness control, provided the other parameters, remain constant. Since the deposition is carried out in normal atmosphere a direct and insist control of thickness is not so easy. To control the film thickness therefore calibration chart may be used. These charts are generally plots of deposition time vs. thickness, and can be prepared at different constant substrate temperatures prior to the preparation of particular experimental samples using the same solution and deposition variables.

4.8 OPTIMIZATION OF THE DEPOSITION PROCESS

To obtain the optimum condition of the film deposition process, it is essential to select at first the requirements with respect to which the process should be optimized. The optimization process is very lengthy because there are a number of process variables. The basic requirement was to get a film of high transparency as well as high electrical conductivity.

For the process of optimization following set of films have been deposited:

The first set of films was deposited at various substrate temperatures, keeping all other deposition parameters constant at an arbitrary level. From the set of films the optimum substrate temperature T_s was selected with respect to the best conducting and transparent films.

After obtaining the optimum value of T_s, second set of films were deposited by varying the substrate to spray outlet distance, d_s using the optimized T_s and other parameters were kept constant to the arbitrary level as they were in the first set. From this second set of films the optimum distance d_s was selected corresponding to the best film.

Fixing the distance d_s and substrate temperature T_s, a third set of films were deposited by varying the pressure of the carrier gas P_a. From this set, optimum carrier air pressure P_a was selected. Keeping T_s, d_s and P_a as fixed fourth set of films were deposited by taking spray rate S_r as variable parameters. From this set, optimum spray rate S_r was selected. The fifth set of films were deposited keeping T_s, d_s, P_a and S_r at their optimum values. In this case, the solution concentration C was varied for selecting the optimum concentration of the working solution.

Thus in all cases the optimum values of the parameters were selected for deposition of films that exhibit good conductivity and high transparency. The resulting optimization is undoubtedly a tentative one because the process variables are in some degree mutually interdependent.

CHAPTER-V

RESULTS AND DISCUSSION

5.1 INTRODUCTION

The objectives of this study are to characterize pure CoS and $Co_{1-x}Cd_xS$ ($0 \le x \le 1$) thin films synthesized by spray pyrolysis method. Here films deposited by the reduced of the preparation cost and made it economically feasible. In this chapter the results and discussion of the various experimental studies namely surface morphology, structural, optical and electrical properties of $Co_{1-x}Cd_xS$ thin films are presented and discussed step by step.

5.2 DEPOSITION OF $Co_{1-x}Cd_xS$ THIN FILMS

In order to prepare $Co_{1-x}Cd_xS$ thin films the aqueous solution of cobalt acetate [$Co(CH_3COO)_2.4H_2O$], cadmium acetate [$Cd(CH_3COO)_2.3H_2O$] and thiourea [NH_2CSNH_2] were used as the precursor solution. In this work the concentration of the solution was kept at 0.1 M. In the spray deposition, the deposition time was kept 5 minutes, substrate temperature was kept 523 K and substrate to spray nozzle distance was 25 cm and flow rate of solution was kept constant as 2ml/min.

5.3 THICKNESS MEASUREMENT

The thicknesses of the films were measured by the setup of Fizeau fringes method at the Department of Physics, BUET. Thickness of the films for Cd doping concentration value of x = 0.0, 0.2, 0.4, 0.6, 0.8 and 1.0 were found to be 535, 475, 420, 385, 355 and 287 nm respectively.

5.4 SURFACE MORPHOLOGY OF AS-DEPOSITED $Co_{1-x}Cd_xS$ AND ANNEALED $Co_{0.8}Cd_{0.2}S$ THIN FILMS

Surface morphology of the $Co_{1-x}Cd_xS$ and annealed $Co_{0.8}Cd_{0.2}S$ thin films was studied by scanning electron microscopy (SEM) under 1000, 5000 and 10000 magnifications. The films deposition by the Spray pyrolysis is generally polycrystalline or amorphous in structure. The SEM pictures of as-deposited of the $Co_{1-x}Cd_xS$ films of different molar concentrations deposited on glass substrate at temperature 523 K for 5 minutes shown in fig. 5.1(a-f). In as-deposited states the film was very dense with no observable voids or pinholes. Many small round shaped precipitates observed on the surface of the sample in the as-deposited state. The film surface becomes increasingly coarse as Cd increases. The films have inhomogeneous surfaces, less defined grain boundaries. The surface can be described as a conglomerate random roughness, which is characteristic of an amorphous nature. The overall morphology of the layers seems to be due to the growth and clustering of initial nuclei.

Fig. 5.1(a) is a pure CoS thin film shows uniform surface and deposition covers the substrate well and Fig. 5.1(f) is a pure CdS thin film and there Cd precipitation is observed. Fig.5.1 (b-e) describes different Cd incorporation in the CoS thin films and there are some opaque portion of clusters due to Cd and shows that the surface is becoming homogeneous and fairly smooth. So it may be necessary to limit the degree of Cd present in these films for applications like solar cells, particularly when spray pyrolysis is used as the fabrication technique.

Fig. 5.1.(g-i) shows the SEM photographs of the $Co_{0.8}Cd_{0.2}S$ films annealed at the temperatures of 673, 773 and 873 K for one hour in air. The small round shape which shown in as deposited films become grown and change in size after annealing. Freshly deposited films are to be associated with the formation of highly unstable phases along with imperfections and defects. On annealing some of these defects will be diffused out with time and leads to a stable phase.

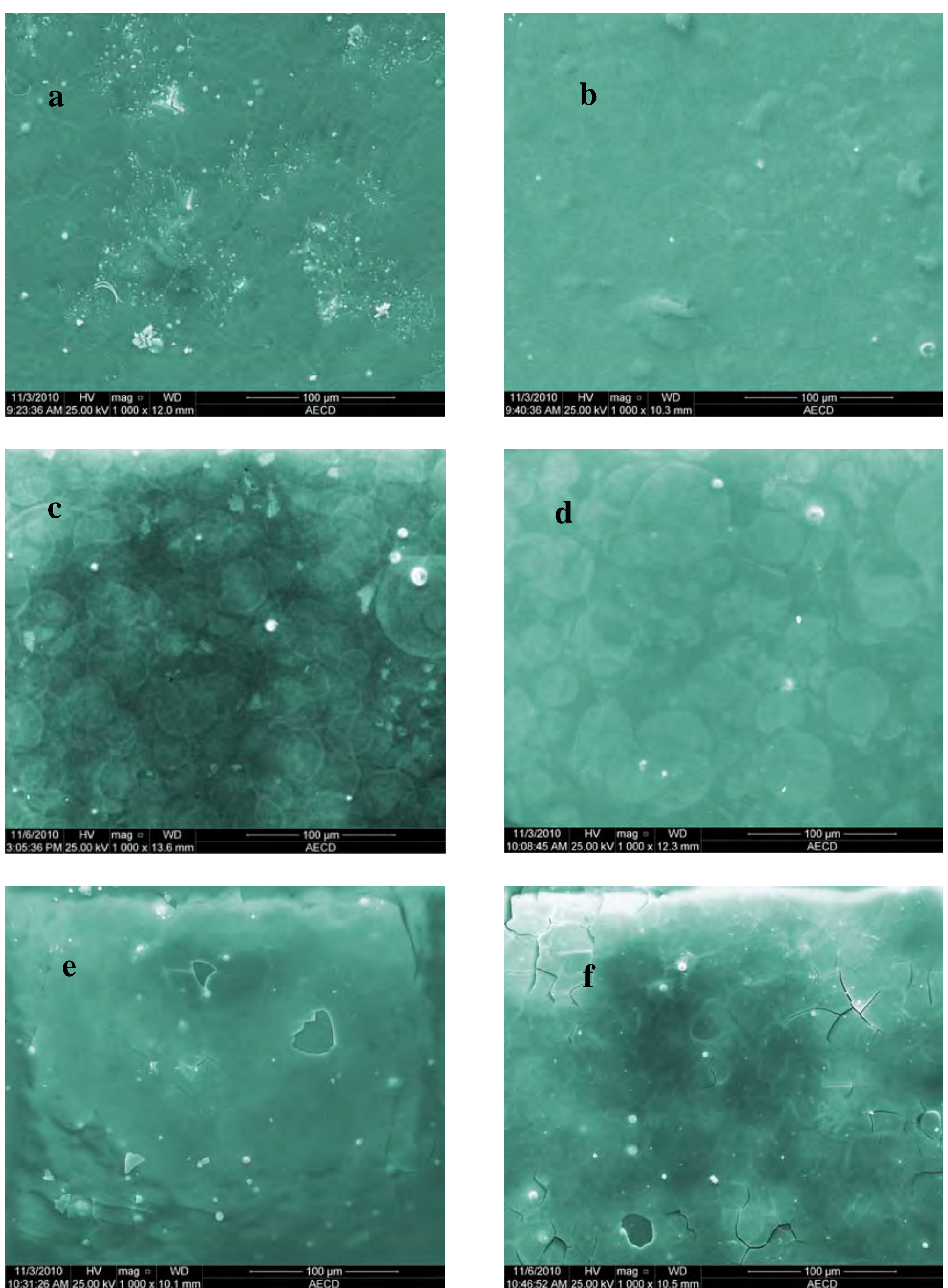

Fig. 5.1(a-f). SEM photographs of as-deposited $Co_{1-x}Cd_xS$ films at x = 0.0, 0.2 0.4, 0.6, 0.8 and 1.0 respectively under 1000 magnification.

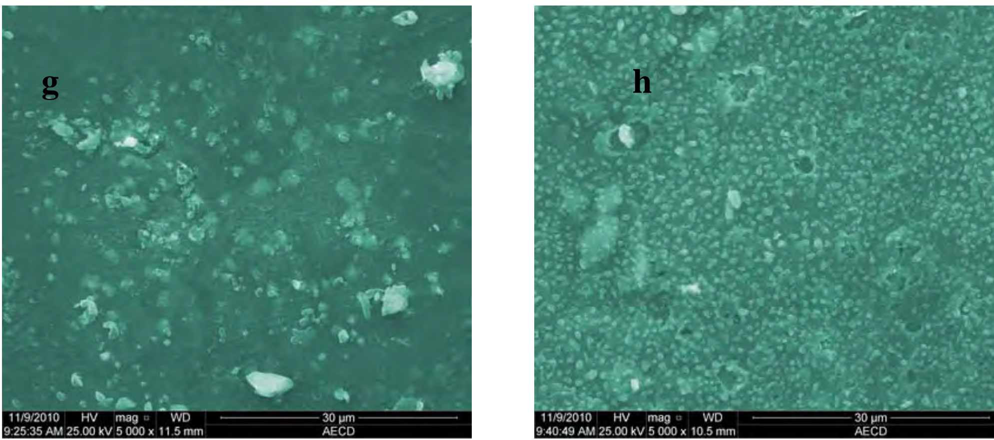

Fig. 5.1(g-h). SEM photographs of $Co_{0.8}Cd_{0.2}S$ annealed films at 673 and 773 K respectively under 5000 magnifications.

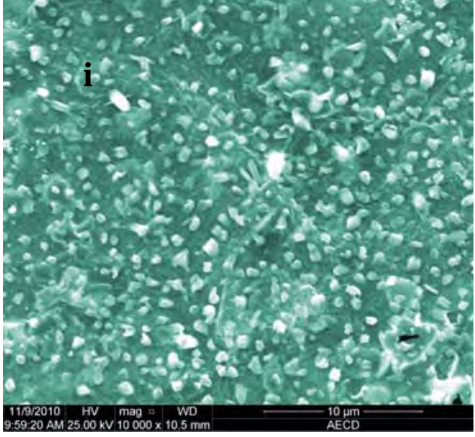

Fig. 5.1(i). SEM photograph of $Co_{0.8}Cd_{0.2}S$ annealed films at 873 K under 10000 magnifications.

At higher temperature the cluster migration mechanism also starts. Hence the smaller clusters move randomly and some of them are absorbed by the larger clusters to increase their radius and height. As a consequence of annealing the atoms started to rearrange themselves periodically and the surface of annealed samples show that the surface is uniform and homogeneous. With the increase of annealing temperature the surface homogeneity, quality, crystallinity of the annealed films increase. With the increase of annealing temperature Cd diffuses over the surface well and becomes more homogeneous. The surface morphology of the as-deposited $Co_{1-x}Cd_xS$ and

annealed $Co_{0.8}Cd_{0.2}S$ thin films are in good agreement reported by Zenrui Yu et al using chemical bath deposition method [10].

5.5 COMPOSITIONAL STUDIES

The quantitative analysis of the as-deposited $Co_{1-x}Cd_xS$ ($0\leq x \leq1$) thin films was carried out by energy dispersive X-ray spectroscopy (EDX). Fig. 5.2(a-d) shows the EDX spectra of as-deposited $Co_{1-x}Cd_xS$ thin films. Table 1.1 shows the composition of elements in $Co_{1-x}Cd_xS$ film in the sprayed solution. Two different peaks corresponding to Co and S in the spectrum, which confirms the CoS thin film. For different concentrations of Cd in the solution, there is also Cd peak in the spectra. It is worth to mention that the as-deposited $Co_{1-x}Cd_xS$ film is stoichiometric. A strong peak is observed which corresponds to Silicon (Si) and an Oxygen (O) peak is also observed both of which are also due to glass substrate. At high operating voltage the electron beam penetrates the film and reaches the glass surface, which results the Si and Oxygen peak. However, sulphur deficiency is observed in all the films. This may be due to the fact that sulphur has great affinity towards oxygen, so it might have converted to SO_2 and then evaporated. EDX result reveals that the deposited films are very close to the nominal composition. From EDX images it is observed that the height of Co peak decreases and Cd peak increases with the increase of Cd doping. From the table 1.1 it is evident that for all the films the amount of Co and S for pure and Co, S and Cd for doped films are present in an excellent ratio.

Table 1.1 Atomic % of different compositions for $Co_{1-x}Cd_xS$ thin films.

Compositions	Co atomic%	Cd atomic%	S atomic%
CoS	56.12	00	43.88
$Co_{0.4}Cd_{0.6}S$	19.89	34.04	46.07
$Co_{.0.2}Cd_{0.8}S$	12.59	37.35	50.06
CdS	00	55.17	44.83

(a)

Intensity (arb. unit)

(b)

Intensity (arb. unit)

Fig. 5.2 (a-b). EDX spectra of $Co_{1-x}Cd_xS$ thin films for (a) x = 0.0 and (b) x = 0.6 respectively.

(c)

Intensity (arb. unit)

(d)

Intensity (arb. unit)

Fig. 5.2 (c-d). EDX spectra of $Co_{1-x}Cd_xS$ thin films for (a) x = 0.8 and (b) x = 1.0 respectively.

5.6 X-RAY DIFFRACTION (XRD)

The X-ray diffraction (XRD) of pure and Cd doped CoS thin films has been done using a diffractometer, PHILIPS model "X'Pert PRO XRD System. XRD has taken to check the status and homogeneity of as-deposited $Co_{1-x}Cd_xS$ and annealed $Co_{0.8}Cd_{0.2}S$ films at 673, 773 and 873 K temperatures using molybdenum CuK_α (λ = 1.54178 Å) radiation. The XRD patterns of pure CoS and $Co_{1-x}Cd_xS$ thin films for different doping concentration (x) are presented in fig. 5.3(a) and 5.3(b) respectively. Fig.5.3. (a) shows the as-deposited film has a broad peak indicating its amorphous nature. $Co_{0.8}Cd_{0.2}S$ film annealed at 673 K shows that the film is still in amorphous but the formation of crystalline nature of the film is started at 2θ = 37.0751° peak of (130) preferential orientation. Crystallinity of the films increased with increasing annealing temperature. This indicated by the appearance of some highly resolved characteristic peaks. For 773 K annealing temperature the characteristic sharp peaks are observed at 2θ = 19.3943°, 29.3016° and 36.9160°. Miller indices (hkl) of these peaks are identified (111), (310) and (130) from JCPDS chart for $Co_{0.8}Cd_{0.2}S$ thin films. The sharp peak, 2θ = 36.9689° at preferential orientation of (130) is easily observed at 873 K annealed states for the $Co_{0.8}Cd_{0.2}S$ thin films. Grain size of the film has been determined from the stronger peaks of (130) from each XRD patterns using Scherrer formula,

$$D_g = \frac{0.9\,\lambda}{\Delta \cos\theta}$$

where, D_g is the average grain size, λ is the wavelength of the radiation used as the primary beam of CuK_α, θ is the angle of incidence in degree and Δ is the full width at half maximum (FWHM) of the peak in radian, which is determined experimentally after correction of instrumental broadening (in the present case it is 0.05°). Average grain size of the film has been determined in the range of 15 to 61 nm, which indicates the nanometric size of $Co_{0.8}Cd_{0.2}S$ grains has developed in the film. Average grain size of the film increases with the increase of annealing temperature.

Structure of the material is identified as cubic. Lattice constant has been calculated using the dominant peaks for $Co_{0.8}Cd_{0.2}S$ and the average value obtained, a ≅ 7.661 Å which is close to the standard value.

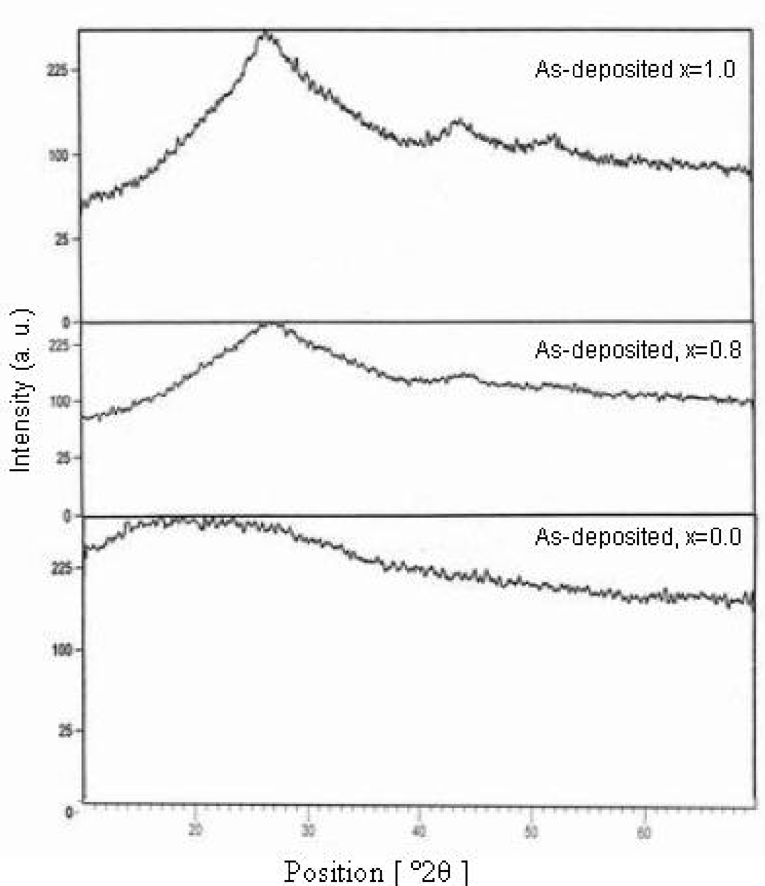

Fig. 5.3. (a) X-ray diffraction patterns of as-deposited $Co_{1-x}Cd_x$ S thin films.

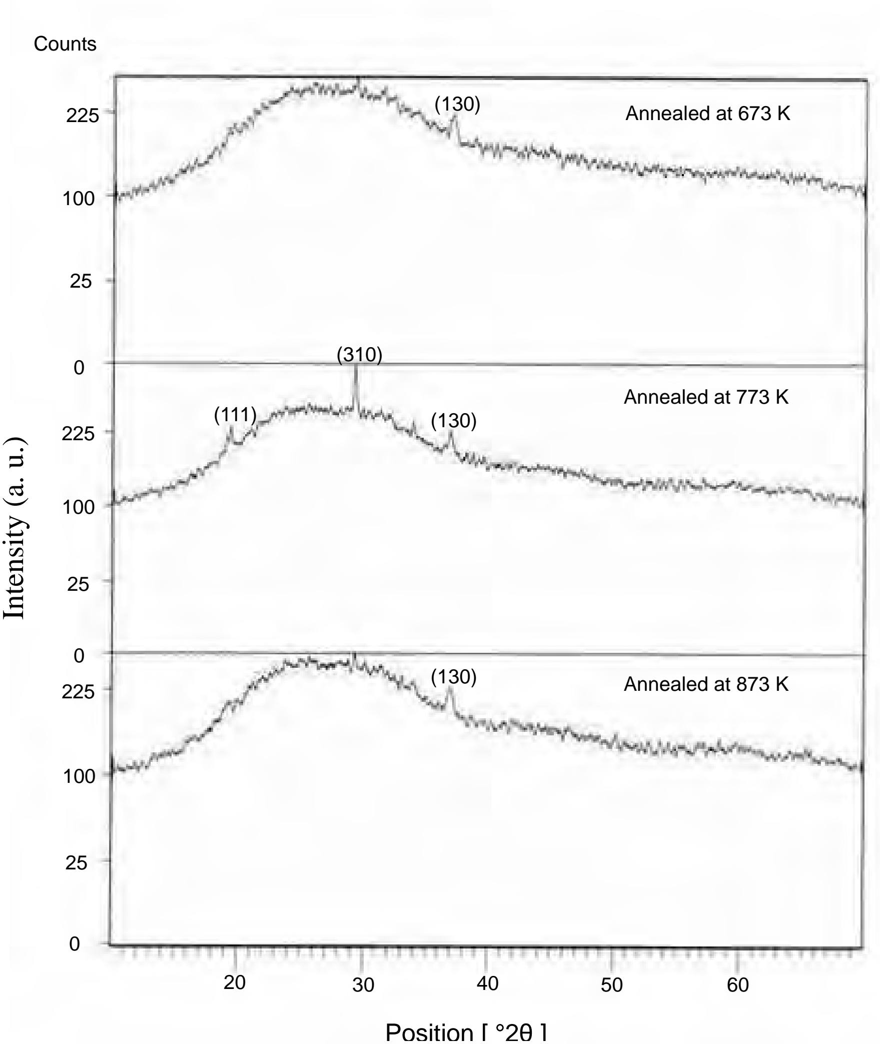

Fig. 5.3. (b) X-ray diffraction patterns of annealed $Co_{0.8}Cd_{0.2}S$ thin films.

5.7 OPTICAL PROPERTIES

5.7.1 ABSORBANCE AND TRANSMITTANCE

The optical absorbance and transmittance spectra of the as-deposited $Co_{1-x}Cd_xS$ thin films with respect to plain glass substrate have been taken using UV spectrophotometer (UV-1601PC Shimadzu, Japan) for wavelength range 300 to1100

nm at room temperature. The absorbance spectra of the as-deposited thin films of $Co_{1-x}Cd_xS$ ($0 \leq x \leq 1$) having different concentrations are shown in Fig. 5.4(a). These spectra reveal that films grown under the same parametric conditions have low absorbance in the visible and near infrared regions from 500 to 1100 nm. However, absorbance is high in the ultraviolet region. Fig. 5.4(a) shows that absorption increases with the increasing incorporation of Cd in the solution.

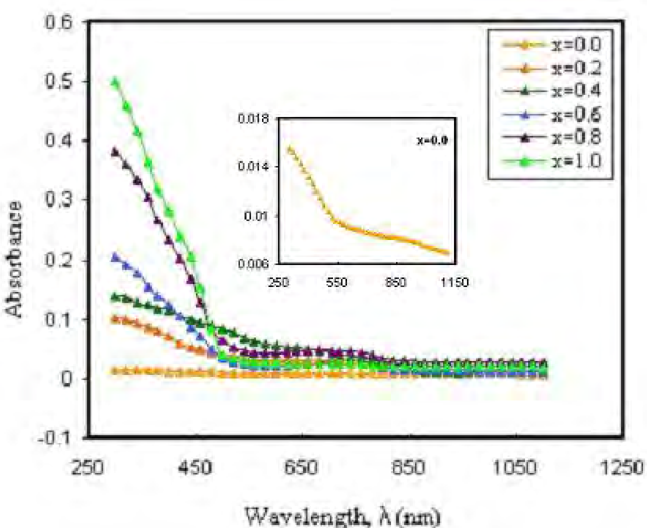

Fig. 5.4. (a) Variation of absorbance as a function of wavelength for $Co_{1-x}Cd_xS$ films for different concentrations. Inset shows the plot for x = 0.0 value.

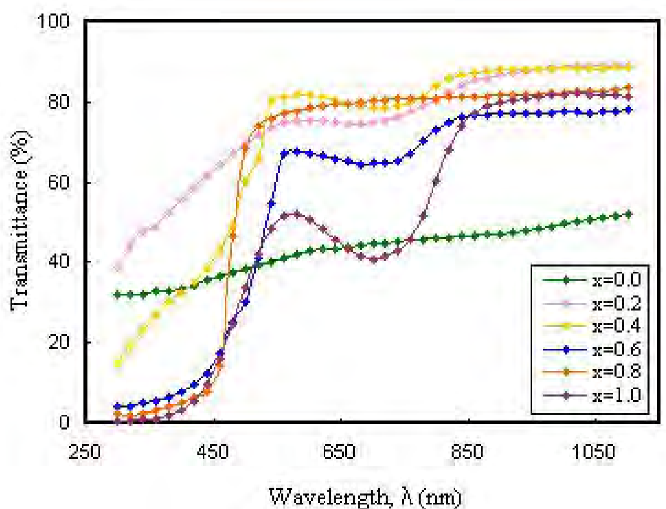

Fig. 5.4(b). Variation of transmittance as a function of wavelength for $Co_{1-x}Cd_xS$ films for different concentrations.

Fig. 5.4(b) shows the optical transmittance spectra for the $Co_{1-x}Cd_xS$ thin films. All the films demonstrate more than 70% transmittance at wavelengths longer than 800 nm. Transmittance is very high in the high wave length range i.e. at 850 to 1100 nm range. From 550 to 800 nm range, transmittance increases slightly. Below 500 nm there is a sharp fall in the %T of the films, which is due to the strong absorbance of the films in this region. It has been observed that the over all %T decreases with increasing incorporation of Cd in the solution. This result is quite similar to that of the film deposited by chemical bath deposition technique [19].

5.7.1.1 ABSORPTION COEFFICIENT AND OPTICAL BAND GAP

Absorption coefficient, (α) of the film is calculated from the absorbance data using Beer-Lambert's formula,

$$\alpha = \frac{2.303A}{d}$$

where, d is the film thickness and A is the optical absorbance of the film. Fig. 5.4 (00) shows the variation of 'α' against photon energy, (hν) for different doping concentrations, (x) of as-deposited $Co_{1-x}Cd_xS$ thin films. From the fig. 5.4(c) it is seen that the 'α' of the as-deposited $Co_{1-x}Cd_xS$ thin films increases with increasing Cd in the solution. The 'α' depends on thickness of the film. From fig. 5.4(c), it is seen that the value of 'α' is very low in the lower energy level and increases slowly in this region. Finally value of 'α' tends to become saturated at higher energy level i.e. above 2.5 eV. In the higher energy level 'α' is very high which is due to the strong absorbance of the films in this region.

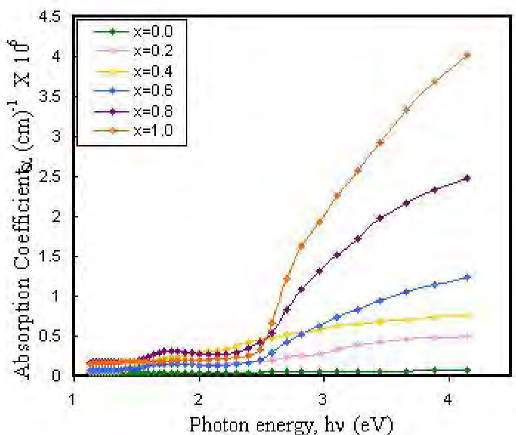

Fig. 5.4(c). Variation of Absorption coefficient as a function of photon energy for as-deposited $Co_{1-x}Cd_xS$ films.

The energy gap in a semiconductor is responsible for the fundamental optical absorption edge. The fundamental absorption process is one in which a photon is absorbed and an electron is excited from an occupied valance band state to an unoccupied conduction band state. If photon energy is less than the energy gap, such process is impossible and photon energy (hν) will not be absorbed. Such inter band absorption process are possible only if the photon energy is higher than the gap energy. Since 'α' is used to describe the reduction in intensity of light in a medium as a function of distance, therefore higher values of 'α' is an indication of more reduction in intensity. Fig. 5.4(d-i).shows the plots of $(\alpha h\nu)^2$ vs. hν for direct transition of as-deposited $Co_{1-x}Cd_xS$ thin films. The optical band gap (E_g) is determined from the plots of $(\alpha h\nu)^2$ vs. hν for direct transition for $Co_{1-x}Cd_xS$ thin films. The direct E_g of the films have been obtained from the intercept on the energy axis after extrapolation of the straight line section of $(\alpha h\nu)^2$ vs. hν curve. E_g of the films varies between 2.20 to 3.10 eV with the increase of Cd in the $Co_{1-x}Cd_xS$ system, which indicates that the presence of Cd in the films greatly affects the direct E_g. Calculated E_g values are found in good agreement with the E_g of as-deposited $Co_{1-x}Cd_xS$ films reported by M. Bedir et al [17]. The effects of increasing E_g due to the exchange interactions of the conduction and valence band electrons with the Cd^{2+} d electrons. The E_g of the compound is altered depending upon the concentration of Cd ions and the 3d levels of transition metal ions are located in the E_g region and d-d

transition dominates. The nature of this variation in the E_g may be useful to design a suitable window material for fabrication in solar cells.

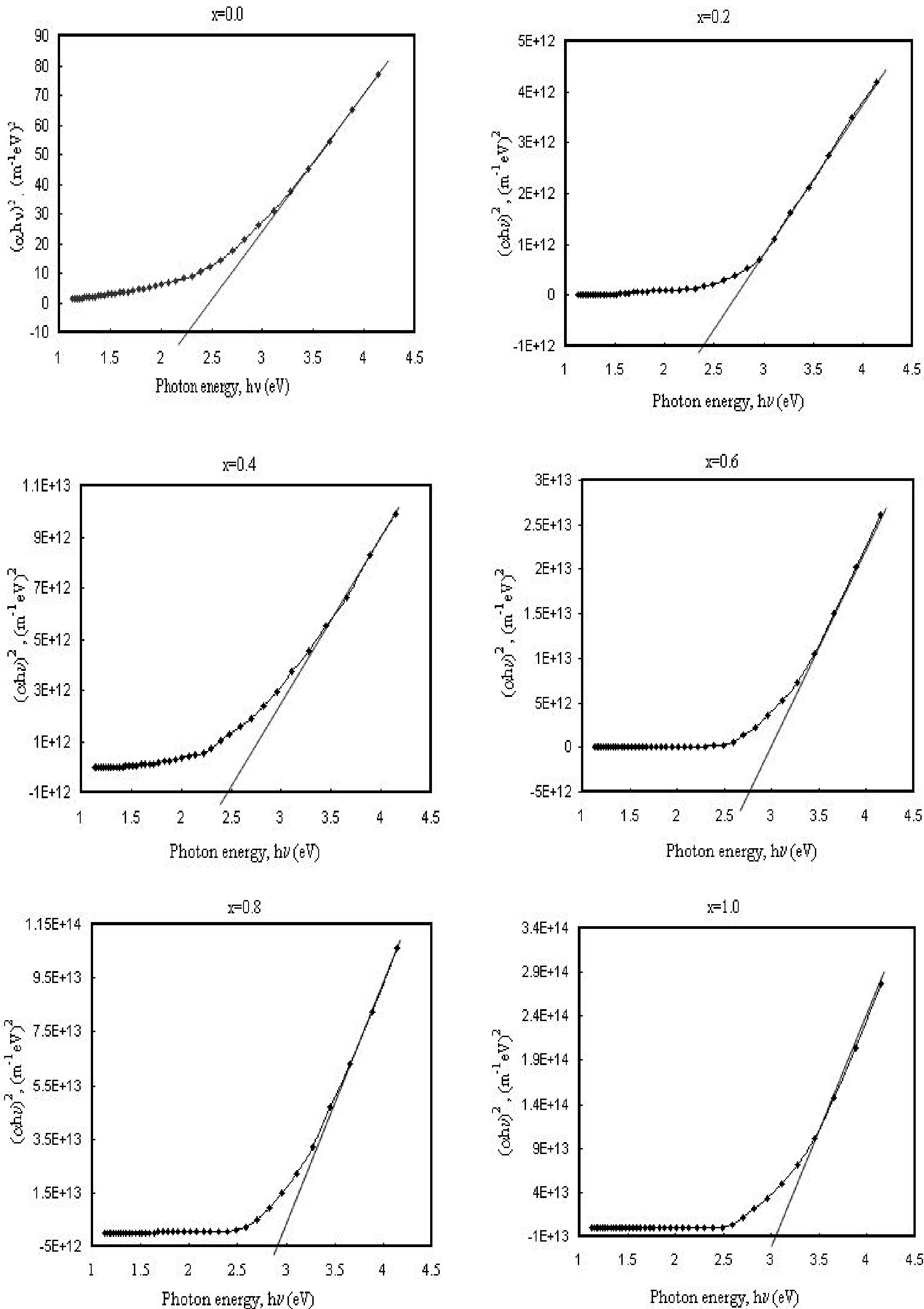

Fig. 5.4(d-i). Plots of $(\alpha h\nu)^2$ vs. hν curves for as-deposited $Co_{1-x}Cd_xS$ thin films.

Table 1.2: Variation of thickness and direct band gap with the doping concentration value, (x = 0-100 % Cd doping) of $Co_{1-x}Cd_xS$ thin film.

DopingConcentration values, (x= 0-100%) of $Co_{1-x}Cd_xS$ film.	**Thickness, d (nm) of $Co_{1-x}Cd_xS$ film.**	**Band gap, E_g (eV) of $Co_{1-x}Cd_xS$ film.**
0 %	535	2.2
20 %	475	2.4
40 %	420	2.5
60 %	385	2.75
80 %	355	2.8
100 %	287	3.1

Table 1.2 shows the variation of E_g with different molar concentration of the films for direct transitions. From the table 1.2 it is seen that the E_g increases slightly with increasing molar concentrations (x = 0 to 1). E_g obtained for direct transition of the films of different molar concentration and different thickness are also shown in the table 1.2. From the table 1.2 it is seen that in both cases the direct E_g increases slightly with decreasing thickness and that of increasing molar concentration i.e. increase of Cd incorporation in the solution.

5.7.2 EXTINCTION COEFFICIENT

The extinction coefficient, (k) is the imaginary part of the complex index of refraction, which also relates to light absorption [57]. The 'k' obtained from the relation, $k = \frac{\alpha\lambda}{4\pi}$ where, λ is the wavelength and α is the absorption coefficient, calculated from observed absorbance data using Beer Lambert's formula, $\alpha = 2.303\left(\frac{A}{d}\right)$ where, A is the optical absorbance and d is the thickness of the film. 'α' is a quantity that characterizes how easily a material or a medium can be penetrated by a beam of light.

The variation of 'k' with wavelength is shown in Fig. 5.5. It is observed that the 'k' increases with the increase of Cd incorporation. The rise and fall in the 'k' is due to the variation of absorbance. The fall in the 'k' may be due to the absorption of light

at the grain boundaries. From figure it is evident that ‘k’ decreases rapidly with increasing wavelength from 300 to 500 nm and then increases slowly in the wavelength range from 550 to 750 nm after that the value of ‘k’ remains constant. The ‘k’ is almost constant in the higher wavelength region and when the energy exceeds E_g it increases rapidly.

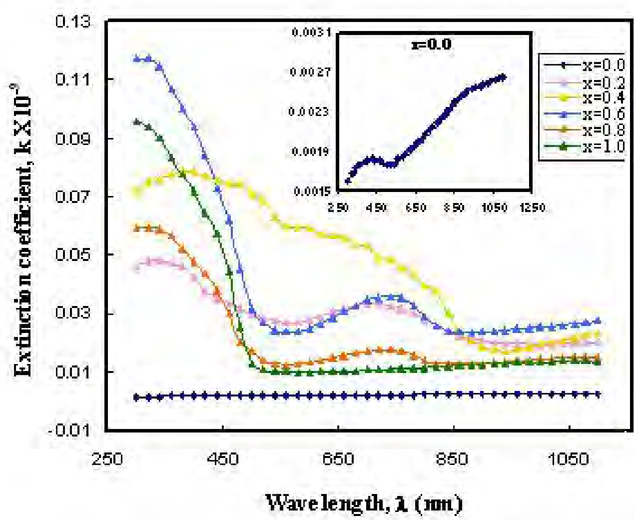

Fig. 5.5. Variation of extinction coefficient as a function of wavelength for $Co_{1-x}Cd_xS$ films of different concentrations. Inset shows the plot for x = 0.0 value.

5.7.3 REFRACTIVE INDEX

In order to calculate the refractive index of the films, the reflectance data of the films were calculated from UV-VIS spectroscopy. The refractive index, (n) has been calculated using the relation,

$$n = \left(\frac{1+R}{1-R}\right) + \sqrt{\left(\frac{4R}{(1-R)^2} - k^2\right)}$$

where, k is the extinction coefficient and R is the optical reflectance, calculated from the absorbance data,

1 = Transmittance + Absorbance + Reflectance

Reflectance, R = 1 – (Transmittance + Absorbance) .

The 'n' as a function of the wavelength for various compositions is shown in Fig.5.6. From Fig. 5.6 it is evident that 'n' increases sharply in the wavelength range from 300 to 480 nm, then decreases from 500 to 560 nm and then increases slowly from 580 to 820 nm. After that the value of 'n' remains constant. The 'n' of the as-deposited thin film decreases with the increase of Cd in the system. Low 'n' occurs due to successive internal reflections. It is also attributed to the variety of different impurities and defects.

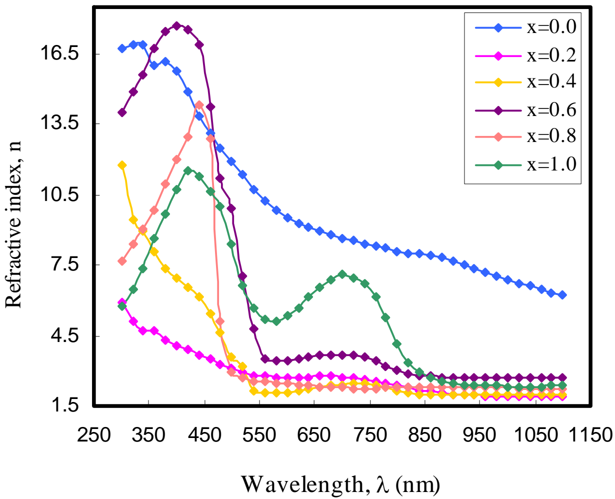

Fig. 5.6. Variation of refractive index as a function of wavelength for $Co_{1-x}Cd_xS$ films of different doping concentrations.

5.7.4 DIELECTRIC CONSTANTS

The real ε_r and imaginary ε_i parts of the dielectric constant were determined using the formula $\varepsilon_r = n^2 - k^2$ and $\varepsilon_i = 2nk$ where, n is the refractive index and k is the extinction coefficient. The complex dielectric constant is fundamental intrinsic material property. The real part ε_r is the normal dielectric constant and imaginary part ε_i represents the absorption associated of radiation by free energy.

The variation of ε_r and ε_i parts of the dielectric constant for different film concentrations are illustrated in Fig. 5.7(a, b).

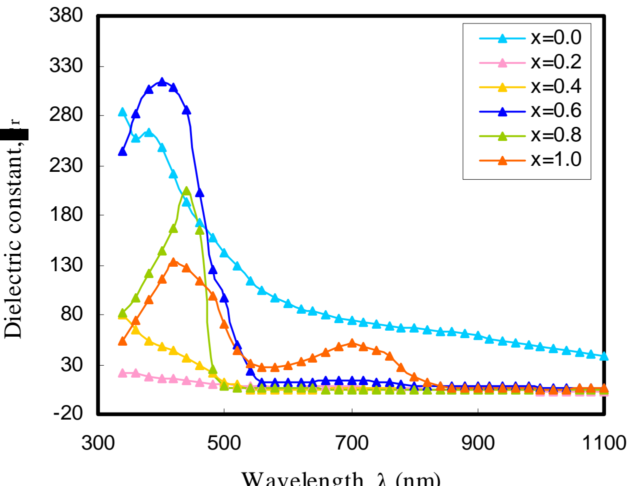

Fig. 5.7(a). Variation of real part of dielectric constant as a function of wavelength of as-deposited $Co_{1-x}Cd_xS$ films of different doping concentrations.

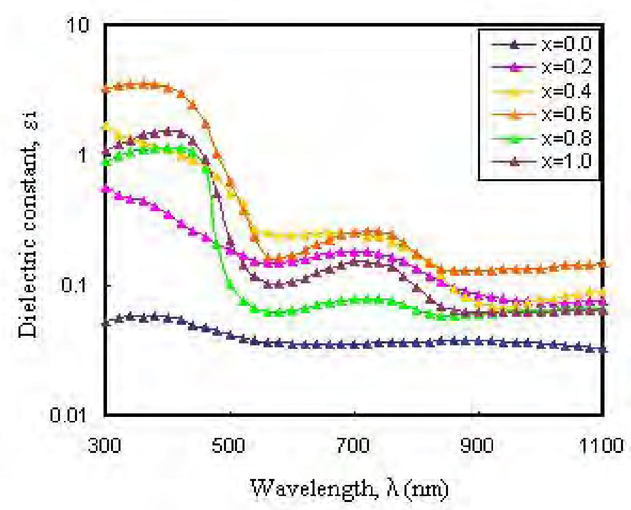

Fig. 5.7(b). Variation of imaginary part of dielectric constant as a function of wavelength of as-deposited $Co_{1-x}Cd_xS$ films of different doping concentration.

Fig. 5.7(a, b) revealed that the value of the ε_r is higher than that of the ε_i of the dielectric constant. The ε_r and ε_i part of the dielectric constant increases in the UV region shown in fig. 5.7(a, b). It is observed that both ε_r and ε_i decrease with increasing wavelength. From the optical data, it is observed that the ε_r and ε_i part of the dielectric constant follow the same pattern. The complex dielectric constant high at the higher energy of the hν and is more or less constant at the lower incident hν.

5.7.5 DIELECTRIC LOSS

Dielectric loss is a loss of energy that goes into heating a dielectric material in a varying electric field. The variations of dielectric loss with hν are shown in Fig. 5.8 for the as-deposited $Co_{1-x}Cd_xS$ thin films.

The dielectric loss is given by,

$$\tan\delta = \varepsilon_i / \varepsilon_r$$

and loss angle, $\delta = \tan^{-1}\left(\frac{\varepsilon_i}{\varepsilon_r}\right)$

where, ε_r and ε_i are the real and imaginary parts of the dielectric constant [58]. From figure it is observed that dielectric loss increases with the increase of photon energies.

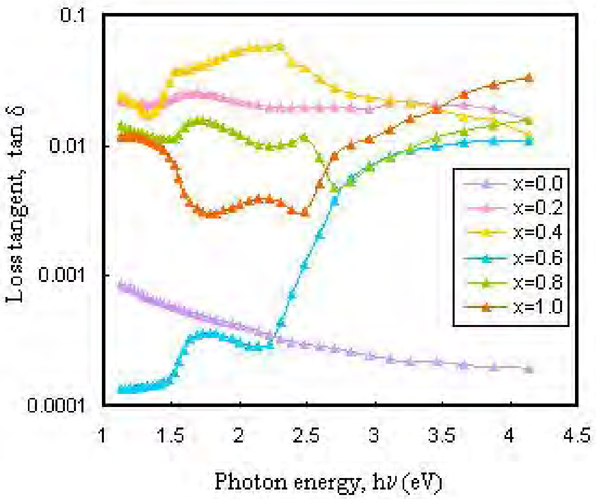

Fig. 5.8. Variation of dielectric loss as a function of photon energy for $Co_{1-x}Cd_xS$ films of different doping concentrations.

5.7.6 OPTICAL CONDUCTIVITY

The optical conductivity, σ_{opt} was determined by using the relation,

$$\sigma_{opt} = \alpha nc / 4\pi$$

where, c is the velocity of light, n is the refractive index and α is the absorption coefficient of the films [59].

Fig. 5.9 shows the variation of σ_{opt} with the incident hν. From Fig. 5.9 it is observed that the σ_{opt} of the films increases at high hν i.e. in the ultra violet region due to the high absorbance in that region. The figure revealed that the σ_{opt} increases with the increasing Cd in the system.

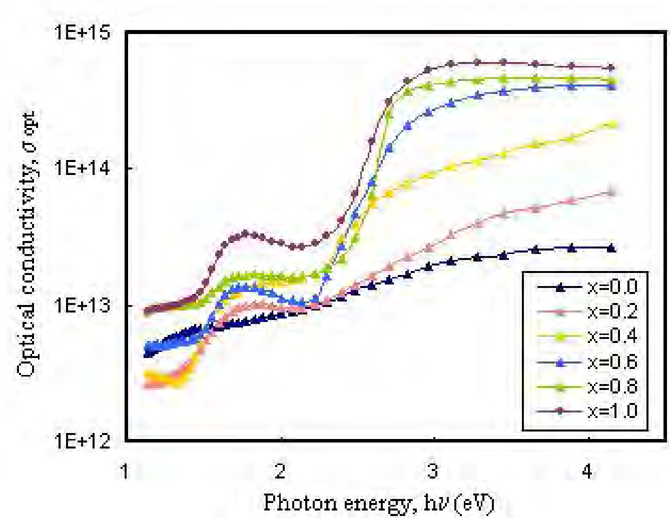

Fig. 5.9. Variation of optical conductivity as a function of photon energy for $Co_{1-x}Cd_xS$ films of different doping concentrations.

5.8 OPTICAL PROPERTIES OF ANNEALED $Co_{0.8}Cd_{0.2}S$ THIN FILM

Annealing was performed on $Co_{0.8}Cd_{0.2}S$ thin film at temperatures of 673, 773, and 873 K for duration of 1 hour in closed furnace.

5.8.1 ABSORBANCE, TRANSMITTANCE AND OPTICAL BAND GAP OF ANNEALED $Co_{0.8}Cd_{0.2}S$ THIN FILM

The absorbance spectra of the annealed thin films of $Co_{0.8}Cd_{0.2}S$, at different annealing temperatures are shown in Fig. 5.10(a). It is seen that absorbance increases with increasing of annealing temperature.

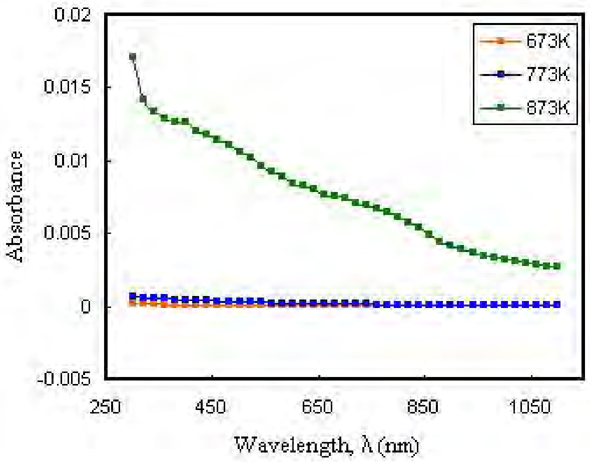

Fig. 5.10 (a). Variation of absorbance as a function of wavelength for annealed $Co_{0.8}Cd_{0.2}S$ films.

Fig. 5.10(b) shows the optical transmittance spectra for the annealed thin films of $Co_{0.8}Cd_{0.2}S$, at different annealing temperatures. It is seen that transmittance decreases with increasing of annealing temperature.

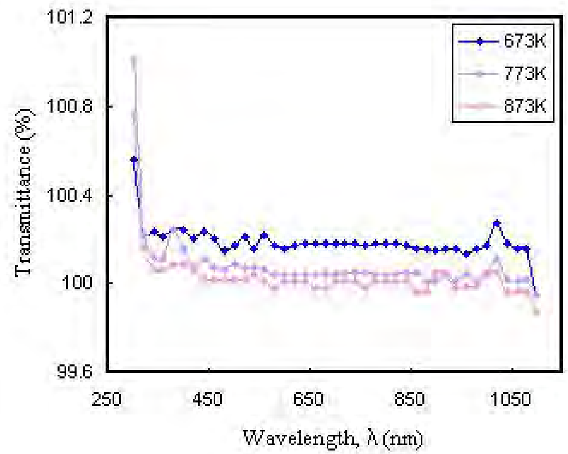

Fig. 5.10 (b). Variation of Transmittance as a function of wavelength for annealed $Co_{0.8}Cd_{0.2}S$ films.

Fig. 5.10(c-e) shows the plots of $(\alpha h\nu)^2$ vs. hν for direct transition. The E_g is determined from the plots of $(\alpha h\nu)^2$ vs. hν for direct transition for the annealed thin films of $Co_{0.8}Cd_{0.2}S$ at different annealing temperatures. The direct E_g of the films have been obtained from intercept on the energy axis after extrapolation of the straight line section of $(\alpha h\nu)^2$ vs. hν curve.

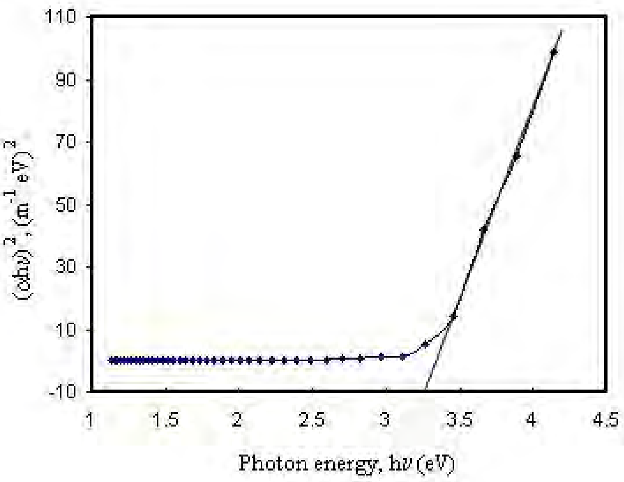

Fig. 5.10(c). Plots of $(\alpha h\nu)^2$ vs. hν for annealed $Co_{0.8}Cd_{0.2}S$ films at 673 K.

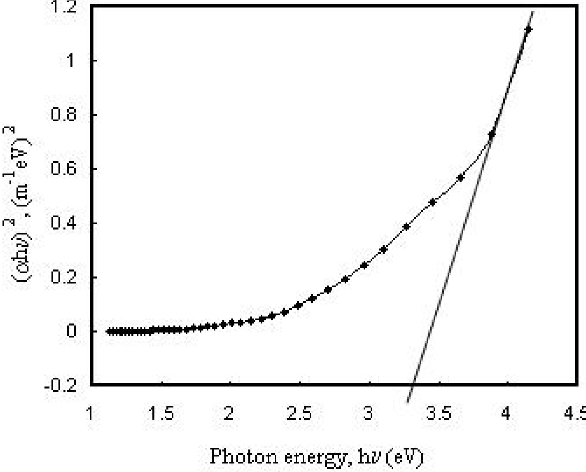

Fig. 5.10(d). Plots of $(\alpha h\nu)^2$ vs. hν for annealed $Co_{0.8}Cd_{0.2}S$ films at 773 K.

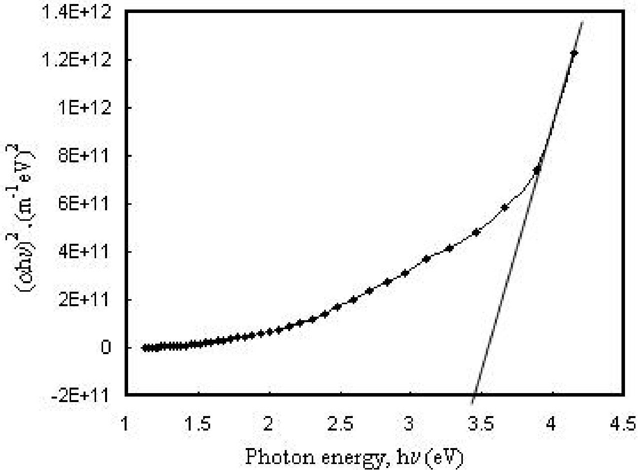

Fig. 5.10(e). Plots of $(\alpha h\nu)^2$ vs. hν for annealed $Co_{0.8}Cd_{0.2}S$ films at 873 K.

The variations of E_g with different annealing temperatures are shown in the table 1.3. The E_g of the annealed $Co_{0.8}Cd_{0.2}S$ films varies between 3.25 to 3.45 eV with the increasing of annealing temperature, which indicates that annealing temperature greatly affects the E_g of the films. This is in agreement with the observed increase in the crystallite size as the annealing temperature increases, which further consolidates the suggestion that annealing enhances the crystallinity of the films. The observed calculated Eg values of annealed $Co_{0.8}Cd_{0.2}S$ films are in good agreement with the other reported value by RF sputtering method [60]

Table 1.3 Variation of direct E_g with different annealing temperatures for annealed $Co_{0.8}Cd_{0.2}S$ thin films.

Annealing temperatures	**Band gap, E_g (eV)**
673 K	3.25
773 K	3.30
873 K	3.45

5.8.2 EXTINCTION COEFFICIENT

The variation of 'k' of annealed $Co_{0.8}Cd_{0.2}S$ films with wavelength is shown in Fig. 5.11. It is observed that the 'k' increases with the increase of annealing temperature. From figure it is clear that 'k' decreases slowly with increasing wavelength range from 300 to 700 nm and after that the value of 'k' remains constant.

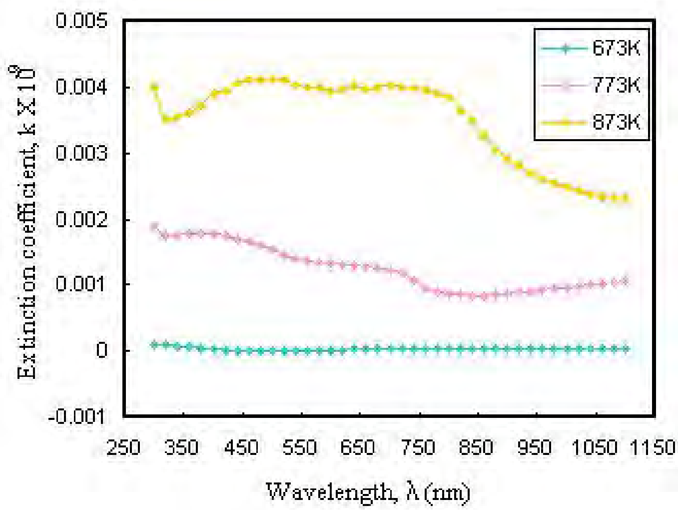

Fig. 5.11. Variation of extinction coefficient as a function of wavelength for annealed $Co_{0.8}Cd_{0.2}S$ films.

5.8.3 REFRACTIVE INDEX

The variation of 'n' of annealed $Co_{0.8}Cd_{0.2}S$ films with wavelength for different annealing temperatures is shown in Fig. 5.12. From the optical data, it is observed that the value of 'n' decreases with the increase of annealing temperature. From figure it is evident that the 'n' increases in the wave length range from 320 to 450 nm and after that the value of 'n' remains constant.

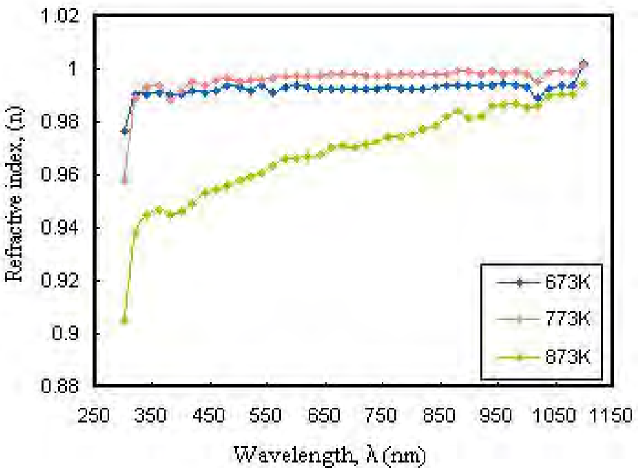

Fig. 5.12. Variation of refractive index as a function of wavelength for annealed $Co_{0.8}Cd_{0.2}S$ films.

5.8.4 DIELECTRIC CONSTANTS

The variation of the ε_r and ε_i parts of the dielectric constant with wavelength for annealed $Co_{0.8}Cd_{0.2}S$ films are illustrated in Fig. 5.13(a, b). The dielectric constant of the film for real part decreases and imaginary part increases with the increase of annealing temperature. From figures it is seen that the values of the real part are higher than that of the imaginary part.

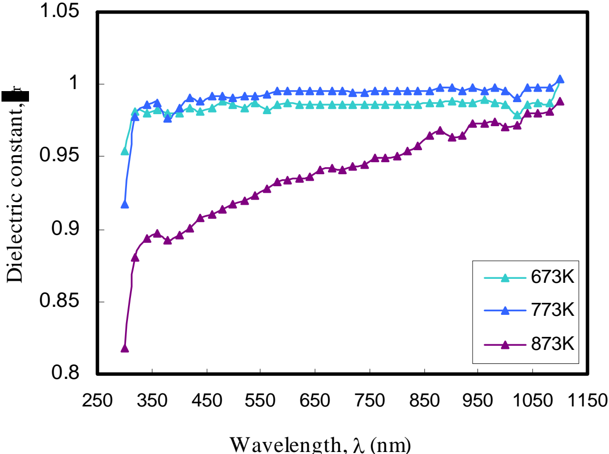

Fig. 5.13(a). Variation of real part of dielectric constants as a function of wavelength for $Co_{0.8}Cd_{0.2}S$ films.

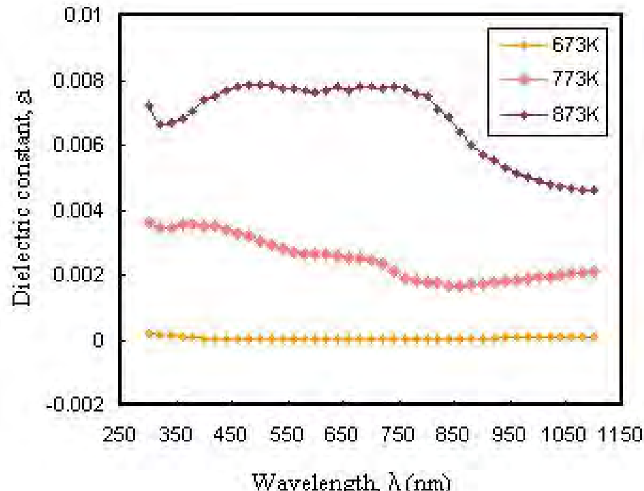

Fig. 5.13(b). Variation of imaginary part of dielectric constants as a function of wavelength for annealed $Co_{0.8}Cd_{0.2}S$ films.

5.8.5 DIELECTRIC LOSS

The variations of dielectric loss of annealed $Co_{0.8}Cd_{0.2}S$ films with hν are represented in Fig. 5.14. From Fig. 5.14 it is observed that dielectric loss decreases for the increase of annealing temperature.

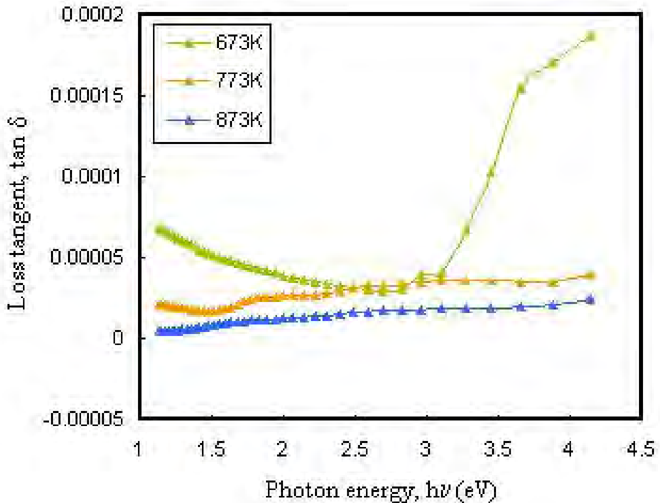

Fig. 5.14. Variation of dielectric loss as a function of photon energy for annealed $Co_{0.8}Cd_{0.2}S$ films.

5.8.6 OPTICAL CONDUCTIVITY

Fig. 5.15 shows the variation of optical conductivity, (σ_{opt}) with the incident hν for the annealed $Co_{0.8}Cd_{0.2}S$ thin films. It is seen from figure that the σ_{opt} increases in the higher energy level due to the high absorbance of the films in that region. It is observed that σ_{opt} increases with the increase of annealing temperature.

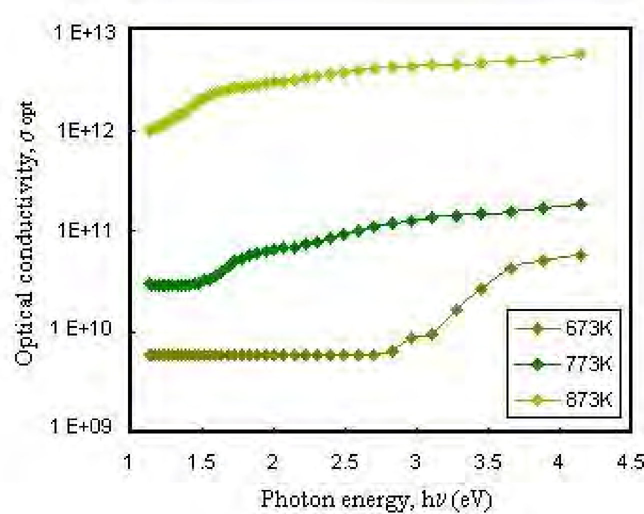

Fig. 5.15. Variation of optical conductivity as a function of photon energy for annealed $Co_{0.8}Cd_{0.2}S$ films

5.9 ELECTRICAL PROPERTIES OF AS-DEPOSITED $Co_{1-x}Cd_xS$ THIN FILMS

Electrical parameters like resistivity, conductivity, sheet resistance, activation energy etc. of the as deposited $Co_{1-x}Cd_xS$ ($0 \le x \le 1$) films were measured by the van-der Pauw method. D.C electrical resistivity measurements were made in air for freshly deposited films from room temperature 303 to 408 K by van-der Pauw method and data were taken by increasing the temperature of the film slowly. On increasing up to a maximum temperature (408 K) and then the film cooled down slowly to room temperature. Variation of current and voltage corresponding temperature recorded in data and then calculated electrical parameters. For dc conductivity measurement, a 15 V dc fixed bias was maintained. A power supply (Heath kit, Model: IP-2717A)

was used to pass a constant dc current through the test sample. An electrometer (Keithley, Model: 614) was used to monitor the current through the sample and a digital multimeter (Model: DM-206) was used to measure the potential differences across each sample. The glass substrate was heated by a specially designed heater and the temperature was measured by a chromel-alumel thermocouple placed on the middle of the substrate.

5.9.1 VARIATION OF RESISTIVITY WITH TEMPERATURE

The variation of electrical resistivity with temperature for as deposited $Co_{1-x}Cd_xS$ ($0 \leq x \leq 1$) thin films is shown in Fig. 5.16.

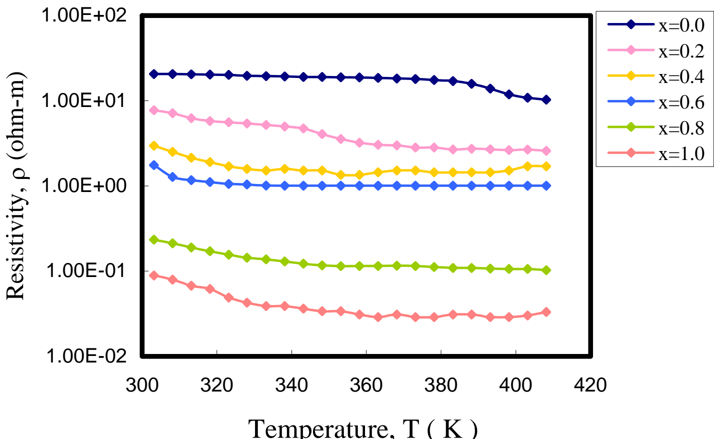

Fig. 5.16. Variation of electrical resistivity with temperature for $Co_{1-x}Cd_xS$ thin films.

From the figure it is seen that resistivity decreases with the increase of temperature. This type of variation indicates the semiconducting behavior of the films. The resistivity decreases with the increase of cadmium concentration in the system.

5.9.2 VARIATION OF ELECTRICAL CONDUCTIVITY WITH TEMPERATURE

The variation of electrical conductivity with temperature for as deposited $Co_{1-x}Cd_xS$ ($0 \le x \le 1$) thin films is shown in Fig. 5.17. From the figure it is seen that the conductivity increases with the increase of temperature. This type of variation indicates the semiconducting behavior of the films. The conductivity increases with the increasing of cadmium concentration. In semiconductor, the numbers of carriers available for electrical conduction are increased with temperature. In the n-type semiconductor conductivity is controlled by electrons. As the temperature increases more and more electrons are released to the valance band. Hence the conductivity is increased with temperature.

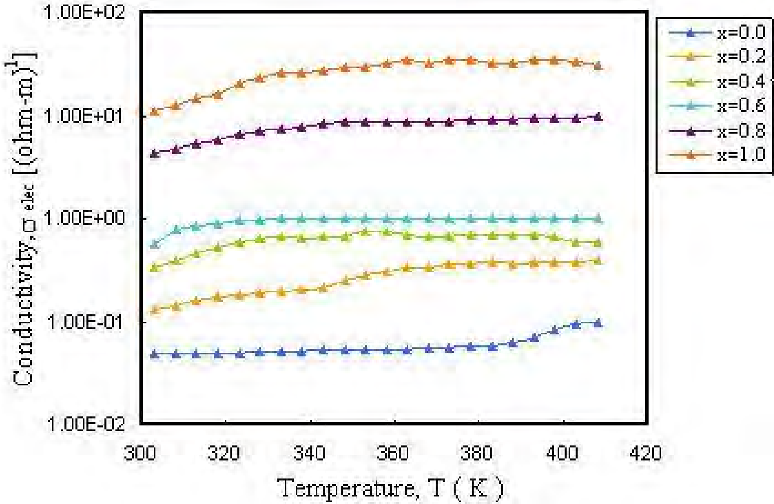

Fig. 5.17. Variation of electrical conductivity with temperature for $Co_{1-x}Cd_xS$ thin films.

In general for a semiconducting material, dc conductivity increases exponentially with temperature indicates that the conductivity is a thermally activated process. Mathematically, it can be expressed by the well-known Arrhenius relation as, $\sigma_{dc} = \sigma_o \exp (-\Delta E / 2 kT)$ where, σ_o is called pre-exponential factor, ΔE is called the activation energy, T is the absolute temperature and k is Boltzmann constant. These parameters are of significance to differentiate the nature of various conduction

mechanisms. Fig. 5.17 shows temperature dependence of dc conductivity σ_{dc}, for $Co_{1-x}Cd_xS$ films of compositions x = 0.0 to 1.0 respectively. The electrical conduction of the films follows a mechanism in which the electron or hole hops from one localized site to the next. Localized state is a state of motion in which an electron may be found anywhere within a region of a material of linear extent smaller than that of the materials. Whenever it is transferred to another site, the surrounding molecules respond to this perturbation with structural changes and the electron or hole is temporarily trapped in the potential well leading to atomic polarization. The electron resides at this site until it is thermally activated to migrate to another site. Another aspect of this charge hopping mechanism is that the electron or hole tends to associate with local defects. So, the activation energy for charge transport may also include the energy of freeing the hole from its position next to the defects [61. 62].

5.9.3 VARIATION OF SHEET RESISTANCE WITH TEMPERATURE

The variation of sheet resistance with temperature for as-deposited $Co_{1-x}Cd_xS$ $(0\leq x\leq 1)$, thin film is shown in Fig. 5.18. It is seen from the graph that the sheet resistance decreases with increasing temperature. The sheet resistance decreases with the increasing of Cd concentration. This is due to the fact that the resistivity of as-deposited $Co_{1-x}Cd_xS$ thin film is decreased with temperature.

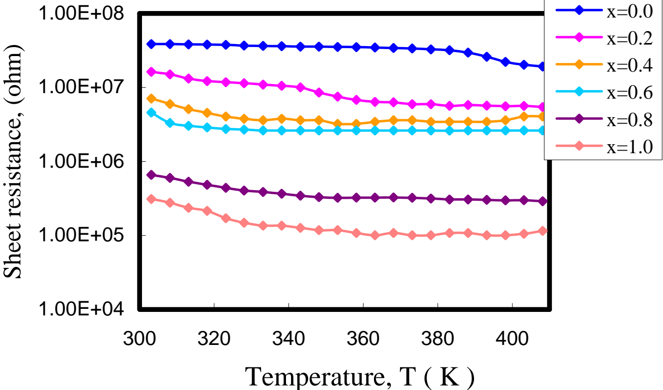

Fig. 5.18. Variation of sheet resistance with temperature for as deposited $Co_{1-x}Cd_xS$ thin films.

5.9.4 VARIATION OF ACTIVATION ENERGY

The lnσ versus 1/T graph for the as-deposited $Co_{1-x}Cd_xS$ thin films is shown in Fig. 5.19. The straight lines for the films of different doping concentrations (0≤x≤1) are drawn by least mean square fitting method (not shown here). From the slope, the activation energy of the films of different doping concentrations (0≤x≤1) has been calculated. Table 1.4 represents the variation of activation energy of different doping concentration (0≤x≤1) for the as-deposited $Co_{1-x}Cd_xS$ thin films. It is reveled from the table 1.4 that the activation energy increases between 0.25 to 0.5 eV with the increase of Cd incorporation in the system. These observed values may be due to size effects that are arising because of quantum confinement of charge carriers within the particles. The low values of the activation energy may be associated with the localized levels due to the excitation of carriers from donor level to the conduction band. The increase in conductivity may be attributed to the increasing number of oxygen vacancies present in the sample. The activation energy of the as-deposited $Co_{1-x}Cd_xS$ thin film is quite similar to the reported value of others [10, 63]

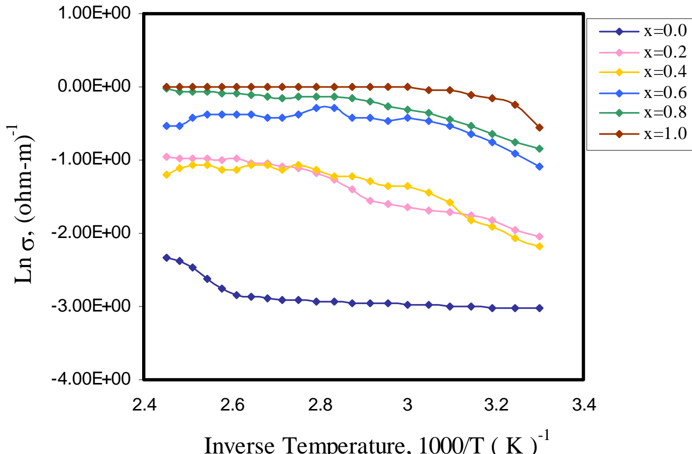

Fig. 5.19 Plot of lnσ versus 1000 / T for as-deposited $Co_{1-x}Cd_xS$ thin films.

Table 1.4 Variation of activation energy with different compositions of $Co_{1-x}Cd_xS$ thin films.

Compositions	Activation energy, eV
CoS	0.25
$Co_{0.8}Cd_{0.2}S$	0.35
$Co_{0.6}Cd_{0.4}S$	0.38
$Co_{0.4}Cd_{0.6}S$	0.40
$Co_{0.2}Cd_{0.8}S$	0.45
CdS	0.50

5.9.5 VARIATION OF TEMPERATURE COEFFICIENT OF RESISTANCE (T.C.R)

Fig.5.21 shows the variation of temperature coefficient of resistance (T.C.R) with temperature for as-deposited $Co_{1-x}Cd_xS$ thin films. It is seen in fig.5.21 that the value of T.C.R is negative which indicates that the as-deposited $Co_{1-x}Cd_xS$ thin films are n-type semiconductor in nature. The T.C.R value is almost same for all doping concentrations shown in figure 5.21.

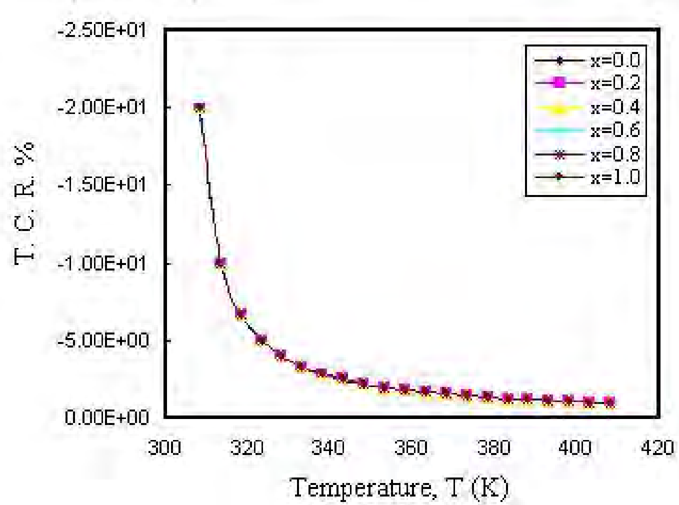

Fig. 5.20. Variation of T.C.R with temperature for as-deposited $Co_{1-x}Cd_xS$ thin films.

CHAPTER-VI

CONCLUSIONS AND SUGGESTIONS FOR FUTURE WORK

6.1 CONCLUSIONS

The purpose of this chapter is to summarize the results obtained in this work. In the light of the experimental investigation and analysis on the surface morphological, structural, optical and electrical studies of pure and Cd doped CoS thin films of different compositions and thicknesses deposited by cost effective and convenient spray pyrolysis technique, the following conclusions may be drawn**:**

In this work, it is observed that the deposition of $Co_{1-x}Cd_xS$ films depends on various parameters such as substrate temperature, concentration of the solution, distance between spray nozzle and the glass substrates and deposition time etc. Film deposited at 523 K substrate temperature is found to be good one in terms of their uniformity of thickness and color.

The SEM micrographs of the $Co_{1-x}Cd_xS$ films of different Cd concentrations deposited on glass at substrate temperature 523 K and $Co_{0.8}Cd_{0.2}S$ films annealed at 673, 773 and 873 K for 1 hour were taken. The SEM micrographs of as-deposited films show that the film surface becomes increasingly coarse as Cd increases. In as-deposited states the film was very dense with no observable voids or pinholes. The surface could be described as a conglomerate random roughness, which was a characteristic of an amorphous nature. The overall morphology of the layers seemed to be due to the growth and clustering of initial nuclei. With the increase of annealing temperature the surface homogeneity, quality, crystallinity of the annealed films increased. With the increase of annealing temperature the defects and surface roughness of the films also reduced.

The elemental compositions of $Co_{1-x}Cd_xS$ thin films have been analyzed by EDX which revealed the presence of Co and S in the system. It is also clear from the EDX result that the Cd ions are acting as dopants in the $Co_{1-x}Cd_xS$ structure. It is worth to mention that the as-deposited $Co_{1-x}Cd_xS$ film is stoichiometric.

XRD analysis reveals that the as-deposited $Co_{1-x}Cd_xS$ thin film is amorphous in nature and the annealed $Co_{0.8}Cd_{0.2}S$ films show the formation of crystalline in nature. Average grain size of the films increases from 15 to 61 nm with increasing annealing temperature. Structure of the material is identified as cubic.

The absorbance spectra of the as-deposited $Co_{1-x}Cd_xS$ ($0\leq x \leq 1$) thin films show that the absorbance is low in the wavelength range from 500 -1100 nm and high in the ultraviolet region. Transmittance of the deposited films increases in the near infrared region. Transmittance of the prepared thin films decreases with increasing incorporation of Cd in the solution. Direct band gap (E_g) of the films varies between 2.20 to 3.10 eV with the increase of Cd in the $Co_{1-x}Cd_xS$ system, which indicates that presence of Cd in the films greatly affects the optical band gap. The measured values of the E_g are found in good agreement with the value reported by others. The 'k' and 'σ_{opt}' of the films increases in the higher energy level with the increasing Cd in the system. The 'n' decreases with the increase of Cd in the system. The value of the ε_r of the dielectric constant is higher than that of the ε_i. The dielectric loss increases in the high photon energy level.

Transmittance of the annealed $Co_{0.8}Cd_{0.2}S$ thin films decreases as the annealing temperature increases. The direct E_g of the annealed $Co_{0.8}Cd_{0.2}S$ films varies between 3.25 to 3.45 eV with increasing of annealing temperature, which indicates that annealing temperature greatly affects the E_g of the films. This is in agreement with the observed increase in the crystallite size as the annealing temperature increases, which further consolidates the suggestion that annealing enhances the crystallinity of the films. The 'k' and the 'σ_{opt}' increase with the increase of annealing temperature. The 'n' and dielectric loss decreases with the increase of annealing temperature.

The electrical resistivity decreases and the conductivity of the as-deposited $Co_{1-x}Cd_xS$ films increase with the increase of temperature range from 303 to 408 K. This indicates that the behavior of $Co_{1-x}Cd_xS$ film is semiconductor. The electrical conductivity increases with increasing Cd concentration. Activation energy of as-deposited $Co_{1-x}Cd_xS$ films increases with increasing Cd in the solution. Activation energy of the films varies in the range of 0.25 to 0.50 eV.

6.2 SUGGESTIONS FOR FUTURE WORK

This is the first time that $Co_{1-x}Cd_xS$ thin films have been prepared in our laboratory by spray pyrolysis technique. In recent years $Co_{1-x}Cd_xS$ thin film has a variety of optoelectronic device applications, such as photo luminescent, photoconductor devices and photodiodes, photovoltaic cells etc. Hence to get better performance of this material the following research work may be extended as follows:

1. The $Co_{1-x}Cd_xS$ thin films may be characterized with respect to different substrate temperature.
2. The Hall Effect and temperature dependence Hall Effect may be studied of the $Co_{1-x}Cd_xS$ thin films.
3. Study of thermoelectric power of $Co_{1-x}Cd_xS$ thin films.
4. Study of photoluminescence (PL) properties of $Co_{1-x}Cd_xS$ the films.
5. Study of luminous and solar transmittance as well as reflectance of the as-deposited $Co_{1-x}Cd_xS$ films for selective surface application.
6. AC measurement of $Co_{1-x}Cd_xS$ thin films should be studied.
7. Mechanical properties of $Co_{1-x}Cd_xS$ thin films may also be also be investigated.
8. Study of magnetic properties of $Co_{1-x}Cd_xS$ thin films.

CHAPTER-I

GENERAL INTRODUCTION

CHAPTER-II

THIN FILM DEPOSITION TECHNIQUES AND PROCESSES

CHAPTER-III

THEORETICAL PRINCIPLES OF FILM CHARACTERIZATION

CHAPTER-IV

EXPERIMENTAL DETAILS

CHAPTER-V

RESULTS AND DISCUSSION

CHAPTER-VI

CONCLUSIONS AND SUGGESTIONS FOR FUTURE WORK

References

[1] Kumar, A., Chung, Y. W., Moore, J. J. and Smugeresky, J. E., “Surface Engineering Science” The Minerals, Metals & Material Society, Warrendale, 1999.

[2] Gloker, D. A. and Shah, S. I., “Hand Book of Thin Film Process Technology” Inst. Phys. Publishing, Bristol and Philadelphia, 1998.

[3] Bhowmik, N. C., Rahman, J., Alam Khan, M. A. and Mozumder, Z. H., “Renewable Energy” Vol-24, Issues 3-4, pp-663, 2001.

[4] Farid Ul Islam, A. K. M., Ph.D. Thesis, University of Rajshahi, Bangladesh, 2005.

[5] Kumar, A., Chung, Y. W. and Chia, R. W. J., “Hard Coatings”, The Minerals, Metals & Material Society, Warrendale, 1999.

[6] Feitosa, A. V., Miranda, M. A. R., Sasaki, J. M. and Araujo-Silva, M. A., “A new route for preparing CdS thin films by chemical bath deposition using EDTA as Ligand”, Brazilian Journal of Physics, Vol- 34, No-2B, 2004.

[7] Ezema, F. I. and Osuji, R. U., “Band gap shift and optical characterization of chemical bath deposited CdSSe thin films on annealing”, Chalcogenide letters, Vol-4, No-6, pp 69-75, 2007.

[8] Murray, C. B., Kagan, C. R., Bawendi, M. G., “Self Organization of CdSe Nanocrystallites into Three Dimensional Quantum Dot Superlattices” Science, Vol-270, pp 1335-1338, 1995.

[9] Mathur, N., Joshi, K., Rakesh, Subbaraju, G. V., Sehgal, H. K., “Solution grown $Pb_{1-x}Co_xS$ semiconductor nanoparticle films” Vol-23, pp 56-60, 2004.

[10] Zenrui, Yu., Jinhui, Du., Shuhua, Guo., Jiayou, Zhang, Yasuhiro, Matsumoto, “CoS thin films prepared with modified chemical bath deposition” Thin Solid Films, Vol-415, pp 173-176, 2002.

[11] Mishack, Nnabuchi, N., Chinedu, Ekuma, E., “Synthesis and characterization of chemical bath deposited CdCoS thin film” Vol-07, No-01, pp 31-38, 2010.

[12] Ezema, F. I. and Osuji, R. U., “Preparation and optical characterization of chemical bath deposited $CdCoS_2$ thin films” Vol-6(8), pp1827-1832, 2006.

[13] Sathyamoorthy, R., Sudhagar, P., Balerna, A., Balasubramanian, C., Bellucci, S., “Surfactant-assisted synthesis of $Cd_{1-x}Co_xS$ nanocluster alloys and their structural, optical and magnetic properties” Journal of Alloys and Compounds, Vol-493, pp 240-245, 2010.

[14] Chandramohan, S., Kanjilal, A., Sarangi, S. N., Majumder, S., Sathyamoorty, R. and Som, T., "Implantation-assisted Co-doped CdS Thin films: Structural, optical and vibrational properties" 2009.

[15] Lewicki, A., Schindler, A. I., Miotkowski, I., Crooker, B. C. and Furdyna, J. K., "Specific heat of $Cd_{1-x}Co_xS$ and $Cd_{1-x}Co_xSe$ at low temperatures" Physical Review B, Vol-l43, No-07, 1991.

[16] Bacaksiz, E., Tomakin, M., Altunbas, M., Parlak, M. and Colakoglu, T., "Structural, optical and magnetic properties of $Cd_{1-x}Co_xS$ films prepared by spray pyrolysis" 2008.

[17] Bedir, M., Kayali, R., Oztas, M., "Effect of the Zn concentration on the characteristic parameters of $Zn_xCd_{1-x}S$ thin films developed by spraying pyrolysis method under the nitrogen atmosphere" Turk J. Phys, Vol-26, pp121-126, 2002.

[18] Raji, P., Sanjeeviraja, C. and Ramachandran, K., "Thermal and structural properties of spray pyrolysed CdS thin film" BULL MATER. Sci., Vol- 28, pp 233-238, 2005.

[19] Ugwu, E. I. and Onah, D. U., "Optical characteristics of chemical bath deposited CdS thin film characteristics within UV, Visible, and NIR radiation" Vol-08, No-01, pp155-160, 2007.

[20] BRUS, L. E., "Quantum crystallites and nolinear optics" Appl., Phys., Vol-53, pp 465-474, 1991.

[21] Wang, Y. and Herron, N., "Nanometer-sized semiconductor clusters; Materials synthesis, Quantum size effects and photophysical properties" J. Phys. Chem., Vol-95, pp 525, 1991.

[22] Ortega-Borges, R., Lincot, D., "Mechanism of chemical bath deposition of cadmium sulfide thin films in the ammonia-thiourea system" J., Electrochem., Soc. Vol-140, pp 3464, 1994.

[23] Cruz-Vazquez, C., Inoue, M., Inoue, M. B., Barnal, R., Espinja-Beltran, F. J., "Electrical and spectroscopic properties of amorphous copper sulfide films treated with iodine, lithium iodide and sodium iodide" Thin Solid Films, Vol-373, pp-01, 2000.

[24] Basu, P. K., Pramanik, P., "A solution grown technique for the deposition of cobalt sulphide thin film" J. of Materials Sci. Lett., Vol-5, pp 1216-1218, 1986.

[25] Maissel, L. I., Glang, R., "Handbook of Thin Film Technology" Mc. Graw-Hill Company, 1970.

[26] Smith, D. L., "Thin Film Deposition, Principles & Practice" McGraw-Hill Professional, 1995.

[27] Bashar, S. A., “Study of Indium Tin Oxide (ITO) for Novel Optoelectronic Devices” PhD Thesis, King’s College London, University of London, Department of Electronic Engineering, 1998.

[28] Senturia, S. D., “Microsystem Design” Springer, 2001.

[29] Chawla, V., Jayagantan, R., Chawla, A. K., Chandra, R., “Morphological study of magnetron sputtered Ti thin films on silicone substrate”, Mater Chem. Phys., Vol-111, pp 414-418, 2008.

[30] Dunlap, R. A., Gaudet, J. M., Hatchard, T. D., “A Mössbauer effect and X-ray diffraction study of Fe- Ga- Al thin films prepared by combinatorial sputtering” J. Magnetism & Magnetic Mater, Vol-320, pp 2730-2736, 2008.

[31] Zhao, Q. X., Bian, F., Zhou, Y., Gao, Y. F., et al., “Optical emission, electron temperature and microstructure of Cu film prepared by magnetron sputtering” Mater Lett., Vol-62, pp 4140-4142, 2008.

[32] Zhang, B., Dong, X., Xu, X., Zhao, P., Wu, J., “Characteristics of zirconium-doped indium tin oxide thin films deposited by magnetron sputtering” Solar Energy Mater Solar Cells, Vol-92, pp1224-1229, 2008.

[33] Shiung Hsi C, Houng B, Yi Hou B, Ju Chen G, Li Fu S. “Effect of Ru addition on the properties of Al-doped ZnO thin films prepared by radio frequency magnetron sputtering on polyethylene terephthalate substrate” J. Alloys Comp, Vol-464, pp 89-94, 2008.

[34] Suwanboon, S., “The properties of nanostructured ZnO thin Film via solGel coating” Naresuan University Journal, Vol-16(2), pp173-180, 2008.

[35] Rinaldi, F., “Basics of Molecular Beam Epitaxy (MBE)” Optoelectronics Department, University of Ulm, Annual Report 2002.

[36] Mooney J. B. and Radding S. B., “Spray pyrolysis processing” Ann. Rev. Mater. Sci. Vol-12, pp 81-101, 1982.

[37] Chopra, K. L., “Thin Film Phenomena” McGraw-Hill Book Company, New York, 1969.

[38] Langmuir, I., Phys. Rev., vol-8, pp149, 1916 & J. Frenkel, Z. Physik, Vol-26, pp 117, 1924.

[39] Semenoff, N., Z. Phys., Chem., No-B7. pp 741, 1930.

[40] Volmer, M. and Weber, A., “Keimbildung in Ubersattigten” Z. Phys, Chem., Vol-119, pp 277, 1926.

[41] Becker, R. and Doring, W., “Kinetische Behandlung der Keimbildung in uebersattigten dampfen” Ann, Physik, Vol-24, pp719, 1935.

[42] Volmer, “Kinetic der phasenbildung” theodor steinkupf verlagsbunchandlung, Dresden Leipzig, Steikopf, 1939.

[43] Pound, G.. M., Simnad, M. T. and Yang, L., “Heterogeneous nucleation of crystals from vapor” J. Chem. Phys., Vol-22, No-07, pp1215-1219, 1954.

[44] Andrade, E. N., trans., Farady. Soc, Vol-31, pp1137, 1935.

[45] Uyeda, R., Proc. Phys. Math. Soc., Japan, Vol-24, pp809, 1942.

[46] Levistein, H., J. Appl. Phys., Vol-20, pp306, 1949.

[47] Pashley, D. W. and Stowell, M. J., in S. S. Breese (Ed.), Proc.5th Intern. ‘Cogner. Electron microscope’, P.GGI. Academic press Inc; New York, 1962.

[48] Smith, D. L., in “Thin Film Deposition”, McGraw Hill Book Company, New York, 1995.

[49] Goswami, A., “Thin Film Fundamentals”, New Age Int.(P) Ltd. Publishers, New Delhi, 1996.

[50] Howland and Benatar, L., “A Practical guide to Scanning Probe Microscopy” Park Scientific Instruments, 1997.

[51] Cullity, B. D., ‘Elements of X-ray Diffraction’ Addison-Wesley Publishing Company. Inc. USA, 1959.

[52] Vankar, D., Das, S. R., Nath, P. and Chopra, K. L., “Structure of vacuum, evaporated $Cd_xZn_{1-x}S$ thin films” Phys. Stat. Sol., (a), Vol-45, pp 665, 1978.

[53] Hirsch, P. B., Howie, A., Nilcholson, R. B., Pashly D. W. and Whelan, M. J., “Electron Microscopy of Thin Crystals” Butterworths, Washington D. C., 1965.

[54] Davies, E. A. and Mott, N. F, “Conduction in non-crystalline system, Optical absorption and photoconductivity in amorphous semiconductors”, Philos. Mag. Vol-22, pp 3, 1970.

[55] Tolansky, S., “Multiple Beam Interferometry of Surfaces and Films” Clarendon Press, Oxford, 1948.

[56] Ghos S. N. and Deb, S., ‘A Synopsis of Physics’ The World Press Ltd, Calcutta, Vol-671, 1937.

[57] Xiao, H., Xianogyan, Z., Uddin, A. and Leu, C. B., "Preparation and characterization of electronic and optical properties of plasma polymerized nitrites'', Thin Solid Films, Vol-477, pp 81-87, 2005.

[58] Wang, J., Xiang, J., Duo, S., Wenkui, L., Mingsheng, L., Lingyun, and B., "Microstructure, optical and dielectric properties of compositional graded (Ba, Sr) TiO_3 thin films derived by RF magnetron sputtering" J. Mater Sci, Vol-20, pp 319-322, 2009.

[59] Sharm, P., Sharma V., Katyal, S. C., "Variation of optical constants in $Ge_{10}Se_{60}Te_{30}$ thin film" Chalcogenide Letters, Vol-3, pp 73-79, 2006.

[60] Assali, K. EL., Boustani, M., Khiara, A., Bekkay, T., Outzourhit, A., Ameziane, E. L., Bernede, J. C. and Pouzet, J., "Some structural and optical properties of CdS thin films prepared by RF sputtering", Phys. Stat. Sol., Vol-178, pp 701, 2000.

[61] Hossain, M. S., Islam, R. and Khan, K. A., "Electrical conduction mechanisms of undoped and vanadium doped ZnTe thin films" Chalcogenide Letters, Vol-5, pp 01-09, 2008.

[62] Khan, M. K. A., Rahman, M. A., Shahjahan, M., Rahman, M. M., Hakim, M. A., Saha, D. K. and Khan, J. U., "Effect of Al-Doping on optical and electrical properties of spray pyrolytic nano-crystalline CdO thin films" Current Applied Physics, Vol-1748, pp-7, 2009.

[63] Ubale, A. u., Junghare, A. R., Wadibsme, N. A., Daryapurkar, A. S., Mankar, R. B., Sangwar, V. S., "Thickness dependent structural, electrical and optical properties of chemically deposited nanopartical PbS thin films", Turk J. Phys., Vol-31, pp 279-286, 2007.